THE UNIVERSITY OF MANITOBA

STACKING FAULT ENERGY DETERMINATION AND ITS APPLICATION TO ALPHA ZIRCONIUM

by

THOMAS FRANK MALIS

A THESIS

SUBMITTED TO THE FACULTY OF GRADUATE STUDIES

IN PARTIAL FULFILMENT OF THE REQUIREMENTS FOR THE

DEGREE OF MASTER OF SCIENCE

DEPARTMENT OF MECHANICAL ENGINEERING

WINNIPEG, MANITOBA

February 1971

ABSTRACT

Through its control over the equilibrium dissociation of dislocations, the stacking fault energy has a marked influence on various aspects of dislocation movement, such as climb and cross-slip, which, in turn, affect such properties as work hardening, creep and recovery. The presence of stacking faults can play an important role in two phase alloy strengthening and phase transformations. Thus it is desirable to know the value of the stacking fault energy as accurately as possible and many methods have evolved for its determination. Each of the techniques is briefly reviewed and the strong and weak points listed. Remarks are made concerning the methods in general, particularly when applied to hexagonal close-packed metals. It is seen that there has been little previous work to determine the stacking fault energy of HCP zirconium. What work there is, has been vague and/or inaccurate. In this work an attempt has been made to measure the stacking fault energy in Zr by means of the loop annealing method, since this is a reasonably accurate method particularly applicable to high stacking fault energy metals. This method involves a comparison of the annealing rates of faulted and perfect quenched-in vacancy loops in a metal. In this study, however, the necessary loops were found impossible to generate because of experimental contamination (hydriding) and impurities present in the starting material. The difficulties encountered are discussed in terms of the parameters affecting loop formation, together with the theoretical possibility of forming quenched-in loops in Zr. The discussion of alternative possibilities for estimating the stacking fault energy of Zr, even though they may be less attractive, for experimental and theoretical reasons, then follows.

TABLE OF CONTENTS

LIST OF TABLES

LIST OF FIGURES

LIST OF PHOTOGRAPHS

STACKING FAULT ENERGY DETERMINATION AND ITS APPLICATION TO ALPHA ZIRCONIUM

1 INTRODUCTION

Defects in the crystal structure of metals have long been known to affect, in varying degrees, many of their physical and mechanical properties. Thus, before improving upon the desirable properties in any given application or diminishing any which are undesirable, a thorough determination of the type and quantity of defect present, and the degree of its effect on the relevant properties, is a necessary prerequisite. To accomplish this, the nature of the defect itself must be understood.

Defects are generally classified in three categories; point defects, such as vacancies or interstitials, line defects, such as dislocations, and planar defects, such as stacking faults or grain boundaries. It is the latter category, namely stacking faults, which shall be closely examined in this study.

The physical description of a stacking fault and how it may arise in the crystal lattice, is of primary importance. Since any system will tend towards its lowest possible energy state, the area of stacking fault will be dependent upon a certain surface energy above that of the perfect lattice, which, in relation to the energies of various other defects, will determine the probability of the fault occurring. Hence, if the presence of faults can be shown to affect a given mechanical property, a knowledge of the magnitude of this stacking fault energy, hereafter denoted as SFE (or Greek symbol γ), could then help predict to what extent the property will be affected.

Accordingly, a great deal of work has been done to determine the SFE of many metals and alloys. The methods of determination may be generally classified as either direct or indirect. The direct methods involve a visual observation of faults or faulted defects followed by appropriate calculations from the defect geometry. The indirect methods rely on observations of some parameter intimately connected with the SFE to obtain an estimate of its magnitude.

Of the three major metallic crystal lattices; face-centered cubic (FCC), body-centered cubic (BCC), and hexagonal close-packed (HCP), by far the greatest amount of work has been done on FCC metals and alloys, primarily because of their commercial importance. The relatively simple FCC lattice geometry has aided these studies a great deal. The BCC metals, because of their complex stacking sequence of the atomic layers have, on the whole, been considered to have SFE's too high to be of prime interest. HCP metals, because of a somewhat complicated lattice geometry and smaller commercial usage have also been little studied with respect to SFE. Accordingly, in this work the applicability of the various methods of HCP metals is explored and evaluated. In particular, determination of the SFE of alpha zirconium, important in nuclear reactor technology, has been attempted.

1.1 FAULT CLASSIFICATIONS

If the atoms in a crystal lattice can be approximated by hard spheres, the FCC and HCP structures arise through different stacking sequences of layers of close-packed atoms. Thus if one layer of atoms is designated as occupying 'A' positions (see Fig. 1), the next layer could

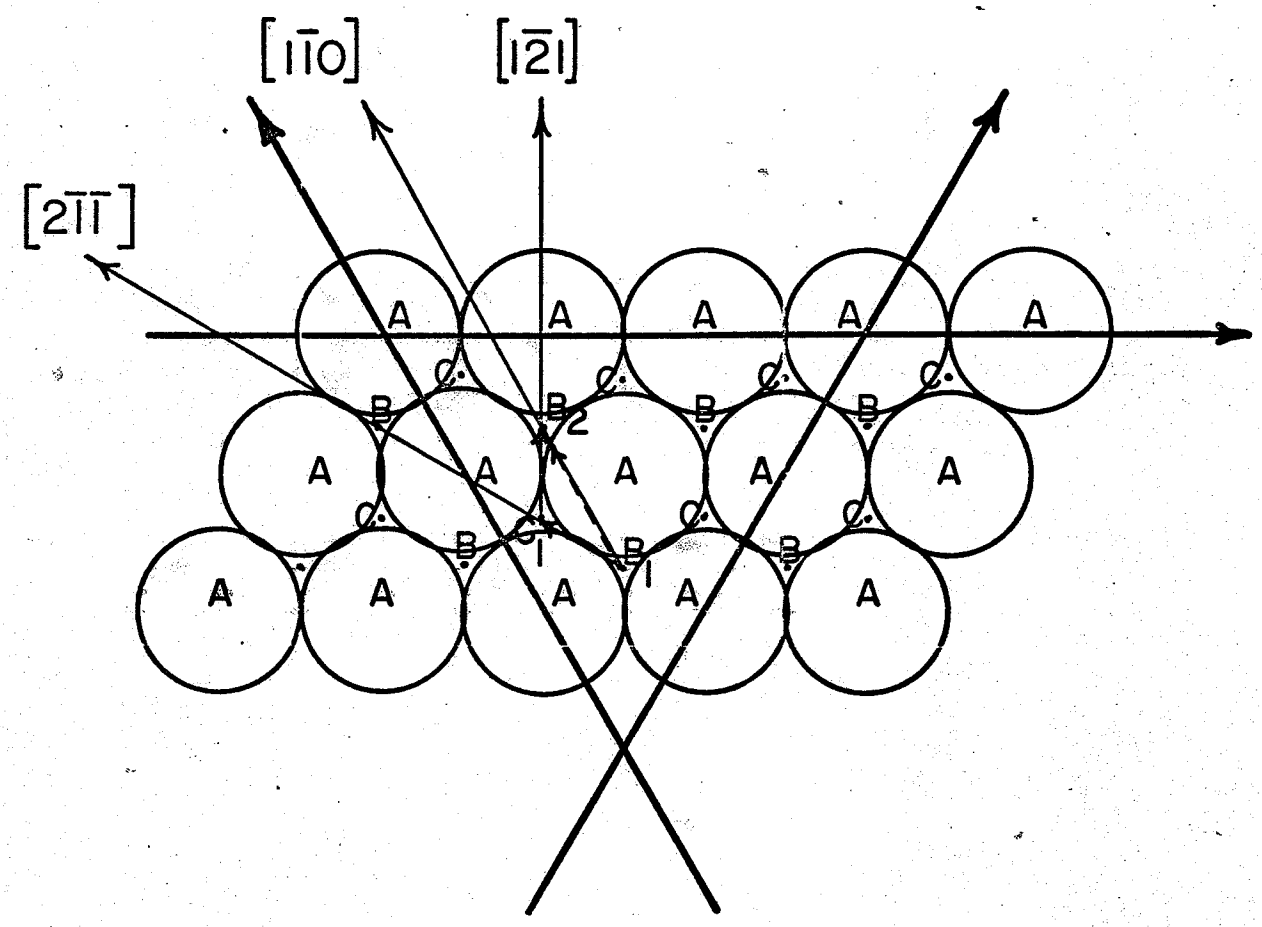

PLANES { (111) - FCC
(0001) - HCP

DIRECTIONS { <110> - FCC
<11$\bar{2}$0> - HCP
<112> - FCC
<10$\bar{1}$0> - HCP

Fig.1 Close packed plane in the FCC or HCP lattice

then be placed in either the 'B' or 'C' positions. Thus the FCC lattice arises from one layer in the 'A' position, the next in the 'B' position and the third in the 'C' position whereas the HCP lattice has the third layer back in the 'A' position.

Given these two ideal stacking sequences, a stacking fault arises when an error occurs in the sequence through either removal, insertion or shear of an atomic plane. The SFE is then the extra energy created above that of the perfect lattice and is composed of a surface energy due to the faulted area and an elastic energy due to the line tension of the bounding partial dislocations, i.e. dislocations whose Burgers vectors are less than the full slip distance of a perfect dislocation. Splitting of a perfect dislocation into two partials bounding a faulted area occurs only when it is energetically favorable (except under unusual circumstances), as in the reaction:

$$\frac{a}{2}[1\bar{1}0] \rightarrow \frac{a}{6}[1\bar{2}1] + \frac{a}{6}[2\bar{1}\bar{1}]$$

perfect dislocation → 2 Shockley partials

where the configurational energy (taken as the square of the Burgers vectors[1]) is

$$\frac{a^2}{2} \rightarrow \frac{a^6}{6} + \frac{a^6}{6} = \frac{a^2}{3}$$

This may also be deduced intuitively, it being easier to produce a shift from B_1 to B_2 by way of C_1 rather than straight from B_1 to B_2, as shown in Fig. 1. This separation of the partials is then given by a balance between their mutual elastic repulsion and an attraction arising from the tendency to decrease the surface energy of the faulted area.

Various means of classifying the possible types of faults have arisen, one early method being that of having either growth or deformation faults. Growth faults are defined as those having the fault boundary separating crystal portions having a twin orientation, while deformation faults separate regions of parallel orientation. Another method has been to classify faults as either intrinsic[2], where, for an intrinsic fault, the atomic pattern of each half of the crystal extends to the composition plane (whether or not this is an atomic plane) and, for an extrinsic fault, the composition plane is an atomic plane which is foreign to the lattice structure on either side of it. As an example, removal of a layer of atoms (vacancy condensation) would correspond to an intrinsic fault, while insertion of an extra layer (interstitial condensation) would lead to an extrinsic fault.

Guided by these rules (where applicable), the various types of FCC and HCP faults can then be classified in a fairly orderly manner as seen in Table 1, using the del (Δ) notation of Frank[3] and Frank and Nicholas[4]. Thus the regular FCC sequence is $A_\Delta B_\Delta C_\Delta A_\Delta B_\Delta C_\Delta A$ and the regular HCP sequence is $A_\Delta B_\nabla A_\Delta B_\nabla A$. Where the operators Δ and ∇ respectively indicate shears of (A→B, B→C, C→A) and B→A, C→B, A→C), i.e. the former represents an ABC-type sequence, while the latter represents a CBA-type sequence. The faults in this table are the common ones and more complex stacking sequences are best regarded as clusters of simple faults. It is also evident that, while the FCC faults can be easily seen to conform to the classifications, the HCP faults are often rather difficult to visualize since the rules were originally derived for the FCC lattice.

TABLE 1

COMMON FAULTS IN FCC AND HCP LATTICES

FCC

1) $A_\Delta B_\Delta C_\Delta A_\Delta B_\Delta C_\Delta A$ - a 1∇, intrinsic, deformation fault corresponding

→ $A_\Delta B_\Delta C_\Delta A_\nabla C_\Delta A_\Delta B$ to either removal of a layer of atoms or single shearing of an atomic layer, i.e. B→C, C→A, A→B, etc.

2) $A_\Delta B_\Delta C_\Delta A_\Delta B_\Delta C_\Delta A$ - a 2∇, extrinsic, double deformation fault corres-

→ $A_\Delta B_\Delta C_\Delta A_\nabla C_\nabla B_\Delta C$ ponding to either insertion of a layer of atoms or a double shear, i.e. B→C, C→A→B, A→B→C, etc.

3) $A_\Delta B_\Delta C_\Delta A_\Delta B_\Delta C_\Delta A$ - a growth or twin fault, corresponding to a successive

→ $A_\Delta B_\Delta C_\Delta A_\nabla C_\nabla B_\nabla A$ shearing of layers, i.e. B→C, C→A→B, A→B→C→A, etc.

HCP

1) $A_\Delta B_\nabla A_\Delta B_\nabla A_\Delta B$ - a 1∇ growth fault

→ $A_\Delta B_\nabla A_\nabla C_\Delta A_\nabla C$

2) $A_\Delta B_\nabla A_\Delta B_\nabla A_\Delta B$ - a 2∇, intrinsic, deformation fault

→ $A_\Delta B_\nabla A_\nabla C_\nabla B_\Delta C$

3) $A_\Delta B_\nabla A_\Delta B_\nabla A_\Delta B_\nabla A$ - a 3∇ extrinsic fault

→ $A_\Delta B_\nabla A_\nabla C_\nabla B_\nabla A_\Delta B$

There are various types of faulted defects that can occur in metals. The splitting of perfect dislocations into partials can lead to bands of stacking faults and, if these interact, intrinsic-extrinsic fault pairs, extended dislocation nodes, faulted jogs or faulted dipoles can result. Point defects can coalesce into discs, forming faulted loops, or, in certain cases, faulted tetrahedra may form. All of these may be recognized as faulted defects, using transmission electron microscopy, by a characteristic fringe contrast of alternating dark and light bands, arising from the sinusoidal variation in transmitted electron beam intensity with crystal depth[5,6]. In addition, a great deal of work has been done in analyzing slight differences in the visual appearance of these fringes in order to partially classify the defects as per Table 1, or to distinguish them from other fringe-producing defects such as grain boundaries, twin boundaries and microtwins.[7,8,9,10,11]

The detailed formation of the more common of these defects will be discussed later, but first we shall consider their influence on the mechanical properties of a metal.

1.2 STACKING FAULTS AND MECHANICAL PROPERTIES

Any attempt to review the effects of a given defect upon the properties of a metal must of necessity be somewhat simplified, unless these effects are the prime topic of discussion. Hence, in this work, the relations between stacking faults and mechanical properties will be dealt with in a short, descriptive manner. To do otherwise would result in so great an amount of theory, observations and explanations that the principle objectives of the work would become blurred.

1.2.1 CLIMB AND CROSS SLIP

In the previous section, the fundamental aspect of faulting, i.e. extended dislocations, was established. This has a marked effect on dislocation movement, notably climb and cross-slip.

Many models have been postulated to describe the process of cross-slip, whereby a dislocation moves from its glide plane on to a plane intersecting the glide plane, in order to bypass some obstacle blocking its movement. Most of these, including the most common one of Seeger and Schock[12] require the contraction of a certain length of an extended dislocation under the pile-up stress caused by the dislocations lying against the obstacle, into a perfect dislocation, before cross-slip can occur. Thus the lower the SFE, i.e. the greater the partials extension, the lesser will be the ease of cross-slip.

The process of climb of a perfect dislocation may be regarded as the condensation of point defects, usually vacancies, on to the extra half plane of the dislocation, resulting in its shrinkage. For an extended dislocation, as the partials climb, the fault between them must also climb by means of a continuous shearing action, as proposed by Barnes[13] and others. A process of both vacancy condensation and shear or even vacancy condensation after constriction would intuitively appear more difficult than one of simple condensation, hence climb should be more difficult, the lower the SFE.

1.2.2 WORK HARDENING

Work hardening, or the increase in resolved shear stress with increasing resolved shear strain, has been separated, for FCC metals, into three main stages, each involving changes in the type of dislocation movement,

as originally suggested by Seeger et al[14]. Unfortunately, the work hardening of HCP metals is more complex due to the lattice geometry and variations in the primary slip system amongst the HCP metals, and has not been studied as extensively. Nonetheless, for some HCP metals, many of the same principles are basically applicable.

Stage 1 or the easy glide region of work hardening (see Fig. 2) in FCC single crystals is thought to mainly involve dislocation movement on the primary slip plane. As these dislocations encounter obstacles and new sources are exhausted, dislocations begin moving on secondary slip planes. Because movement on these planes is more difficult a higher hardening rate develops, called Stage 2 or the linear hardening region. As these secondary dislocations encounter pile-ups, tangles or Lomer-Cottrell locks, a stress builds up which can be relieved by cross-slip around the obstacle. Thus the hardening rate falls off, leading to Stage 3 or the parabolic hardening region. Obviously then, the SFE will have a marked effect on the onset of parabolic hardening, as schematically shown in Fig. 2, due to its influence on the ease of cross-slip. The ease of cross-slip from basal to prism planes in HCP metals will be similairly affected. This effect forms the basis for the indirect, deformation methods of SFE determination, as shall be seen later.

1.2.3 RECOVERY

The process of recovery in metals, in which the stored energy of a deformed metal is lowered through elimination of dislocation tangles, pile-ups, etc., leads to restoration of properties that have been reduced by severe cold-working, e.g. ductility, formability or conductivity. Since this process can involve both climb and cross-slip of dislocations, a low SFE could then greatly hinder the rate at which recovery occurs.

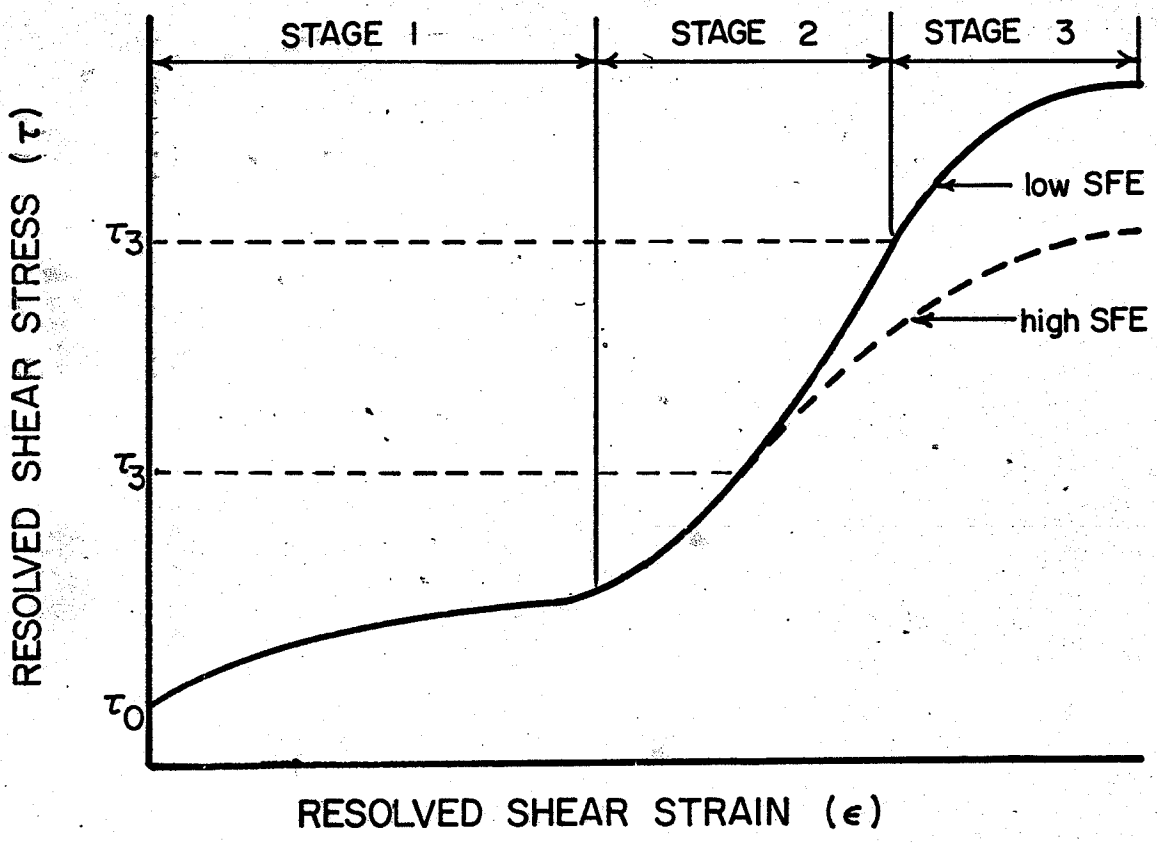

Fig.2 Typical stress-strain curve for an FCC single crystal

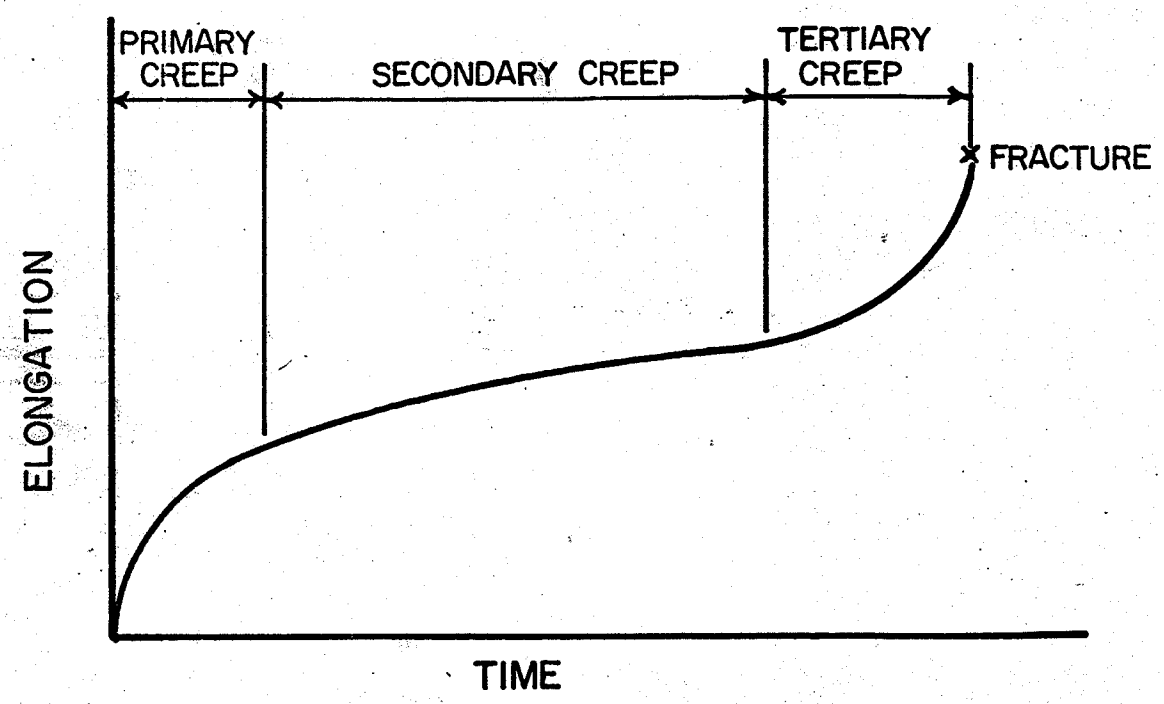

Fig.3 The three stages of recovery creep

1.2.4 CREEP

The time-dependant elongation of a metal under a stress greater than its yield stress but less than its fracture stress is known as creep. The most common type of creep, recovery creep, can be separated into three main stages, as shown in Fig. 3. The onset of accelerated, or tertiary creep, leading to fracture, is determined by the length of the secondary or recovery stage, in which a balance exists between recovery and strain hardening. The recovery in this region has been proposed as resulting from both cross-slip[15] and a combination of climb and cross-slip[16] of dislocations. Thus, as above, the SFE will have some influence on the rate of recovery and, along with other factors, thus influence the creep life of a metal.

1.2.5 PRECIPITATION AND PHASE TRANSFORMATION

With the advent of more complex alloys in recent years to meet new technological demands, the effect on mechanical properties of precipitate particles in association with stacking faults has aroused a good deal of interest. Apart from their influence on work hardening, the faults, along with undissociated dislocations, strengthen because they are constrained by the precipitates.

Two notable examples of this arose from the work of Hirsch and Kelly[17] and Honeycombe et al[18]. Simply treated, Hirsch and Kelly reasoned that if coherent precipitates of a lower SFE than the matrix existed in an alloy, extended dislocations, in passing into these regions, would dissociate further, as shown in Fig. 4. Therefore to pull these dislocations away from the particles, some extra work, i.e. an increase in strength, would have to be supplied to constrict them to their original

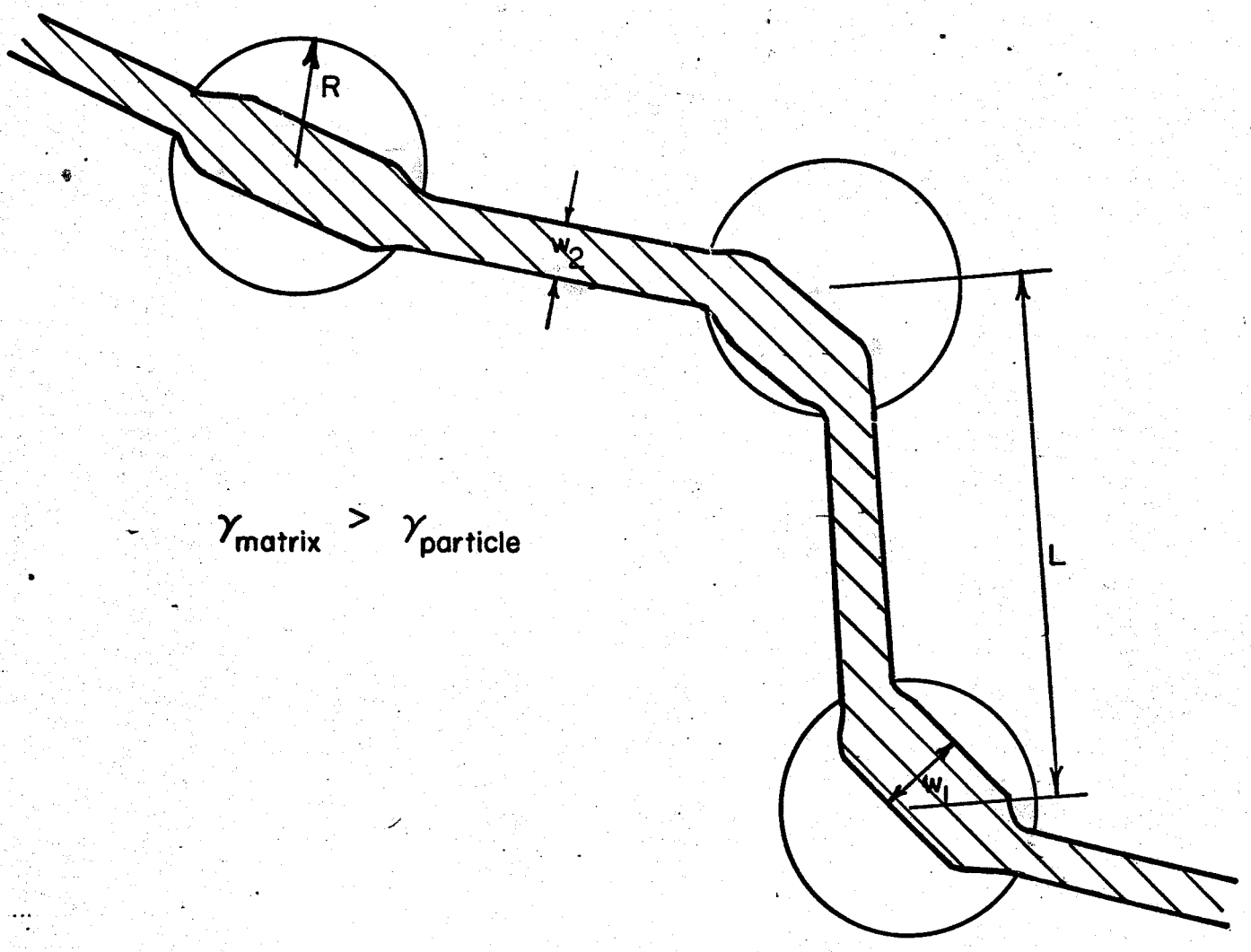

Fig.4 Schematic diagram of an extended dislocation held at precipitate particles (after Hirsch and Kelly, ref.17)

width. The same reasoning would apply if the matrix was of lower SFE except now the dislocations would be repelled by the particles and an extra force would be necessary to move them past the particles. Expressions can be developed for this strengthening effect as a function of the parameters shown in Fig. 4, with varying amounts of strengthening between the two extremes of $R >> w_2$ and $R << w_2$. The important conclusion is that the strengthening is directly proportional to the SFE difference between matrix and precipitate and yield stress values from this theory agreed quite well with experimental results for Al-Ag and Al-Zn, and to some extent for Cu-Co[17].

A somewhat different process was observed by Honeycombe et al[18], where, for NbC and TiC precipitation on both faults and dislocations in austenitic steels, the optimum yield and ultimate strengths were obtained from an ageing process that resulted in extensive faulting with widespread precipitation on the faults. Silcock and Tunstall[19] postulated a mechanism for this which involved climb of Frank partials (from splitting of sessile dislocations[20]) around the particles to relieve the misfit strain from the larger Nb or Ti atoms. Once these particles are imbedded, a strengthening of the Hirsch-Kelly type might result while the particle remains coherent, with a change to another mechanism when they become incoherent. Along with several other factors the authors concluded that a low SFE matrix was necessary for this mechanism. Further study has confirmed this type of mechanism[21,22] and, in one study of Fe-Mn austenites[23], a direct correlation between faulted area and hardness was also established.

From the nature of the stacking sequences of various faults in FCC and HCP metals, it can be deduced that a certain regular distribution of faults in one structure is equivalent to the other structure. For example, a growth fault on every second plane of the FCC lattice is equivalent to the HCP lattice. In other words, if solute addition to an FCC metal lowers the SFE, the faulting density may increase to a point where the structure becomes HCP, i.e. a phase transformation has taken place. This type of transformation is thought to be the correct one for several systems, such as Ag-Al[24] and Cu-Ge[25]. A slightly different mechanism has been proposed[26] for the nucleation of martensitic phases in austenitic stainless steels involving Shockley partial movement on alternating close-packed planes, but the important point is that heavy faulting is a prerequisite.

The above sections list but a few examples of properties affected by the SFE since this energy will affect, to some extent, any property dependent upon dislocation movement and/or configuration. The important point to remember is that, in all of the examples given, the SFE is only one of several parameters which may affect a given property. For example, work hardening is generally considered[27] to be influenced by metal purity, orientation, deformation temperature, crystal size and surface condition as well as SFE. Thus a true picture of the quantitative effects of stacking faults must usually be a rather complex one which attempts to account for every other variable.

Having thus established the marked influence of the SFE on many important properties, the next logical step would be to estimate the magnitude of this energy for as many metals as possible, as accurately as possible.

2 STACKING FAULT ENERGY DETERMINATION

2.1 DIRECT METHODS

2.1.1 NODE METHOD

This method was the first of the direct methods, suggested by Whelan in 1959[28] for extended nodes in stainless steel. Nodes can be formed by the interaction of extended dislocations and can result from interactions on the same plane, as in Fig. 5, or, by means of cross-slip, from interactions on intersecting planes, as in Fig. 6. The nodes normally tend toward a screw character ($\alpha = 0$ in Fig. 7), since screw nodes have a slightly lower energy (and are therefore slightly larger) as determined by Brown[29].

Whelan's simplified analysis assumed elastic isotropy and took no account of the interaction energy of nearby partial dislocations, and of the variation of line tension along the curved dislocation. He calculated the force balance between points A,B and C, Fig. 5c, as one between the line tension, T, of the partials and the surface energy of the fault, γ, as

$$\gamma = T/R \quad \ldots\ldots\ldots\ldots\ldots\ldots\ldots\ldots \quad (2.1)$$

where $T \simeq Gb^2/2$

R = node radius of curvature

G = shear modulus

b = Burgers vector of the partial dislocation

Unfortunately such modifying factors as repulsion of partials, solute impedance effects, image forces near free surfaces, interactions with nearby dislocations and node character were not accounted for.

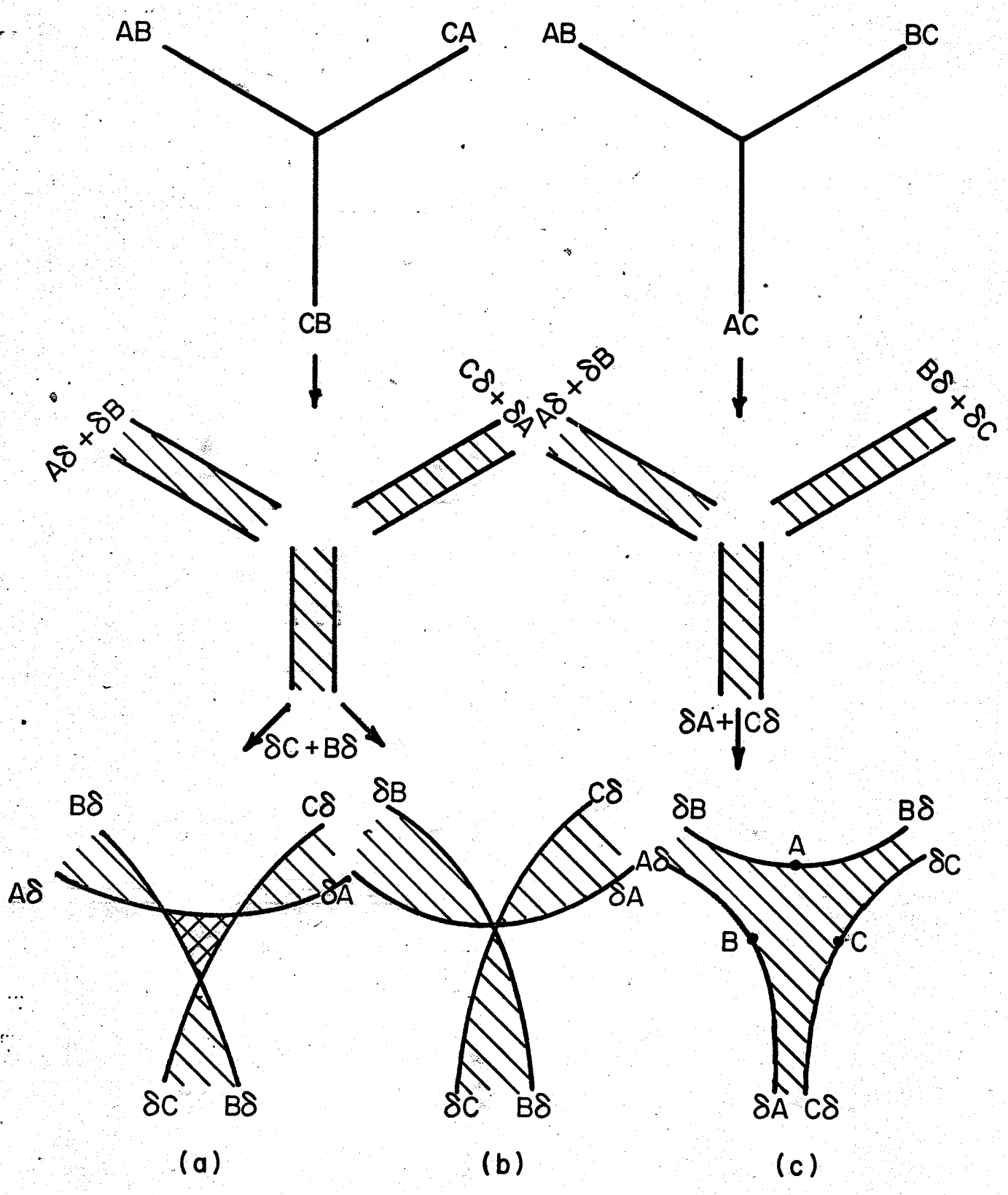

Fig.5 Extended dislocations on the same plane interacting to form

a) an extrinsic extended node

b) an intrinsic contracted node

c) an intrinsic extended node

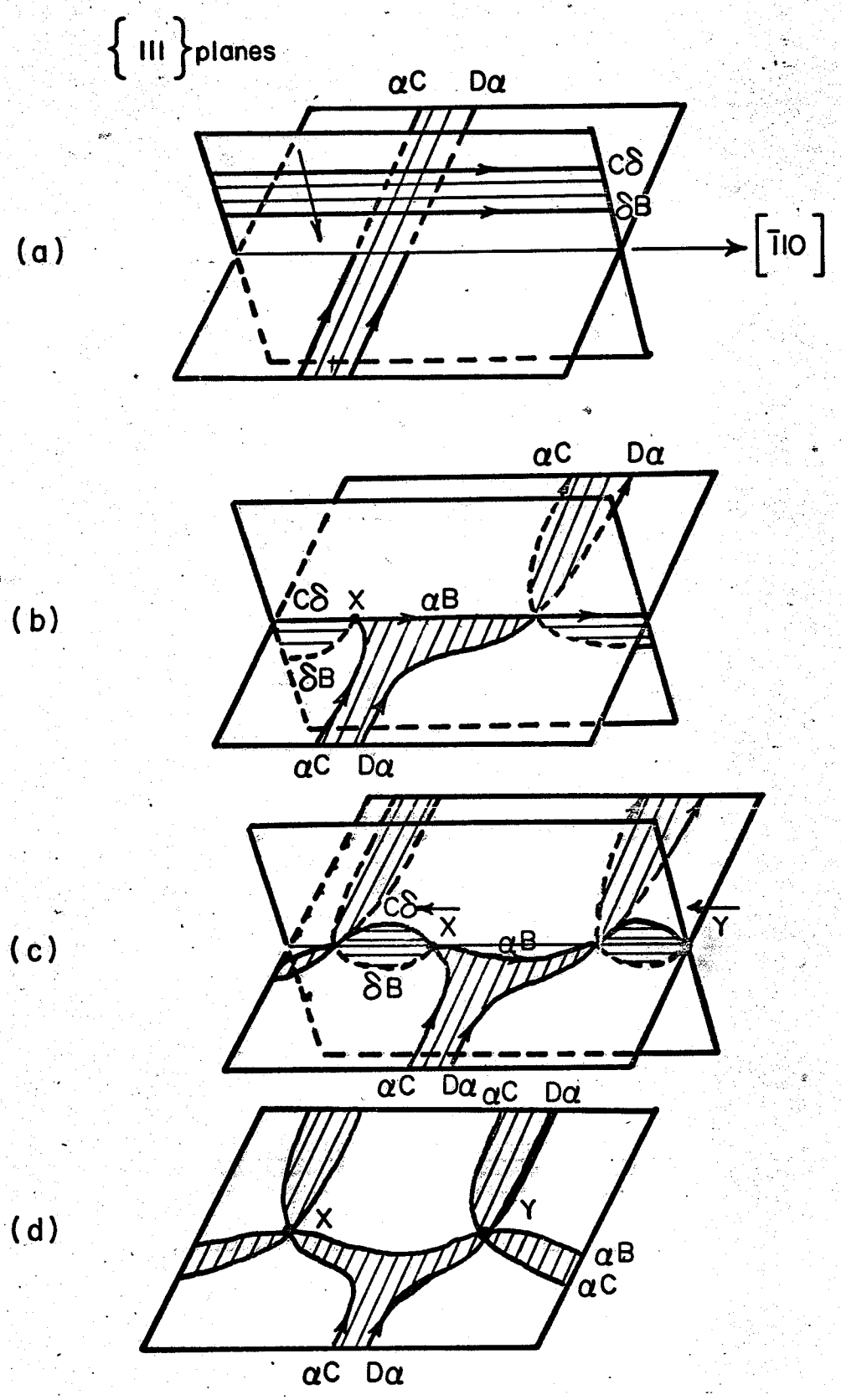

Fig.6 Interaction of extended dislocations on intersecting planes producing a nodal network on one plane (after Whelan, ref.28)

In several reappraisals of the theory these factors have gradually been taken into consideration. Siems et al[30] and Thornton et al[31] considered interaction of partials. Mader[32] investigated the effect of surrounding nodes and Brown[29] accounted for the node character effect on line tension. The most recent analyses, which give concurring values of SFE, are the numerical one of Brown and Tholen[34] and the analytical one of Siems[35]. Besides R, these also utilize the inscribed node radius, w, and the separation of the partials in the arms, d (see Fig. 7). Their equations, while appearing rather cumbersome, involve parameters that are generally easily obtained if the nodes are large and suitably symmetric. They are:

Brown and Tholen:

a) $$\gamma R/Gb^2 = 0.27 - 0.08(\nu/1-\nu)\cos 2\alpha + \{0.104(2-\nu/1-\nu) + 0.24(\nu/1-\nu)\cos 2\alpha\}\log R/\varepsilon \quad (2.2)$$

b) $$\gamma w/Gb^2 = 0.055(2-\nu/1-\nu) - 0.06(\nu/(1-\nu)^2)\cos 2\alpha + \{0.018(2-\nu/1-\nu) + 0.036(\nu/1-\nu)\cos 2\alpha\}\log R/\varepsilon \quad (2.3)$$

Siems:

a) $$R = \frac{Gb^2}{4\pi\gamma}\,\frac{w}{w-d/\sqrt{3}}\,\{1 + (\nu/1-\nu)(3\cos 2\alpha/2 + 1/2)\}\ln R/\varepsilon \quad (2.4)$$

b) $$R = \frac{w\sqrt{3}}{(\sqrt{3}w/d)-1}\,\{1 + 5\nu\cos 2\alpha/(2-\nu)\,(1 + 2\cos 2\alpha)\}\ln R/\varepsilon \quad (2.5)$$

where $$d = \frac{Gb^2(2-\nu)}{8\pi\gamma(1-\nu)}\,(1 - \frac{2\nu\cos 2\alpha}{2-\nu}) \quad (2.6)$$

ν = Poisson's Ratio

ε = cutoff or core radius of partial (usually taken as its Burgers vector)

Thus measuring errors are minimized by use of more than one parameter, although each has its own limitations. R is often difficult to fit to a node, especially asymmetric ones, although it is the largest parameter.

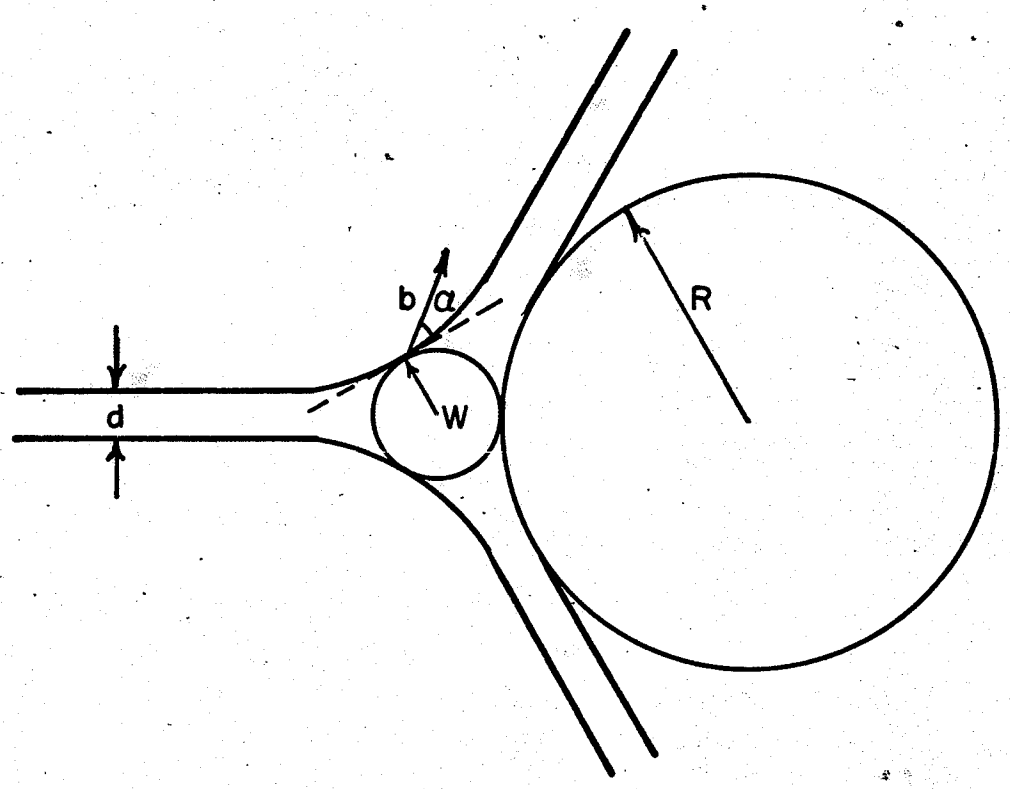

Fig.7 Extended node parameters (after Gallagher, ref.33)

The separation d is almost impossible to measure in most metals and alloys since its equilibrium value is usually of the same order as the partials image width. The inscribed radius w, while easiest to measure, is only valid down to a critical node size of roughly one-third the extinction distance (roughly 75 Å) due to anomolous contract effects which occur for smaller nodes[9]. G and ν can be modified if the material is highly anisotropic and, at present, the value of $\varepsilon \simeq b$ is only an order of magnitude estimate. The R and w values of nodes inclined to the electron beam should be multiplied by a geometric correction factor while those of a size approaching the foil thickness are not useable since the surface reduces the line tension, anomolously increasing the curvature[36a], i.e. the nodes should be reasonably far from, and parallel to, the foil surface. Annealed nodes are desired in alloys since solute impedance effects may result in asymmetric configurations due to solute pinning of the partials. Even when symmetric, the node size could be larger in regions of slightly higher solute concentration (lower SFE), therefore a large number should usually be measured, especially in alloys. When these limitations are taken into consideration and corrected for, the values obtained by this technique are generally considered to be the most accurate of all the present techniques and are often used as a base reference with which to compare values from others. The major limitation of this method is the fact that it is limited to relatively low SFE materials, with the upper limit being around 30 ergs/cm^2.[37] Thus, while it is often used in studies on alloys, when alloying lowers the SFE, it cannot be used directly on most of the pure metals.

2.1.2 TETRAHEDRON METHOD

Silcox and Hirsch[38] first observed faulted, tetrahedral-shaped defects in quenched Au and explained their presence as due to a combination of vacancy condensation and dislocation glide as per Fig. 8, which is still one of the most widely accepted models for formation of quenched-in tetrahedra. Tetrahedra growth by direct vacancy condensation onto jogs on the tetrahedron itself has been proposed by de Jong and Koehler[39] and Kimura et al[40]. It has also been found[41,42,43] that these defects can be formed solely through deformation, by Frank loop formation from cross-slip of extended dislocations at superjogs and further dissociation from there into the tetrahedron. An example is given in Fig. 9.

Silcox and Hirsch[38] were the first to try and relate the edge length (l_o) of the maximum stable tetrahedra in quenched metals to the SFE by a somewhat simplified energy balance as;

$$\frac{l_o}{\ln(l_o/r_o)} = \frac{2Ga^2}{9\sqrt{3}\pi(1-\nu)\gamma} \qquad \ldots\ldots\ldots\ldots\ldots\ldots\ldots\ldots (2.7)$$

where r_o = core radius

a = lattice constant

This relation did not take into account dislocation interaction energies or the dissociation of the Frank loop. First Czjzek et al[44] and then Jossang and Hirth[45] attacked the problem much more comprehensively through development of a general energy expression for the configuration of partials and faulted area as a function of the height of the truncated tetrahedron, i.e. a more general case where the tetrahedron may not be fully formed. In plotting this expression vs. a parameter involving the

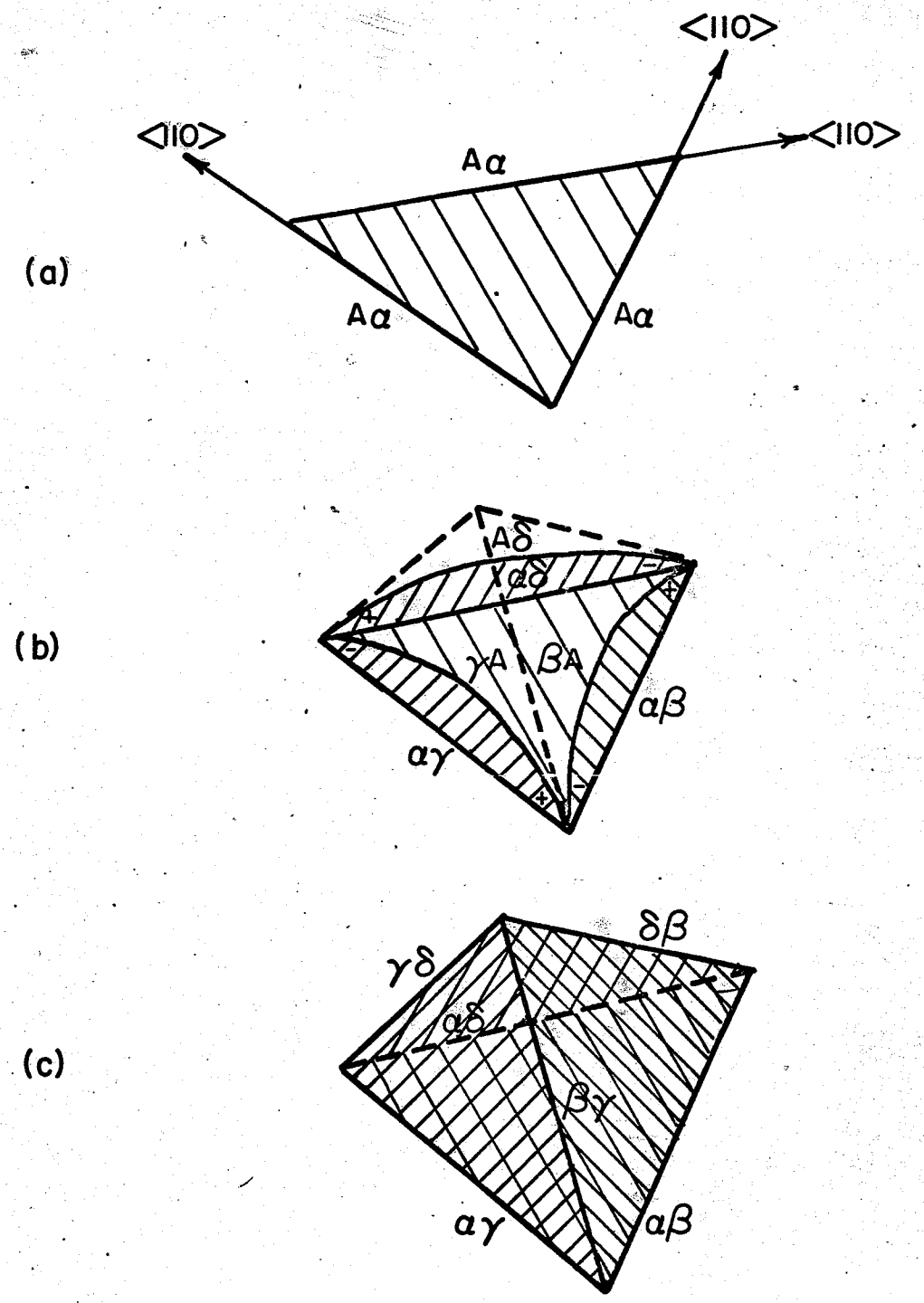

Fig.8 Formation of quenched stacking fault tetrahedra

a) vacancies collapse on a {111} plane, forming a loop bounded by Frank sessile dislocations

b) the Franks dissociate into stair-rod and Shockley dislocations, the Shockleys spread out on other {111} planes

c) the Shockleys combine to form three more stair-rods

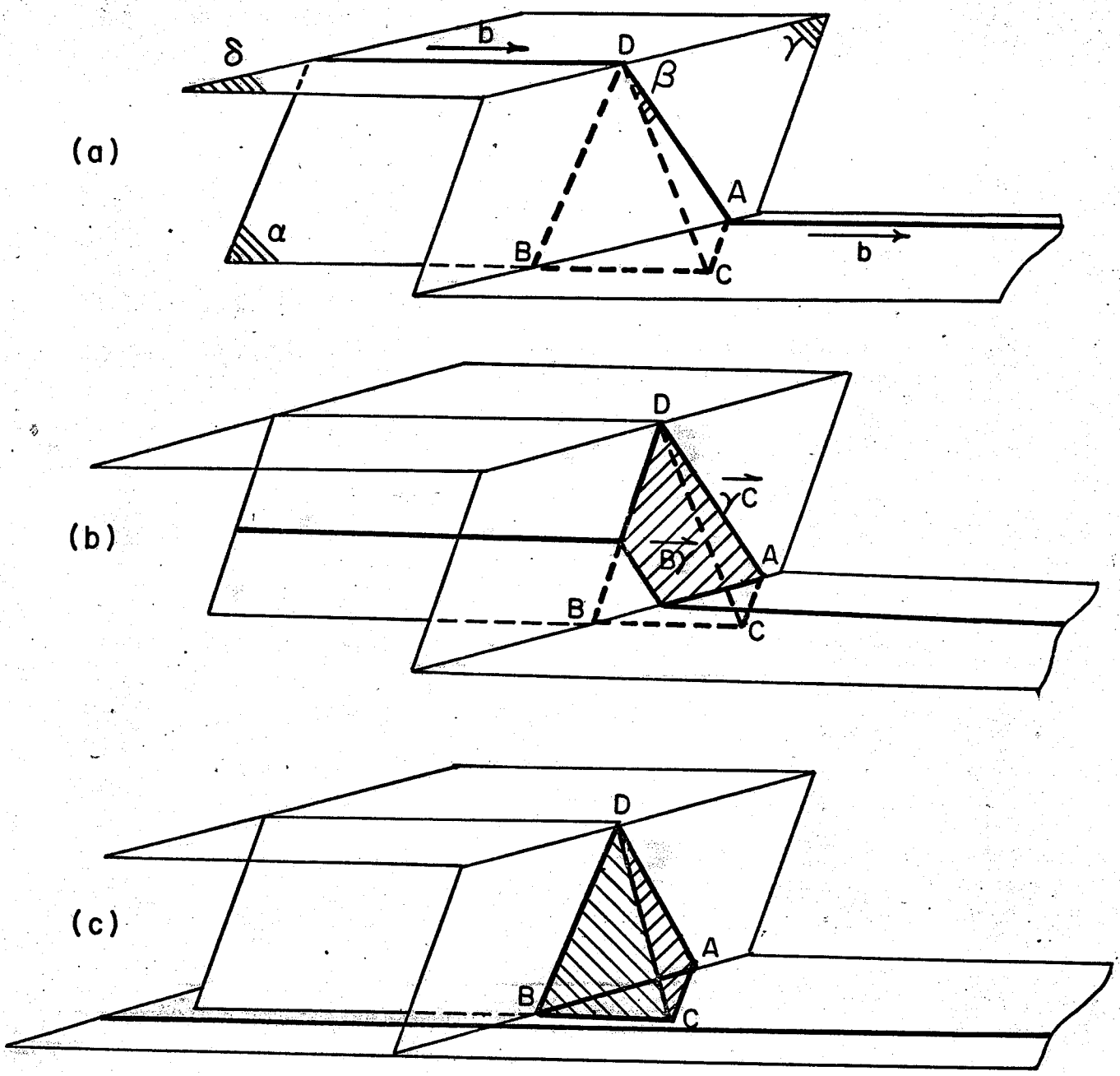

Fig.9 Deformation tetrahedron formation (after Loretto et al, ref.44)

a) screw dislocation with edge superjog AD (Burgers vector BC)

b) AD dissociates as: $\vec{BC} \rightarrow \vec{B\gamma} + \vec{\gamma C}$ (Shockley plus Frank) as screw cross-slips on α plane and glides on δ plane. New jogs DB and AB also dissociate as AD, with Shockleys annihilating, leaving complete Frank loop

c) Loop dissociates to tetrahedron as per fig.8

height for various l_o's, it was found that, below a certain critical size of l_o, the tetrahedral defect was stable, and, above a much larger value of l_o, only the Frank triangle was stable. In between there was a range where both tetrahedra and loops could be stable.

It is of interest to note that for Au the size for Frank triangle stability was found to be very large ($\simeq$ 5800 Å) which would explain why tetrahedra are in the vast majority in this low SFE metal. Quite probably then, this critical size is much reduced for a high SFE metal such as Al so that only loops are stable, as found experimentally. Thus the mixture of loops and tetrahedra observed in Ni[46] might indicate that it's SFE is at least close to, if not lower than, that of Al, in contradiction to most other estimates.

At any rate, the value of the SFE is then found by an iterative process in which plots of the energy of the configuration vs. a function of the height are drawn for different γ values until one value gives a plot with a horizontal inflection point (denoting the loop-tetrahedron transition) at l_o = maximum edge length observed in the metal.

Humble et al[47] refined Jossang and Hirth's energy expression by more accurately taking into account the curvature of the Shockley partials and, most important, accounting for any energy that might have to be overcome for the loop-tetrahedron transformation, i.e. an activation energy. This would not influence quenched tetrahedra due to the absence of any applied stress, but could definitely affect deformation tetrahedra where the applied stress might be enough to push the loop over this barrier before the equilibrium transformation is reached, resulting in an overlap between the size of the largest tetrahedron and the smallest loop. Thus

a mean value of these should be used, resulting in slightly lower values than Jossang and Hirth's, but still compatible with node results. This point is especially important since it is now believed that, because quenched tetrahedra could conceivably grow due to a vacancy supersaturation, only deformation tetrahedra can give accurate results for the SFE.

This method extends the range of SFE measurement up to roughly 100 ergs/cm^2 and complements the node method, especially in enabling more accurate extrapolations to be made in plots of γ vs. alloying content (for example, Humble et al[46]). As with the node method, only tetrahedra away from the foil surfaces should be used and, of course, for high SFE metals where 1_o may be as small as 100 Å, extreme care must be taken in measurement. Since the largest edge length is of importance, a very thorough search of the thin foil is required. Finally, since the determination is an iterative process, the calculations become quite tedious and are best computerized.

2.1.3 OTHER DIRECT METHODS

Another direct method that has recently been extensively used is the loop annealing method which shall be discussed in detail later since it was chosen as the experimental method. The remaining direct methods have either not been given much credence, have only seen limited use or apply to materials of little interest here. Therefore they shall be described and commented upon briefly.

2.1.3.1 RIBBON METHOD

This method utilizes the equilibrium spacing between the partials of a dissociated dislocation to determine the SFE as;

$$\gamma = \frac{Gb^2(2-\nu)}{8\pi d(1-\nu)} \left(1 - \frac{2\nu\cos 2\alpha}{2-\nu}\right) \quad \ldots\ldots\ldots\ldots\ldots\ldots \quad (2.8)$$

using Read's isotropic elasticity theory[48].

where d = partial's separation

α = angle between partials and total Burgers vector of extended dislocation

The major limitation of this method is that, for any amount of accuracy, d must be fairly large, implying a low SFE. If 300 Å is taken as a rough limit for accurate measurement, so that the actual separation is reasonably larger than the partials image width, the method then becomes limited to SFE's less than roughly 5 ergs/cm^2, thus eliminating practically all metals and their alloys. This method has been applied successfully to layer-type structures[49], i.e. structures such as graphite, talc, bismuth, etc. whose main glide planes are almost invariably parallel to their cleavage or growth planes, resulting in long dislocation ribbons of measurable spacing due to the low SFE's of these materials.

Great care has to be taken that the configurations are equilibrium ones, i.e. they have not been influenced by external stresses such as foil handling or beam heating. Faulted loops which grow sufficiently large to cut the foil surface may also appear to be widely extended dislocations. Surface image effects have to be especially watched for due to the structure of these materials and the large size of the ribbon configurations.

2.1.3.2 GRAIN BOUNDARY INTERSECTION METHOD

This method is based upon a comprehensive determination of the ratio of twin boundary free energy to grain boundary energy from the coherent twin boundary-grain boundary intersection configuration (Murr et al[50]). Only one investigation[51] has thus far been reported, which duplicates this work for SFE rather than twin boundary energy. Rather than requiring any equilibrium spacing measurement, this method hinges on two main assumptions; that the interfacial free energy of the high-angle grain boundary and the stacking fault is thermodynamically equivalent to the corresponding tensions, and that the balance of these tensions can be resolved in any direction in terms of the true dihedral angles, ϕ_j, between the intersecting interfaces. Resolving an intersection such as found by Peterson and Queeney[51] (see Fig. 10), parallel to the fault results in;

$$\gamma_{SF} = -\gamma_{GB} (\cos\phi_1 + \cos\phi_2) \quad \ldots\ldots\ldots\ldots\ldots\ldots\ldots (2.9)$$

where forces normal to the grain boundary are thought negligible since it remains straight on either side of the intersection. The true dihedral angles, ϕ_1 and ϕ_2, are determined as per Murr et al[50], from the plan view angles, ψ_1 and ψ_2, and the inclination angles to the foil surface, θ_1, θ_2 and θ_3 which are easily determined once the foil plane and fault plane are known. It does not matter if a single fault or a fault "bundle" is present since γ is a constant and extra faults should not affect the configuration. Although the grain boundary energy is an average value and thus is not the actual value for any given boundary, the deviation from this average value is only around ±6%[51]. The main

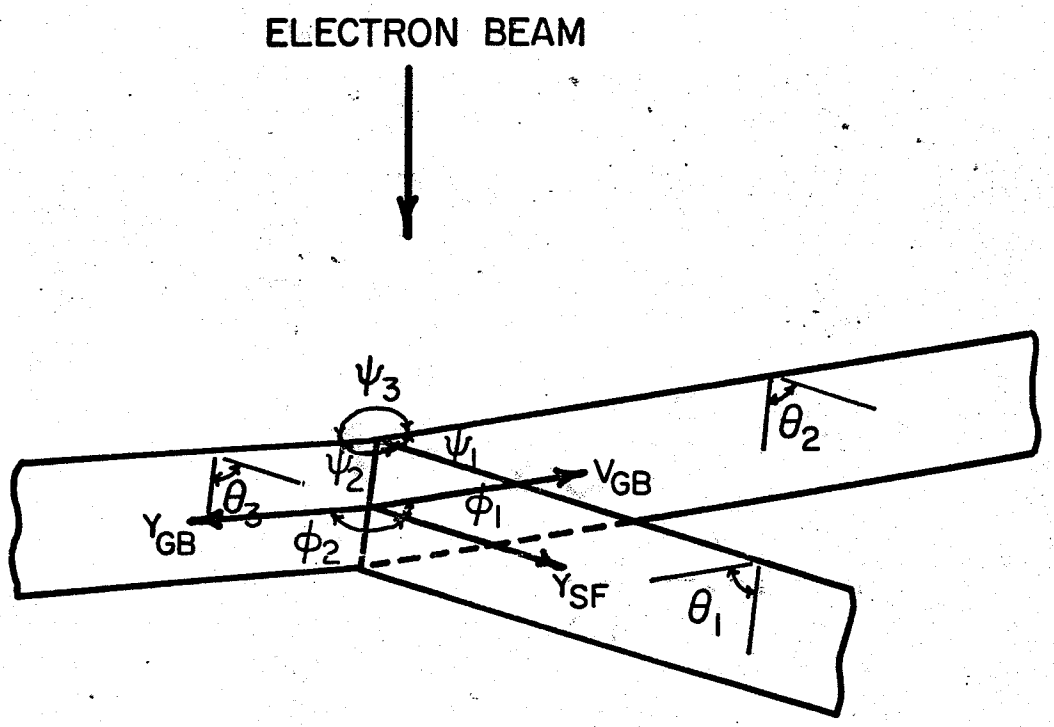

Fig.10 Stacking fault-grain boundary intersection (after Peterson and Queeney, ref.51)

difficulty in this technique would seem to be the scarcity of good, useable intersections, since Peterson and Queeney report only a single measurement in their work on Cu, a risky practice at best. Otherwise, the method appears to hold promise, especially for high SFE metals, since the fault does not have to be of equilibrium length.

2.1.3.3 INTRINSIC-EXTRINSIC FAULT PAIR METHOD

From various considerations, such as relative sizes in intrinsic-extrinsic node pairs[52], X-ray work[53], and the absence of extrinsic faulted tetrahedra[54], it was long held that the extrinsic SFE (γ_{ext}) was larger, in varying amounts, than the usual intrinsic SFE (γ_{int}). This was in disagreement with theoretical perturbation studies[55a] which showed that $\gamma_{int} \simeq \gamma_{ext}$. In support of this, Gallagher[56] and others[57,58] have recently experimentally confirmed this fact, explained the earlier incorrect conclusions to some extent, and in the process have evolved a simple, accurate method of SFE determination. In the definitive paper for this method, Gallagher[56] has explained several intrinsic-extrinsic configurations, the simplest and most useful of which is the one shown in Fig. 11, in which two extended dislocations have joined and interacted, with one "crossing-over" to form the band of extrinsic fault. Because of the fact that the three long partials are parallel and have the same Burgers vector, a relatively simple relationship may be derived from isotropic elasticity theory as;

$$\gamma_{int} = \frac{Gb^2}{2\pi} (1/d_i + 1/(d_i + d_e))(\cos^2\alpha + \sin^2\alpha/1-\nu) \quad \ldots\ldots\ldots \quad (2.10)$$

or $$\gamma_{ext} = \frac{Gb^2}{2\pi} (1/d_e + 1/(d_i + d_e))(\cos^2\alpha + \sin^2\alpha/1-\nu) \quad \ldots\ldots\ldots \quad (2.11)$$

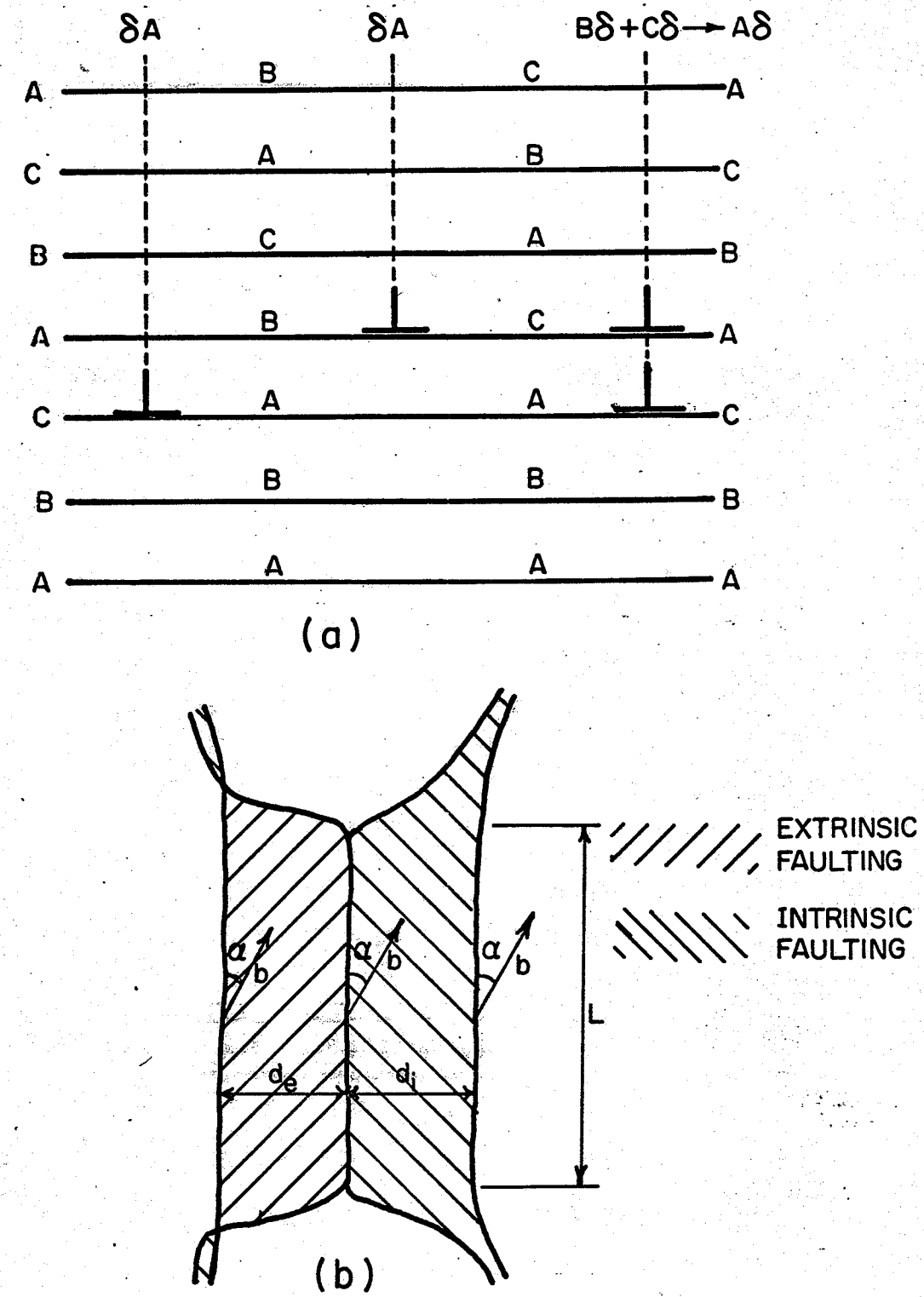

Fig.11 Intrinsic-extrinsic fault pair

a) side view

b) plan view

Care must be taken to measure the d's away from the cross-over points and to correct it for inclination to the foil surface. As with the other direct methods, the accuracy of measurement becomes less as d becomes smaller and the method is limited to SFE's less than about 20 ergs/cm^2. In addition this type of configuration is relatively rare, having been observed thus far only in noble metal alloys. The absence of this defect is thought to be due to some type of formation barrier caused by the strong elastic forces at the cross-over points[59] but not by the greater magnitude of the extrinsic SFE, as previously assumed. One interesting possibility raised by Gallagher[59] is that of annealing multi-layer vacancy loops in quenched high SFE metals, such as Al and Mg, where some intrinsic loops have been found with regions of extrinsic faulting inside them. Unfortunately the only study thus far, on an Al-Mg alloy[60], shows $\gamma_{ext} \simeq 1.4\gamma_{int}$ and it is difficult to say just where the discrepancy might lie.

2.1.3.4 FAULTED DIPOLE METHOD

The dipole method is essentially based upon a transition between the unfaulted and faulted condition of a dipole at some critical separation of the slip planes of the top and bottom dislocations of the dipole, i.e. at separations less than this, the total energy is lowered by dissociation of the dipole dislocations. As first formulated by Steeds[61] in a comprehensive study, this separation can be related to the dipole width in the plane of the foil as a fraction of the extinction distance (ξ_g). Various configurations of dislocations resulting in either S or Z-shaped faulted dipoles (S-shaped involving both intrinsic and extrinsic faults, Z-shaped being similar faults) were determined

and transition curves drawn for each. It was concluded that Z-type dipoles were the most suitable because of the uncertainty of whether intrinsic SFE was equal to extrinsic SFE. In addition the image contrast for different operating reflections was determined, with $\bar{1}\bar{1}1$ being the most suitable. A typical determination on Cu-2at%Al[62] is based on Steed's formula;

$$\gamma = 1.28bP_1/(W_{max} - 0.14) \quad \text{for } \Delta<0.4\xi_g \quad . \quad . \quad . \quad . \quad . \quad . \quad . \quad . \quad . \quad . \quad . \quad . \quad (2.12)$$

where Δ = separation of Shockley partials in the direction of the incident beam

W_{max} = maximum dipole width (along plane of dipole)

P_1 = a material constant

W_{max} is usually determined by microdensometer traces and P_1 is a function of the elastic constants of the material. There are two other possible relations between γ and W_{max}, for $0.8\xi_g > \Delta > 0.4\xi_g$ and for $\Delta \simeq \xi_g$, but in any determination the governing relation is usually easily found. This method extends the range of measurement into approximately the same range as the tetrahedron method. It is not applicable for low SFE's[61] since the favored mechanisms for dipole formation (mutual trapping or superjogs on screw dislocations) become less and less feasible the lower the SFE. Though most of the calculations come from isotropic elasticity theory, anisotropy can be easily taken into account. Some of the other disadvantages are[61];

a) Contrast calculations break down for small dipoles (possibly similar to the aforementioned difficulty with small nodes[9]).

b) The small values of W_{max} used (as low as 100 Å) cast some doubt on the use of linear elasticity theory.

c) Uncertainties in the extinction distance.

d) The usual uncertainty in the values for cut-off radii in the dislocation cores.

In addition the determination of the constant P_1 seems a bit vague, as are some of the quantitative assumptions made during the calculations. The harshest criticism for this method is probably the wide variation in results from different workers as shall be seen later.

2.2 INDIRECT METHODS

2.2.1 X-RAY METHOD

Since stacking faults were first detected by their effects on X-ray diffraction patterns[63], an enormous amount of data and theory has been generated on the effect of faulting on the X-ray intensity profile, with the three early definitive works being those of Wilson[64], Warren and Warekois[65] and Paterson[66]. Their work essentially developed diffracted intensity expressions in which faulting affected the intensity profiles in four main ways; symmetrical or asymmetrical peak broadening and/or peak shifts with either type of broadening. Various systems have been derived to separate out the different types of faulting in FCC and HCP metals[36b], but the end product of these calculations, the deformation stacking fault probability (α), is of interest here. This parameter may be defined as either the product of the dislocation density, dislocation width and close-packed plane spacing or as the probability of a fault forming on a particular plane, given faulting on only one set of planes. As can be intuitively seen, this probability (as well as the growth fault probability, β) should vary in some inverse fashion with SFE, but in just what exact manner has been very difficult to determine. A few attempts have been made[67,68,70] to relate α to γ in an accurate enough manner to obtain reasonable values of SFE, but little success has been

achieved. A more recent effort by Gallagher and Liu[69] has shown some promise, but only for certain systems. In plotting γ/γ_o and $\alpha^{-1}/\alpha_o^{-1}$ vs. e/a ratio (where γ_o and α_o apply to the solvent metal), it was found for the Ag-Sn and Ag-In systems (but not for the Ag-Zn) that the respective curves could, to a certain extent, be approximated by an equation of the form $\gamma/\gamma_o = f(x)\alpha^{-1}/\alpha_o^{-1}$, where x is the atomic % solute. One equation proposed for this[68] is;

$$\alpha = k'N/\gamma \quad \ldots\ldots\ldots\ldots\ldots\ldots\ldots\ldots\ldots\ldots \quad (2.13)$$

where k' = a constant that can be calculated

N = dislocation density.

Using a relation between N and x for the Ag-Zn system, and using faulting probability data, a plot of SFE vs. x gave a line of similair slope to a plot from node data but displaced about 2.6 times lower. This was thought to be due primarily to fundamental theoretical differences between the above type of equation, (2.13), (based on equilibrium partials separation), and X-ray theory (faults extending completely across the crystal). If these theoretical difficulties could be resolved, this method would be very attractive since α can be calculated for even the highest SFE metals. It should be remembered, however, that the higher the SFE, the harder it will be to detect the peak broadenings and shifts upon which α and β are based and the larger the error range will be.

2.2.2 DEFORMATION METHODS

Deformation techniques generally involve a SFE estimation from the plastic behaviour of a metal and are perhaps the most used indirect methods. As comprehensively summarized recently by Ahlers[71], there are three major types of deformation techniques. The first is from the

temperature and strain rate dependence of the critical resolved shear stress (CRSS) of FCC metals, which usually corresponds to the CRSS for basal glide in HCP metals. Based on a forest-intersection type rate controlling mechanism, estimation of the SFE should be possible[72]. However, more recent studies have also indicated the possibility of either Peierl's friction or dislocation-impurity interactions being rate controlling mechanisms. Also, other studies have shown substantial disagreement between the forest dislocation densities predicted from the above theory and those determined using electron microscopy[71]. Thus it is generally considered invalid to obtain SFE values in this manner.

The major technique is undoubtedly the τ_3 method, which utilizes the temperature and strain rate dependence of the cross-slip stress (τ_3) in FCC single crystals. As developed mainly be Seeger and co-workers[73,74] this method essentially relates the cross-slip rate (some fraction of the total strain rate) to an activation energy for cross-slip, through an Arrhenius-type equation,

$$\dot{a}_c = \dot{a}_c(o)\ (U\tau_3/kT) \quad \ldots\ldots\ldots\ldots\ldots\ldots\ldots\ldots \quad (2.14)$$

where $\dot{a}_c$ = cross-slip rate

$\dot{a}_c(o)$ = proportionality factor

$U\tau_3$ = activation energy for cross-slip

This activation energy is in turn logarithmically related to the cross-slip stress as,

$$U\tau_3 = -A\ln\ (\tau_3/\tau_3[0]) \quad \ldots\ldots\ldots\ldots\ldots\ldots\ldots\ldots \quad (2.15)$$

where A = proportionality constant

Taking into consideration the temperature dependence of the shear modulus and Burgers vector, the two relations may be combined to give;

$$kT \ln \dot{a}/\dot{a}_o = A(0) \frac{G(T)b^3(T)}{G(0)b^3(0)} \ln \frac{\tau_3/G(T)}{\tau_3(0)/G(0)} \quad \ldots\ldots\ldots (2.16)$$

where $\dot{a}$ = strain rate

$\dot{a}$ = a proportionality factor

$A(0)$, $G(0)$, $b(0)$ and $\tau_3(0)$ are values at 0^oK.

By separate differentiations, the temperature and strain rate dependences can then be derived, which have been experimentally confirmed, but only at low temperatures. From these equations three parameters, $\dot{a}_o$, $A(0)$ and $\tau_e(0)$, may be determined. $\dot{a}_o$ is very dependent on the metal being tested while $\tau_3(0)$ is related to the SFE through an equation which is a very weak function of γ,

$$\tau_3(0) = \frac{2G(0)}{n} (0.056 - \gamma/Gb) \quad \ldots\ldots\ldots\ldots\ldots\ldots (2.17)$$

where n = number of pile-up dislocations in front of the obstacle.

However $A(0)$ has been related to SFE by Wolf[75], for $Gb/^3A > 4$, through the following relationship:

$$(1 + n/900)(1 + 180\gamma Gb) = 0.352Gb^3/A \quad \ldots\ldots\ldots\ldots (2.18)$$

Although a great deal of work has resulted from this theory, especially since it allows a very wide range of SFE measurement, difficulties and criticisms abound. To begin with, a reasonably long, straight stage 2 of hardening is necessary for a reasonable determination of the τ_3 cross-slip stress, and, with increasingly more accurate studies, it is now thought that this may be one of the hardest parts of the technique. Also, the necessity of using single crystal can often be more than a little difficult and time-consuming. Impurities (or a solute for that matter)

can also have a substantial effect on cross-slip. This effect has been used by Gallagher and Liu[69] to explain the anomolous behaviour of SFE with alloying content arising from the work of Peissker[76] using the τ_3 method. This behaviour, a rise in SFE with alloy content, then a fall, rather than a steady decrease has, incidentally , not been found by any other method (especially node and x-ray results), to the best of the author's knowledge. As shall be seen shortly, the scatter in the results is severe and this method's authenticity has been increasingly criticized of late, e.g. Gallagher[77] or Kuhlmann-Wilsdorf[78]. The latter's criticisms contain the facts that cross-slip has been observed in Au foils at stresses much below those predicted by theory, tying in with the above difficulty of choosing τ_3, and that screw dislocations have been seen to be conspicuously absent in low SFE specimens deformed into Stage 2, probably indicating cross-slip out of the foil prior to Stage 3. She also mentions the fact that long pile-ups of dislocations, essential to the theory, have never been observed in Stage 2. Finally, there generally always exists a large difference between τ_3 values and any others, with the τ_3 values being the higher ones. There still may be something to be said for this method as a means of relative SFE determination for pure, high SFE metals, especially in view of the fact that much of the necessary data is generated in normal deformation studies.

Unfortunately this theory has proved almost impossible to correlate with SFE for HCP metals, mostly due to wide variations in their work hardening curves. Some attempts have been made on Mg[79], Cd[80] and Zn[81], but the results have been given little credence in Ahler's review[71].

The only partial estimation of SFE for HCP metals has arisen through the temperature and strain-rate dependence of the CRSS for prismatic slip (τ_o). This dependence could be due to either cross-slip of dislocations split on the basal plane, or to the initial forest cutting of dislocations on the prism plane. Whatever the model, the SFE will play an important role, and, as in the τ_3 method, the strain rate (or cross-slip rate) can be related to the thermal component of τ_o (τ_o^*). Since τ_o^* is determined by the value of the athermal (temperature independent) component, this value can be critical, unless, as Ahler's suggests, the inverse of the activation volume (v) is plotted against τ_o since τ_o/A (= 1/v) is independent of the athermal component. Therefore a plot of the inverse of the activation volumes (determined from strain rate changes) vs. the CRSS for prismatic slip, at various temperatures, should be linear and of slope 1/A. Unfortunately this is as far as the analysis has developed and a relation between A and γ (eq'n. 2.18), such as in FCC metals, has not been developed. All that can be said is that some type of inverse relationship exists between the two parameters. For example, studies have shown that Gb^3/A for Ti,Zr and some Mg-Li alloys are roughly the same[71], indicating similar SFE's, and should be higher than Gb^3/A for Cd and Co, which are generally conceded to have fairly low SFE's. As with the τ_3 data, there appears to be a good deal of scatter in the experimental results and very few studies, making any conclusions drawn somewhat unreliable.

In addition to these major methods there exist several minor methods worth mentioning. One very early method was a calculation of the fault width from low temperature creep data by Thornton and Hirsch[82],

which provided rough estimates of the SFE of several important metals at that time. However, besides the above difficulties with the strain rate and temperature sensitivity, their model required knowledge of the glide and forest dislocation spacing, unless some assumptions were made as to their relative sizes. Then too, the calculated width had to be related to the SFE (as in the Ribbon Method). Thus it has not been often used, although there is a recent estimate for Zr SFE[83] by this method.

Cousland[84] has recently established a tentative relationship between the SFE and the Cottrell-Stokes Ratio of several FCC metals. Such a correlation seems reasonable since this ratio involves the temperature dependence of the thermal component of the flow stress which depends on short range interactions which, in turn, are dependent to some degree on the SFE. Further correlation and verification could possibly enable this relationship to be used as a means of SFE determination.

Another interesting possibility, as suggested by Tangri[85] is a correlation of the SFE with the required temperature change to produce equal amounts of work softening as found by Cottrell and Stokes[86], since this yield drop upon restraining at higher temperatures is thought to be due to thermally-activated cross-slip. Both of these last two methods would, of course, require accurate knowledge of the SFE of some reference metals.

Finally, it is known that the SFE is related to the stress necessary to produce large, non-equilibrium faults in metals, denoted by the critical tear stress, as described by Saarinen and Miekk-Oja[87];

$$n\tau = \gamma/b \quad \ldots\ldots\ldots\ldots\ldots\ldots\ldots\ldots \quad (2.19)$$

The stress to first produce non-equilibrium faults in a recent study of Ni[88], used in conjunction with an assumed SFE value of 150 ergs/cm^2, did give reasonable values for the number of pile-up dislocations, n. To reverse the determination would require an accurate knowledge of n, possibly through etch-pit studies, but the main advantage of the method would be the extreme simplicity of the relationship, i.e. fewer parameters and fewer sources of error.

2.2.3 TEXTURE METHOD

The effect of cold rolling on FCC metals and alloys is a compression normal to the surface and a tensile force parallel to the rolling direction. The compressive force first rotates primary slip planes parallel to the surface and then finally {110} planes. Similarly the tensile force rotates slip directions parallel to the tensile axis with <112> eventually becoming stable. This is the alloy type or brass texture, indicative of low SFE metals. If extensive cross-slip can take place, further rotation of the slip planes into the {124}-{146}<112> orientation can take place. This is called the pure metal or copper type texture representative of high SFE metals. This connection between texture transition and SFE has been utilized by Dillamore et al[89] to estimate values of the SFE for some common FCC metals. They first estimated the degree of brass texture by the ratio of intensities of {111} poles in the transverse direction to that 20^o from the rolling direction in {111} X-ray pole figures. This ratio was used since the 20^o intensity remained the same for both textures while the transverse peak shifted towards the figure center with increasing copper texture. From Seeger's[73] cross-slip theory, and assuming that single crystal stress-strain curves

of metals of the same γ/Gb values with equivalent thermal activation and orientation are identical if stress is measured as fractions of G, they concluded that γ/Gb could be correlated with the above intensity ratio at equal values of kT/Gb^3 for different metals. Utilizing known values for Ag, Cu and Ni, correlation curves were drawn and SFE values of other metals determined.

As previously noted, an immediately apparent drawback is the accuracy of the values for the reference metals. Also, as noted recently by Liu and Alers[90], the intensity ratio technique is convenient but there is no theoretical reason for any ratio best describing the texture. This method also assumes no temperature dependence of the SFE. Of prime importance is Liu and Alers finding that the texture transition is better described in terms of the "dislocation interaction" hypothesis of texture formation[91], in which the separation of the partials, be they of equilibrium spacing or not, is the controlling factor. Their work on Cu-Al alloys concurred with this theory in that the brass to copper transition took place over a very narrow range of solute content and not gradually as the earlier theory would suggest. Thus there is a functional relationship between SFE and texture, but no one-to-one correspondence. For the alloy content at this critical texture (defined as 50% brass and copper), γ/Gb can be empirically determined, but for no other. In addition, their tabulation shows a low SFE metal, Pb, as having the copper-type texture, while Ag, of almost identical SFE, possesses the brass-type. As if to further complicate matters, recent work by Kamijo and Sekine[92] has suggested that mechanical twinning and not cross-slip

is the prime factor for texture transition. Obviously this method can therefore no longer be regarded as trustworthy, except, perhaps, for the special case at the critical alloy content.

2.2.4 TWIN BOUNDARY METHOD

The geometry of stacking in FCC metals indicates that two coherent twin boundaries (growth faults) lying on adjacent planes have the same stacking sequence as an intrinsic fault. Therefore the SFE should equal twice the twin boundary energy, and this idea was utilized by Fullman[93] to give the first estimates for SFE, on Cu and Al. Using the analogy of twin boundary-grain boundary intersections being under equilibrium surface tensions due to their respective energies, he calculated the ratio γ_{TB}/γ_{GB} from the dihedral angles of the intersections. Since γ_{GB} can be independently calculated[94,95], a value of SFE could then be obtained. This would be especially useful for high SFE metals, where annealing twins can be formed but equilibrium faults cannot. However, several drawbacks exist.

Since the material is annealed at a high temperature to obtain the equilibrium annealing twin-grain boundary intersections, one is essentially measuring the SFE at that temperature and not at room temperature[58]. Since the temperature dependence of the SFE is uncertain at best[37], this could lead to a large variation in results as compared to other methods. Recent work on Cu[96] has indicated that purity, as usual, can affect results significantly, and, in addition, grain orientation must be taken into account. By far the most serious drawback to this method is that, despite reasonable SFE values obtained for Al and Cu, there appears to be no correlation whatever between $2\gamma_{TB}$ and generally

accepted SFE values for Au, Ag, Fe, Ni and Pt[55b] and for Inconel 600 and stainless steel[58]. This suggests that the approximate agreement for Cu and Al is more fortuitous than anything and makes this method extremely risky.

Mention should also be made of the connection between the SFE and frequency of annealing twins, with twins becoming more frequent the lower the SFE. One attempt to graphically correlate SFE with the number of twin intersections/grain[97] showed such a large degree of scatter, however, that no reasonably accurate relationship could be fitted to it.

2.3 THEORETICAL METHODS AND ALLOYING EXTRAPOLATION

Several attempts have been made to estimate the SFE from first principles, but with limited success. As mentioned earlier, some works have demonstrated the approximate equality of the intrinsic and extrinsic fault energies[55,98]. As far as direct SFE determination, several approaches have been attempted. Hirth and Lothe[55b] discussed a method whereby the number of pairs of atoms of separation N, at 0^{o} K, that are not in the proper stacking sequence, are multiplied by the distortional energy/pair and summed over the lattice. Neglecting dilatational forces normal to and within the fault plane, i.e. the usual spherical ball model bound by central forces, values roughly two orders of magnitude lower than normal were obtained by Jossang[99] for several metals using this theory. It is interesting to note that by imposing a 1% compression normal to the fault Jossang then obtained a value for Cu of 50 ergs/cm^2, in fairly good agreement with experiment. This presence of non-central forces is further indicated by the deviations from the ideal c/a ratio in HCP metals, making similar calculations in this lattice

even more difficult.

Recently Ducharme[100] calculated SFE values for Be, Cd and Mg using a non-local optimized model potential theory and obtained values of 225, 12 and 8.7 ergs/cm^2 respectively. As shall be seen shortly, the values for Mg and possibly Cd are quite far off experimental estimates.

Another recent attempt by Krasko et al[101] has met with more success. They calculated the energy of faults in non-transition metals by means of an assumed pseudopotential method in which an effective interatomic interaction potential is affected by the faulting and then summed over the lattice. Their values for Cu, Al, Zn and Mg were in reasonable agreement with experimental values but not accurate enough to be used with any real confidence because of the sensitivity of the SFE value to the chosen potential.

Finally, of great importance, both theoretically and practically, is the effect of alloying on SFE. This has long been held to be related to the free energy difference between the FCC and HCP phases in a system. That is, addition of solute lowers the SFE, enabling creation of more faults until, at the phase boundary, where the SFE is expected to be zero, the entire structure is faulted and equivalent to the other structure, as previously noted in section 1.2.5. This simplified model is not completely accurate, however, as was pointed out recently by Tisone et al[102] in a discussion of the theoretical components of the SFE. They showed that the SFE would go to zero along with the free energy if only first nearest neighbour interactions affected the SFE. Since faulting does affect numbers of other nearest neighbours the SFE is then not necessarily zero when the free energy is zero. This is borne out by many instances

of non zero (although low) values of SFE arising in experimental work where SFE vs. alloying content curves have been extrapolated to a phase change composition. This is further borne out in the simplified theory of SFE decrease due to alloying. Qualitatively, addition of a solute of higher valency adds more free electrons to a metal, which increases the density of states at the Fermi surface, corresponding to the decrease in SFE. This expands the surface until it touches the Brillouin zone, whereupon the energy can be reduced by a phase change, corresponding to a zero SFE. This relatively simple concept of the relation between SFE and free electrons has indeed shown up well in many studies on the faulting probability in monovalent noble metal-higher valency solute systems, e.g. Davies and Cahn[103] or Gallagher's review[37]. For that matter the reverse, or an increase in SFE by addition of a lower valency solute, has been indicated for Pb-Tl alloys[104].

Unfortunately the situation is not always as simple. For polyvalent metals the multiplicity of Brillouin zones leads to a very complex Fermi surface. Since it is the long range interactions which affect the SFE (faulting affects only third, and higher, nearest neighbour distances and numbers), the SFE is likely to be fairly dependent upon the exact (and difficult-to-determine) shape of the Fermi surface, as has been suggested[104,105]. Similarly, Gallagher's review[37] indicates that the effect of multivalent solutes is not as predictable as the case where a clear-cut difference exists between solvent and solute. When solvent and solute are of roughly the same valency the effect of alloying on the SFE may be a substantial decrease (Ni-Co alloys)[106], an increase (Co-Fe alloys)[107], non-existent (Ag-Mn and Cu-Mn alloys)[37], or a simple monotonic variation between the pure metal SFE's (inter-noble metal alloys)[36c]. Thus

alloying can only be qualitatively predicted, as the Fermi surface-Brillouin zone model would indicate.

At this point, a distinction should be made between the absolute or equilibrium SFE (dependent on the electronic contributions) and the apparent or dynamic SFE (dependent on the dislocation spacing). The former is the main concern of the theoretical studies while the latter is of prime importance for any property dependent on the partials spacing, which is the concern of practically all the work previously mentioned in the various methods for SFE determinations. It is this apparent SFE which can show a marked temperature dependence or a marked variation at a given alloy content. The alloying effect can lead to non-equilibrium configurations and a much greater initial decrease in SFE than that predicted by the gradual decrease of the free electron theory. As long as an absolute value is not of prime concern, this is not too important. It does give rise, however, to one of the major failings of the extrapolation technique in that the SFE vs. alloying content curve quite often rises slowly with decreasing alloy content and then suddenly bends upwards at the lowest content, making the pure metal extrapolation very difficult. Of course the accuracy is also dependent on the reliability of the method used to determine the values for the various compositions. Nonetheless, this still remains one of the best checks for a pure metal SFE value as determined by some other method.

2.4 APPLICATION TO HCP METALS

Given the variety of ways that the SFE can be calculated, it is perhaps not too surprising that a large degree of variance should be observed in the many determinations, although some portion would undoubtedly

be due to relatively crude early studies. This is indicated in Tables 2-6 for the common FCC metals, primarily compiled from Gallagher's recent review[37], and in Table 7 for some HCP metals. It is immediately apparent that the results for the HCP metals are fewer and more variable. The main reason for this could be the difficulty of applying the various methods to HCP metals. Because of the very nature of the lattice, multiple intersecting slip planes, as in FCC metals, do not really occur, therefore faulted tetrahedra cannot be formed. For similar reasons the present texture and dipole theories cannot be applied to HCP metals. To the best of the author's knowledge, fault pairs have not been observed in HCP metals. The twin boundary and τ_3 methods cannot be regarded as trustworthy, the one for theoretical and the other for practical reasons. The relatively untried methods, grain boundary intersection, critical tear stress, etc. hold interesting possibilities but need a good deal more theoretical work and/or experimental verification. Eliminating all these as prime possibilities, only the approximate estimation from the temperature and strain rate sensitivity of the prismatic slip CRSS remains in the indirect category (unless a better correlation can be found from X-ray data). Similarly only the node, ribbon and loop annealing methods remain in the direct category. Even with this drastic limitation on the number of choices, there should be no reason why, following a procedure to be shortly stated, these methods could not be utilized to furnish at least one estimation for the SFE. In short, it would appear that lack of accurate studies, not lack of methods, is the primary reason for the scarcity and unreliability of many SFE values for HCP metals.

TABLE 2

STACKING FAULT ENERGY OF SILVER

METHOD	SFE(ergs/cm^2)	REFERENCE
node	21	Loretto et al, 1964 (108)
	20 ± 7	Gallagher, 1964 (109)
	21.9 ± 3.5	Gallagher and Washburn, 1966 (57)
	27 ± 7	Wilkens et al, 1966 (110)
	22.8 ± 4	Ruff and Ives, 1967 (111)
	17 - 32	Clarebrough et al, 1967 (112)
	17 ± 3	Gallagher, 1968 (77)
	19.6 ± 2.3	Gallagher and Liu, 1969 (69)
τ_3	43	Seeger et al, 1959 (73)
	29	Berner, 1960 (113)
	>30	Thornton et al, 1962 (31)
	40	Buhler and Lucke, 1964 (114)
	15 ± 3	Ahlers, 1965 (115)
	65 ± 8	Ahlers and Haasen, 1965 (116)
tetrahedra	<43	Seeger, 1964 (117)
	7.5 ± 1	Loretto et al, 1965 (42)
	17 ± 4	Jossang and Hirth, 1966 (45)
	15	Humble et al, 1966 (47)
dipole	21 ± 6	Haussermann and Wilkens, 1966 (118)
	30.7	Steeds, 1967 (61)
normalized X-ray data	24	Hu et al, 1961 (119)
	18 ± 3.5	Otte, 1967 (70)
fault-pair	30	Gallagher and Washburn, 1966 (57)
creep data	26<35<58	Thornton and Hirsch, 1958 (82)
stress for mechanical twinning	21	Suzuki and Barrett, 1958 (120)

TABLE 3

STACKING FAULT ENERGY OF COPPER

METHOD	SFE(ergs/cm^2)	REFERENCE
τ_3	170	Seeger et al, 1959 (73)
	102 - 165	Haasen and King, 1960 (121)
	163	Berner, 1960 (113)
	>170	Thornton et al, 1962 (31)
	50 ± 6	Peissker, 1965 (122)
twin boundary	40	Fullman, 1951 (93)
	42	Fisher and Dunn, 1952 (123)
	40	Seeger and Schock, 1953 (124)
	24	Inman and Khan, 1961 (125)
	70	Valenzuela, 1965 (96)
tetrahedra	78	Loretto et al, 1965 (42)
	73 ± 15	Jossang and Hirth, 1966 (45)
	59	Humble et al, 1966 (47)
dipole	59	Haussermann and Wilkens, 1966 (118)
	150 ± 30	Steeds, 1967 (61)
	94	Pande, 1970 (62)
extrapolation (node)	48 ± 10	Gallagher and Liu, 1969 (69)
	70	Nordstrom and Barrett, 1969 (126)
grain boundary intersection	46	Peterson and Queeney, 1969 (51)
normalized X-ray data	70 ± 15	Otte, 1967 (70)
creep data	40	Thornton and Hirsch, 1958 (82)
stress for mechanical twinning	33	Blewitt et al, 1957 (127)
theoretical	40	Krasko et al, 1970 (101)
	50	Jossang, 1967 (99)

TABLE 4

STACKING FAULT ENERGY OF GOLD

METHOD	SFE(ergs/cm^2)	REFERENCE
tetrahedra	16	Czjzek et al, 1962 (44)
	12	Seeger, 1964 (117)
	56	Loretto et al, 1965 (42)
	55 ± 11	Jossang and Hirth, 1966 (45)
	45	Humble et al, 1966 (47)
τ_3	30	Seeger et al, 1959 (73)
	10	Berner, 1960 (113)
	13 ± 19	Ahlers and Haasen, 1965 (116)
dipole	42	Haussermann and Wilkens, 1966 (118)
	61	Steeds, 1967 (61)
texture	45	Dillamore et al, 1964 (89)
extrapolation (node)	42 ± 5	Gallagher and Liu, 1969 (69)
creep data	24<33<47	Thornton and Hirsch, 1958 (82)
stress for mechanical twinning	30	Suzuki and Barrett, 1958 (120)

TABLE 5

STACKING FAULT ENERGY OF ALUMINUM

METHOD	SFE(ergs/cm^2)	REFERENCE
loop annealing	210	Kannan and Thomas, 1966 (128)
	200	Clarebrough et al, 1967 (112)
	135 ± 20	Dobson et al, 1967 (129)
	110	Tartour and Washburn, 1968 (130)
twin boundary	200	Fullman, 1951 (93)
	200	Seeger and Schock, 1953 (124)
τ_3	170 - 230	Seeger et al, 1959 (73)
	238	Berner, 1960 (113)
texture	>150	Dillamore et al, 1964 (89)
creep data	>200	Thornton and Hirsch, 1958 (82)
theoretical	260	Krasko et al, 1970 (101)

TABLE 6

STACKING FAULT ENERGY OF NICKEL

METHOD	SFE(ergs/cm^2)	REFERENCE
τ_3	$2.2\gamma_{Cu}$	Haasen, 1958 (131)
	410	Seeger et al, 1959 (73)
	300	Berner, 1960 (113)
	300	Mader, 1963 (32)
dipole	185	Haussermann and Wilkens, 1966 (118)
extrapolation (tetrahedra)	160	Humble et al, 1966 (46)
extrapolation (node and texture)	240	Beeston et al, 1968 (106)
creep data	64<95<140	Thornton and Hirsch, 1958 (82)

TABLE 7

STACKING FAULT ENERGIES OF HCP METALS

METHOD	SFE(ergs/cm^2)	REFERENCE
Beryllium		
extrapolation (node)	155	Saulnier, 1963 (132)
theoretical	225	Ducharme, 1970 (100)
Cadmium		
electronic and deformation data	200 - 400	Seeger, 1955 (133)
creep data	>130 (80^{o}K)	Thornton and Hirsch, 1958 (82)
from presence of dislocation ribbons	<30	Price, 1963 (134)
τ_3	100	Bocek et al, 1964 (80)
loop annealing	205 ± 50	Westmacott, 1970 (167)
theoretical	12	Ducharme, 1970 (100)
Cobalt		
creep data	26 ± 10	Thornton and Hirsch, 1958 (82)
node	31 ± 5	Ericsson, 1966 (199)
Magnesium		
electronic and deformation data	200 - 400	Seeger, 1955 (133)
basal CRSS theory	60	Seeger, 1963 (135)
τ_3	40	Bocek et al, 1964 (79)
prismatic CRSS theory	high, > Ti & Zr	Ahlers, 1970 (71)
loop annealing	280 ± 100	Harris and Masters, 1966 (136)
	125 ± 25	Hales et al, 1968 (137)
	102	Leighly, Jr., 1970 (166)
theoretical	8.7	Ducharme, 1970 (100)

METHOD	SFE(ergs/cm^2)	REFERENCE
Titanium		
HCP-FCC transformation	10	Spreadborough, 1958 (138)
prismatic CRSS theory	high, same as Zr	Ahlers, 1970 (71)
Zinc		
electronic and deformation data	200 - 400	Seeger, 1955 (133)
creep data	>250 (80°K)	Thornton and Hirsch, 1958 (82)
from presence of dislocation ribbons	<30	Price, 1963 (134)
τ_3	134	Lukac and Svaboda, 1965 (81)
loop annealing	300 ± 150	Harris and Masters, 1966 (136)
	290, 220, 230	Dobson and Smallman, 1966 (139)
	140	Hales et al, 1968 (137)
theoretical	96	Krasko et al, 1970 (101)
Zirconium		
ribbon	>65	Roy, 1963 (140)
creep data	250	Ramaswami and Craig, 1967 (83)
prismatic CRSS theory	high, same as Ti	Ahlers, 1970 (71)
theoretical	250	Ramaswami and Craig, 1967 (83)

2.5 GENERAL REMARKS

At the risk of being repetitious, there are a number of relevant points that apply to the usage of the various methods for any metal or alloy.

Some are theoretically suspect (texture, twin boundary), while others (deformation, loop annealing) are greatly dependent on the authenticity of their rate-controlling mechanisms. The various "minor" methods need a good deal more clarification, while the more common approaches (τ_3, dipole) have shown such a wide range of values for the same metal as to make their accuracy difficult to judge. The theoretical estimations are very dependent on the assumed model for displacement effects on interatomic forces, and the extrapolation technique, is, of course, dependent on the methods utilized in it. Even the most accurate calculations (node, fault-pair, ribbon) are limited by their applicability range. Most of the direct methods can be hindered by the difficulty of creating the necessary defects (loop annealing, tetrahedra, fault-pair, dipole, grain boundary intersection). The indirect methods are naturally often criticized because of their usual measurement of a parameter that can often be influenced by several factors, of which SFE is only one, thus its "relative weight" may be difficult to determine.

Finally, there are a number of points that bear mentioning because of their general applicability. Some examples are;

1) accurate measurement of the necessary dimension or parameter, i.e. application of all possible correction factors, such as for inclination to the electron beam of a node, loop, tetrahedron, etc.

2) the likelihood that errors can increase greatly as measurements become finer, e.g. taking dislocation image widths into account when fitting circles to small nodes[58].

3) importance of specimen purity for most methods, or at least some awareness of possible impurity effects.

4) the necessity of a reasonable number of measurements due to the commonplace large variation in defect size.

5) the careful estimation of an error range, e.g. a value of 135 ± 10 ergs/cm^2 is a good deal more valuable than one of 150 ± 100 ergs/cm^2.

6) measurement of a defect in a stress free region of the foil is desirable (e.g. reasonably far from the foil surface) although probably the most difficult requirement to obtain.

From the above and from Tables 2-7 one point becomes quite evident, that of the individuality of each work. That is, there is no "best" method per se, thus the task is to determine the best method for any given metal or alloy. In conclusion then, this might possibly be achieved as follows;

a) Eliminate those methods that cannot be used.

b) If possible, estimate the approximate range that the SFE lies in (high, medium, low) from such sources as X-ray data, work hardening behaviour or dislocation structure, e.g. low SFE tends to co-planar arrays while high tends to a cell structure.

c) Choose the most reliable method in this range, preferably a direct one.

d) If time and equipment are available, choose one or two other methods,

possibly a minor one, to be used either in conjunction with the main method or as a check on it.

e) Be aware of the shortcomings of each method, either to discount them or possibly correct for them.

Good examples of this type of work are Beeston et al's[106] combination of node, tetrahedra and texture data for an extrapolative value of Ni SFE, Gallagher and Liu's[69] use of node, τ_3, X-ray and texture methods on Ag alloys, or Tisone's[107] use of node, fault-pair and tetrahedra techniques on Co-Fe alloys.

3. APPLICATION TO ALPHA ZIRCONIUM

3.1 PREVIOUS WORK

As is evident from Table 7, the estimations for Zr SFE are few and, even more important, somewhat lacking in accuracy. Roy's work[140] was on a Zr alloy (Zircaloy-2) and while it can be said that the SFE of pure Zr is undoubtedly higher, just how much higher is difficult to say. It would seem a little implausible, however, that the relatively small alloying additions in Zircaloy-2 should lower the SFE by a factor of nearly 4, as the other results would indicate. As already noted, the creek data calculations of Ramaswami and Craig[83], based on Thornton and Hirsch's work[82], are subject to several inaccuracies, while their theoretical calculations, based on Chou's theory of extended dislocation width[141], are beset by many of the problems common to all theoretical determinations. The same sense of vagueness applies to the deformation data. If indeed Zr SFE is less than that of Mg, the most accurate value of Mg SFE (125 ergs/cm^2 - loop annealing) would indicate that Zr might even lie in the medium SFE range. This is contradicted by the nature of the dislocation substructure in deformed Zr (e.g. easy tangling) and the absence of faults in any electron microscope studies.

Lele and Anantharaman[142] found α, the deformation fault probability, to be negligible in Zr (as did Mogard and Averbach[143]) and slightly greater in Ti (0.008), while Krishnan[144] concluded that α in both was 0.002 and β (growth fault probability)was 0.013.

All that can be concluded from the above is that the Zr SFE is high and close to that of Ti, although here again difficulty arises in view of Spreadborough's Ti SFE estimation[138] and his observation of profuse faulting in that metal. Thus there is a definite need for a reasonably accurate, quantitative determination of Zr SFE. This is somewhat limited by the aforementioned restrictions on HCP metals, but, if vacancy loops could be created in Zr, the loop annealing method could fill these requirements, especially in view of its extensive use on other high SFE metals such as Al, Mg and Zn. To gain a better insight into this relatively new method, a good understanding of loop formation, while perhaps not essential, would be very helpful.

3.2 VACANCY LOOP FORMATION

Since the loop annealing method requires the presence of both faulted and prismatic loops, this discussion will be limited to those loops formed by rapid quenching rather than by dislocation interactions.

There exists at any temperature, an equilibrium concentration of vacant lattice sites, or vacancies, given by;

$$V_1 = n_1/N = \exp Sv/k \exp(-E_{f1}/kT) \simeq \exp(-E_{f1}/kT) \quad \ldots\ldots (3.1)$$

where Sv = entropy of formation for a vacancy

E_{f1} = energy of formation for a vacancy ≃ 1 electron volt[145]

Similarly, the concentration of di-vacancies is;

$$V_2 = 1/2\, Z \exp(-2E_{f1}/kT) \exp B/kT \quad \ldots\ldots\ldots\ldots\ldots\ldots (3.2)$$

where B = di-vacancy binding energy ≃ 0.3 e.v.

Z = co-ordination no. in the perfect lattice

Substitution of the approximate energy values gives

$$V_2 = 1/2\, Z \exp(-1.7/kT) \quad \ldots\ldots\ldots\ldots\ldots\ldots\ldots\ldots (3.3)$$

Thus V_2 increases as T increases. It can also be seen that V_2/V_1 also increases with T,

$$V_2/V_1 = 1/2\ Z\ \exp(-1/kT)\exp(+0.3/kT) = 1/2\ Z\ \exp(-0.7/kT) \ldots (3.4)$$

as experimentally found by Koehler et al[146].

It has been shown[145] that binding energies increase with increasing number of vacancies in the configuration, i.e. they are increasingly more stable. Results have also shown that the migration energy, i.e. mobility, varies inversely with the binding energy. Studies[145] have determined that the tri-vacancy must dissociate to move, thus it combines low mobility with relatively high stability and can therefore be thought of as the smallest cluster for void formation.

Given then, the large degree of supersaturation of vacancies produced by a rapid quench from near the melting point to room temperature or thereabouts ($V_1 \simeq 10^{-4}$ vs. $V_1 \simeq 10^{-26}$), a qualitative picture of what occurs during the quench would be similar to that proposed by Panseri and Federighi[147]. As already shown, near the melting point, a large number of di-vacancies will be present along with the mono-vacancies. Being highly mobile and reasonably stable, as the quenching begins a significant portion will last long enough to encounter another vacancy, forming the tri-vacancy. As the temperature is dropping, vacancy mobility is being reduced and the chances of a monovacancy reaching a tri-vacancy (or larger cluster) before it diffuses to a sink (foil surface, grain boundary, etc.) correspondingly increase. Thus the clusters grow.

Now if the quench temperature is reduced to, say 0.8 m.p., the vacancy and di-vacancy concentration will be greatly reduced and the clustering time will be higher. Thus the relative proportion of clusters to vacancies and di-vacancies will be greatly reduced.

Further reduction of the quenching temperature to, say, 0.65 m.p., reduces the probability of clustering to nearly zero. The di-vacancy concentration itself is very small due to both decreased number and mobility of single vacancies, so that almost all the quenched-in defects are monovacancies.

There are a multitude of reasons why this is only a qualitative picture. The formation, binding and migration energies of the mono-, di- and tri-vacancies are not all known to a high degree of accuracy, while those for higher order clusters are almost wholly unknown. The formation of clusters or, for that matter, even the concentration of retained monovacancies depends greatly on the sink density and distribution, no easy parameter to evaluate. Further complicating the picture may be dislocations produced by quenching stresses or quench-induced phase transformations, which can act as both sources and sinks of vacancies (to be discussed later). Finally, there are always some amount of impurities present that may be able to form impurity-vacancy complexes. The binding energy of these complexes depends on both the size and electrostatic charge of the impurity atom. Impurities larger than the matrix atoms will tend to form complexes with vacancies while smaller ones will tend to form complexes with interstitials (if present). The electrostatic binding depends on the excess ionic charge of the impurity, Z, and the larger Z is the larger is the Coulombic repulsive force between the impurity and surrounding atoms, thus the easier it is to remove one of

matrix atoms. Since several impurities of varying sizes and concentrations are usually present, the situation becomes quite complex. Indeed, depending on such things as relative sizes, binding energy and type of lattice, some complexes may be reasonably mobile and these impurities (and their vacancies) travel to sinks: Other complexes may be so much slower than single vacancies that the probability of their meeting and growing before they reach a sink is fairly high. Thus they may be regarded, to some extent, as nucleating agents for higher order vacancy clusters. An example of a "fast" complex is Mg in Al[148] while a slow one is Cu in Ni[149]. If enough impurities were present, all of the vacancy supersaturation of roughly 10^{-4} could be used up to form complexes since this would only correspond to 100 ppm impurities (impurities that would form complexes).

As these clusters grow in size during the quench and upon subsequent ageing, one of three things will happen to them:

1) they will remain as roughly spherical voids of varying sizes
2) they will collapse to form dislocation loops
3) they will form tetrahedral defects (in FCC at least)

The second result is the one of interest here and was extensively analysed by the Wilsdorfs in 1960[150], who analysed vacancy condensation in Al from three points of view:

1) whether or not cluster formation was necessary for loop formation
2) the modes, i.e. habit planes, of condensation
3) a mechanism for the cluster-loop transition

Calculating the energies of various loops from,

$$E = 1/2\ Gb^2R/1-\nu\ (\ln R/b + 5/3) \quad \ldots\ldots\ldots\ldots\ldots\ldots (3.5)$$

where R, the loop radius, is obtained from the number of vacancies in the

loop, it appeared that the plane of closest packing appeared to be favored for loop formation. That is, the lowest energy configuration was the faulted (Frank) loop, caused by direct collapse of a single layer of vacancies on a {111} plane. Perfect (prismatic) {111} loops, on the other hand, had a higher energy than double layer condensation on a {110} plane, but it is possible that many of the perfect loops that are experimentally observed result from nucleation of a Shockley partial on the Frank loops. The plots of loop energy/vacancy vs. the number of vacancies are schematically shown in Fig. 12, along with the plot for a void, given by

$$E/n = n^{-1/3}\ 4\ \pi\gamma\ (3a^3/16\ \pi)^{2/3} \quad \ldots\ldots\ldots\ldots\ldots\ldots \quad (3.6)$$

where γ = void surface energy

a = lattice constant

There are three ways to determine the minimum number of vacancies necessary for loop formation. One is that the energy/vacancy must be less than that for a single vacancy, thus the minimum number for each configuration is given by the intersection of its curve and the 0.76 e.v. (the author's assumed value for E_{fl}) line in the graph of Fig. 12. These minima may also be given by the intersections with the void energy curve, curve 0, (shown approximated by a tangent at lower values). Finally, there is the straightforward, geometrical method of calculating, for each configuration, the number of vacancies in the smallest possible loop, i.e., one in which the dislocation cores on opposite sides do not overlap. All three of these indicate that even the smallest minima (curve A) is of the order of 10-20 vacancies, and for the others, rises drastically. In other words, vacancies will meet and cluster in three-dimensional

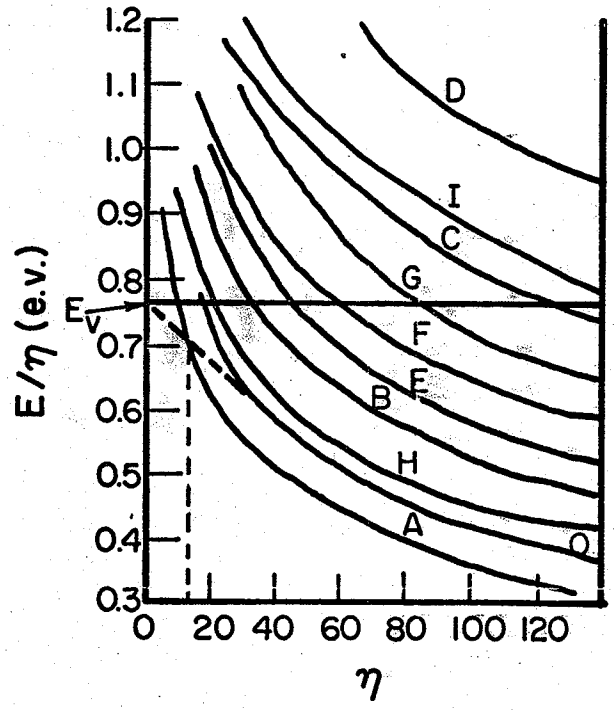

Fig.12 Curves of energy/vacancy vs. number of vacancies for various FCC planes (after Kuhlmann-Wilsdorf and Wilsdorf, ref.150)

CURVE	CONDENSING LAYERS	PLANE	RESULTING LOOP
A	1	(111)	Frank
B	1	(111)	prismatic
C	2	(111)	faulted, may go to prismatic
D	3	(111)	faulted, may go to pr-smatic
E	1	(100)	prismatic
F	2	(100)	faulted, may go to prismatic
G	1	(110)	prismatic
H	2	(110)	prismatic
I	3	(110)	faulted, may go to prismatic

O - void energy curve

aggregates to at least some degree before it is energetically favorable for them to collapse and form a loop.

Two qualitative mechanisms have been discussed for the cluster-loop transition. If the voids are roughly spherical, they will be subject to a uniaxial compressive stress, slightly deforming the cluster into a rotational ellipsoid. This introduces a stress concentration at the circumference, causing vacancy diffusion from the stress-free poles, which subsequently flattens the ellipsoid into a lens shape 2 or 3 atomic planes thick. This then collapses into a loop. A more realistic picture might be to have the void bounded by {111} planes. Then, along the lines of a mechanism similar to, but more complex than, the one above, opposing faces of the void would fuse together as they collapsed, forming a series of concentric loops on the {111} plane which immediately move apart under mutual repulsion. The smaller loops evaporate rapidly and are condensed into the larger ones, leaving as an end result, only one large loop or possibly a pair. Even though these loops may still be unstable with respect to a void, they will remain and grow as loops because of an (unknown) activation energy barrier to reconvert them to voids. This type of mechanism would reconcile the experimental results with the above energy curves since almost all loops and loop pairs (curves A, B and C) will lie on {111} planes, as is found experimentally, even though energy considerations alone indicate that {110} and {100} pairs should be more frequent.

A more recent analysis by Dohkner[151] indicates that an aggregate of only 7 vacancies on a {111} plane in Cu is stable as a loop. Thus this might be the nucleating size for loop growth as the tri-vacancy is thought to be for cluster growth. Dohkner also studied the interaction of nearby vacancies with this loop and found them to be increasingly more bound to the loop within a radius of 3 interatomic spacings around the dislocation bounding the loop. Thus the loop growth is not by a random striking process. He further discovered that the vacancy movement towards the loop was directionally favored to head towards the plane of the loop, i.e. even vacancies directly under the loop would first migrate away from it, then up into the plane of the loop and into the loop itself. This might be qualitatively explained as the vacancies tending to pass into the compressed region around the extra half plane of the dislocation rather than migrate into an already extended region. Quantitatively, Dohkner derived the activation energy for loop growth as $0.8E_m$ (migration energy of a monovacancy far away from the loop) vs. $1.2E_m$ as the activation energy for loop shrinkage.

There are many other points that could be discussed: whether or not there is an activation energy for the void collapse or, what other factors besides energy considerations can have an effect on either the void-loop transition or the condensation plane. However this simplified approach does point out the necessity of the clustering process and explains to some extent just why the loops appear where they do and why they grow.

3.2.1 HCP VACANCY CONDENSATION

Due to the nature of the stacking sequence of HCP metals, the loop formation process is more complex than that for FCC metals. In HCP metals, condensation of a disc of vacancies results in two A or B atoms directly above one another. This can be obviated in two ways:

1) part of the layer above the loop (and only that layer) can collapse as shown in Fig. 13a, i.e. there are three violations of the stacking sequence, with a σS type bounding partial (c/2[0001]), using Berghezan's bipyramidal notation[152].
2) a collapse and shifting of all layers above the loop as in Fig. 13b, i.e. only one violation of the stacking sequence with an AS (1/6[20$\bar{2}$3]) type bounding partial (not perfect as occurs in the FCC lattice with a collapse and a shift) resulting from the reaction of an Sσ Frank and a σA Shockley (a/3[10$\bar{1}$0]).

(1) is a lower energy dislocation but (2) is a lower energy fault so that, barring other factors, the tendency for one type to predominate arises from an energy analysis:

$$E_1 = 1/8(GR - \gamma)c^2 \ln R/R_o + 3\pi R^2\gamma \quad \ldots\ldots\ldots\ldots\ldots\ldots \quad (3.7)$$

$$E_2 = 1/4GR\ \{1/3a^2 + 1/1\text{-}\nu\ (1/3a^2) + 1/2c^2\}\ \ln R/R_o + \pi R^2\gamma \quad \ldots \quad (3.8)$$

taking $c^2 = 8/3a^2$, $\nu = 1/3$, $E_2 < E_1$ for a critical radius

$$R_c \geq \frac{5}{48\pi\gamma} Ga^2 \ln R/R_o \quad \ldots\ldots\ldots\ldots\ldots\ldots\ldots\ldots \quad (3.9)$$

Using typical values for Zn[152],

$$R_o = 5 \times 10^{-8} \text{ cm}$$

$$R \simeq 5 \times 10^{-6} \text{ cm}$$

$$G = 4 \times 10^{11} \text{ dyne/cm}^2$$

$$a = 2.66 \times 10^{-8} \text{ cm}$$

this becomes $R_c \geq \frac{5 \times 10^{-5}}{\gamma}$ cm $\quad \ldots\ldots\ldots\ldots\ldots\ldots\ldots\ldots \quad (3.10)$

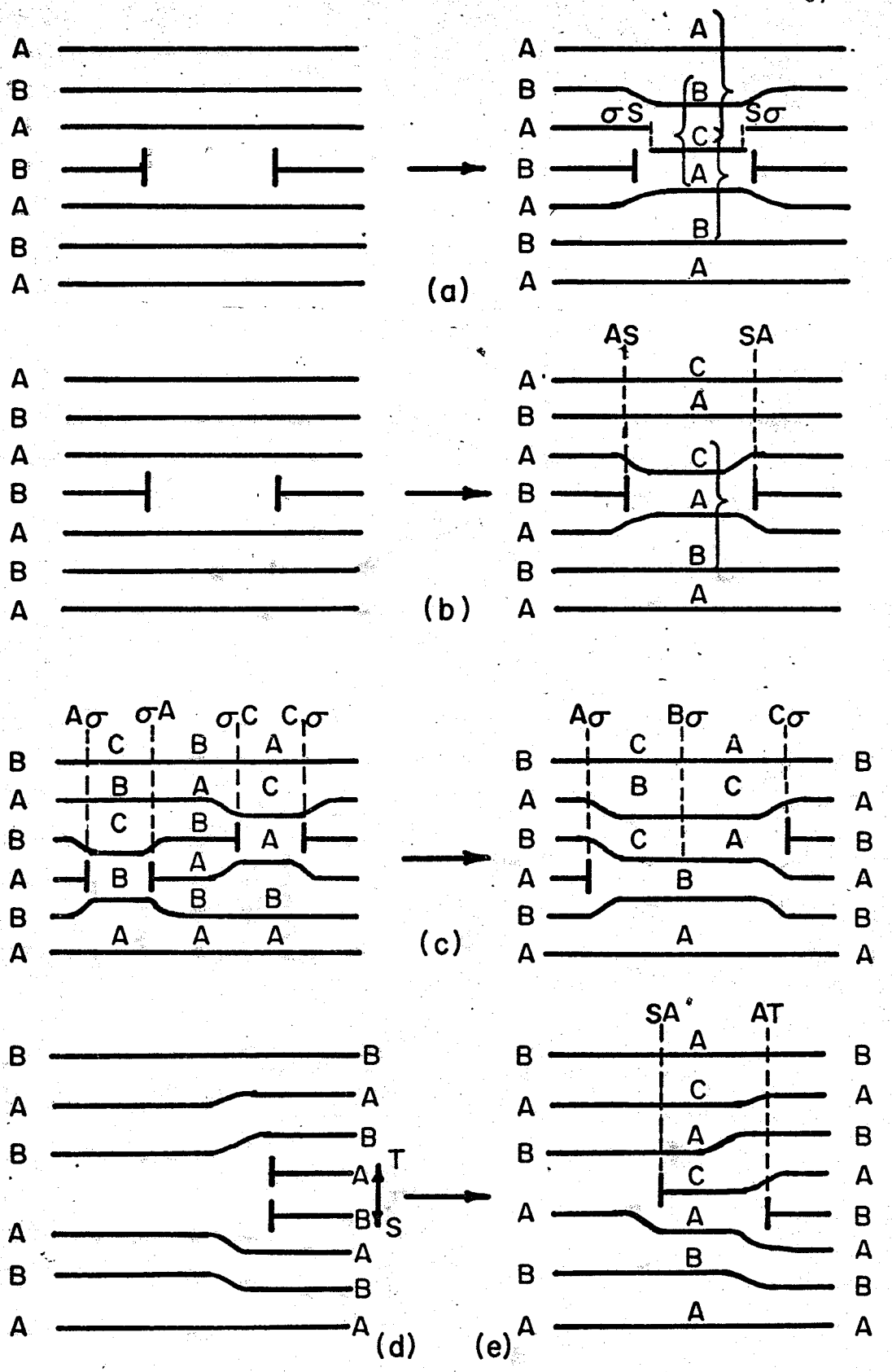

Fig.13 Vacancy condensation in the HCP lattice (after Berghezan et al, ref.152)

so that for γ = 50 ergs/cm^2, R_c > 100 Å will favor (2) and for higher SFE, R_c will be even smaller. Thus the low energy fault is favored for all but the smallest loops and lowest SFE's.

A less likely but nonetheless possible occurrence is for condensation to take place on two adjacent planes as in Fig. 13c, i.e. two adjoining loops with a partial dislocation separating the areas of different stacking.

It might be thought that two layers of vacancies could condense to give a prismatic loop as in Fig. 13d, however, due to energy considerations this ST type dislocation would almost immediately dissociate into an SA and an AT dislocation with an attendant decrease in energy, shown in Fig. 13e, i.e. an annulus of low energy fault bounded by two partials. Thus it is unlikely to have very many prismatic loops initially formed. However, foil heating or ageing can often result in loop shrinkage (or growth), with the inner loop shrinking at a slower rate than the outer one. Thus the fault is gradually eliminated and the two partials then combine to form a prismatic loop of Burgers vector ST or SA/TB (depending on the signs of the initial partials). The prismatic loop may also shrink, but at a different rate since there is no fault energy to consider. This difference in shrinkage (or growth) of faulted and prismatic loops forms the basis of the loop annealing method of SFE determination.

3.3 LOOP ANNEALING METHOD

If faulted loops are present in a metal, it might be tempting to expect to obtain SFE values from their dimensions, as per extended nodes or fault-pairs. Unfortunately this is not the case and it appears

that loop size is governed solely by the manner in which the vacancies aggregate, which, in turn, is determined primarily by quenching temperature, quench rate, ageing procedure and metal purity.

It seems unlikely that large faulted loops could remain stable in high SFE metals since the added energy due to the fault would appear sufficient to nucleate a Shockley partial which would sweep the loop and convert it to a prismatic one. Neglecting external stresses or thermal fluctuations, the necessary stress has been estimated at $G/30$[153] - $G/10$[159]. This leads to a value of SFE of around 150 ergs/cm^2, above which, only perfect loops are stable, thus only faulted loops have been found in low SFE Au or Cu while both are found in high SFE Al, with perfect being easier to obtain. However, if a loop energy criterion is used[154], i.e. equating the energies of the Frank and prismatic configurations, an upper limit of SFE of 40 ergs/cm^2 is calculated for the smallest loops (100 Å). This apparent anomoly can be resolved by consideration of an activation energy barrier to the Shockley nucleation. Calculations taking this into account[155] give an upper limit for SFE of about 200 ergs/cm^2 up to which faulted loops of several thousand Angstroms diameter are metastable with respect to prismatic loops.

A similar problem of Shockley nucleation, etc. does not really apply to HCP metals since, as already seen, Shockley nucleation still leaves a faulted loop with an SA type partial dislocation.

If, however, the loops are heated to the point where the vacancies in them are sufficiently thermally activated to diffuse away from the loop, the rate of shrinkage would be governed by the total energy of the loop, which includes the SFE.

The original theory for this method was laid down by Silcox and Whelan[156]. Studying the annealing rates of prismatic loops in quenched Al, they utilized the earlier work of Friedel[157] who determined the climb velocity of a dislocation due to vacancy diffusion, in terms of the movement of jogs, as;

$$V_c = \frac{Z\nu_a b}{\sin\psi} \exp\{-(E_f + E_m)/kT\}\{\exp(F_c b^2/kT) - \exp(F_s b^2/kT)\}. . . (3.11)$$

where Z = atomic co-ordination number of the lattice

ν_a = atomic frequency $\simeq 10^{13}$cps

ψ = angle between Burgers vector, b, and the dislocation line

E_f = energy of formation of a vacancy and E_m = the activation energy for movement of a vacancy

F_c = force due to any applied stress and due to the stress fields of other segments of dislocations.

F_s = force due to the chemical stress resulting from any deviation in the vacancy concentration from the equilibrium value.

The physical interpretation of this equation would be that of a unit jog (height b) on the extra half plane of the dislocation emitting vacancies under the influence of F_c and moving so as to shrink the loop, while F_s would tend to recombine vacancies with the jog, thus the expanding loop.

The climb rate of the loop is therefore

$$dR/dt = - V_c C_c . . . . (3.12)$$

where C_c is the jog concentration b/x (x = average distance between jogs), and the (-) sign indicates a net shrinkage. A detailed analysis of a prismatic loop gives a maximum rate of $1/2V_c$, i.e. $C_c \simeq 1/2$, and

this was assumed to hold for all segments of the loop.

It is evident in equation (3.11) that the important parameters are the "driving" forces, F_c and F_s. The force F_s is given by,

$$F_s = kT/b^2 \ln c/c_o \quad \ldots\ldots\ldots\ldots\ldots\ldots\ldots\ldots \quad (3.13)$$

where c and c_o are respectively the actual and equilibrium vacancy concentrations at temperature T. Thus if a large proportion of the quenched-in vacancies have gone into loop formation and there exists a reasonable sink distribution (especially the free surface in a thin foil), it can be shown that, upon heating, the remaining free vacancies plus the vacancies emitted by the loops will diffuse to these sinks rapidly enough so that no super-saturation builds up, i.e. $c \simeq c_o$, and thus $F_s \simeq 0$. This leads to an "emission-controlled" mechanism, i.e. the governing factor is the rate at which vacancies are released by the loop. When the vacancies cannot diffuse away as fast as they are emitted, i.e. $F_s \neq 0$, a "diffusion-controlled" mechanism results, which is currently held[129] to be the correct one. However, both theories give rate equations differing mainly in pre-exponential constants and not in the rate-controlling portion, thus, in view of the other uncertainties and assumptions made in both, it is necessary to develop both to clearly establish a preference for either one. Therefore, substituting $F_s = 0$ in (3.11),

$$dR/dt = \frac{-C_c Z \nu_a b}{\sin \psi} \exp(-U_d/kT)(\exp F_c b^2/kT - 1) \quad \ldots\ldots\ldots \quad (3.14)$$

where $U_d = E_f + E_m$ = activation energy for self-diffusion and Frank[158] gives $F_c = \frac{Gb^2}{4\pi(1-\nu)R} \ln R/R_o$

For a faulted loop, the SFE must be added and the resulting energy is[159]

$$E = Gb^2R/2(1-\nu)\ \ln R/R_o + \pi R^2\gamma \quad \ldots\ldots\ldots\ldots\ldots\ldots \quad (3.15)$$

By differentiating with respect to R and equating the components, it was found that the second term predominates for $R/b \gg 5$ ($b \simeq R_o$) in a high SFE material. Since R/b is usually of the order of several hundred, the first term in (3.15) can be neglected and

$$dR/dt = C(\exp \gamma B^2/kT - 1) \quad \ldots\ldots\ldots\ldots\ldots\ldots \quad (3.16)$$

where $C = \dfrac{-C_c Z \nu_a b}{\sin \psi} \exp(-U_d/kT)$ = a constant

B^2 = cross-sectional area of a vacancy in the close-packed plane (better approximation than b^2 since some relaxation takes place around a vacancy)

As the loop shrinks, the line tension has more and more effect until finally it predominates and the rate is essentially that of equation (3.14). Silcox and Whelan discovered that a plot of the reciprocal of $(\exp F_c b^2/kT - 1)$ vs. R/b gave essentially a straight line, thus $\exp F_c b^2/kT$ could be approximated by a parameter, $\alpha b/R + 1$, giving

$$dR/dt = C(\exp \gamma B^2/kT\ (\alpha b/R + 1) - 1) \quad \ldots\ldots\ldots\ldots \quad (3.17)$$

where α = a constant, varying slightly with temperature

$$= \frac{Gb^4}{6\pi(1-\nu)RkT} \ln (1/R_o)$$

Since $\exp \gamma B^2/kT \gg 1$, (-1) can be neglected and integration finally yields

$$t = \frac{1}{C \exp \gamma B^2/kT} \{R - \alpha b \ln (1 + R/\alpha b)\} \quad \ldots\ldots\ldots\ldots \quad (3.18)$$

i.e. a straight line graph valid over nearly all loop radii can be obtained in which the only unknown in the slope is γ. Similarly, for a perfect loop,

$$t = \frac{1}{C} (R^2/2\alpha b) \quad \ldots\ldots\ldots\ldots\ldots\ldots\ldots\ldots \quad (3.19)$$

Unfortunately, the one weak point is the value used for U_d. As pointed out by Saada[160], the effect of U_d in equation (3.17) is severe since it is of the order of 1 ev vs. 0.1 ev for γB^2. Thus even a small error in U_d would cause a large error in γ. To overcome this, Dobson and Smallman[139] proposed the now standardized method of comparative annealing between prismatic and faulted loops, if both are present. The slopes of the two plots of t vs. the function in brackets in (3.18) and (3.19) will differ solely due to the extra driving force of the faulted area as in Fig. 14a. The ratio of the slopes of (3.18) and (3.19) then gives

$$S_p/S_f = \frac{b_f \sin\psi_p}{b_p \sin\psi_f} \exp \gamma B^2/kT \quad \ldots\ldots\ldots\ldots\ldots\ldots \quad (3.20)$$

where 'f' denotes faulted and 'p' denotes prismatic. Thus both U_d and the other uncertain parameter, C_c, are cancelled out. It should be noted that this type of annealing should apply in principle to faulted loops of substantially different radii. Unfortunately, at the large radii where the theory holds best and the graphs have the least scatter, the SFE term predominates so much in even the smaller of the loops that the results would be little, if any, better than those obtained by using single measurements and the best value of U_d.

Finally, the question arises of whether or not Silcox and Whelan's original assumption of an emission-controlled mechanism is valid. They concluded this by considering two cases of diffusion. In the first, they considered a loop of radius R at a distance L between the foil surfaces and the vacancies diffusing to the surface along the cylinder of the loop. Calculating the fluxes for emission and for diffusion control,

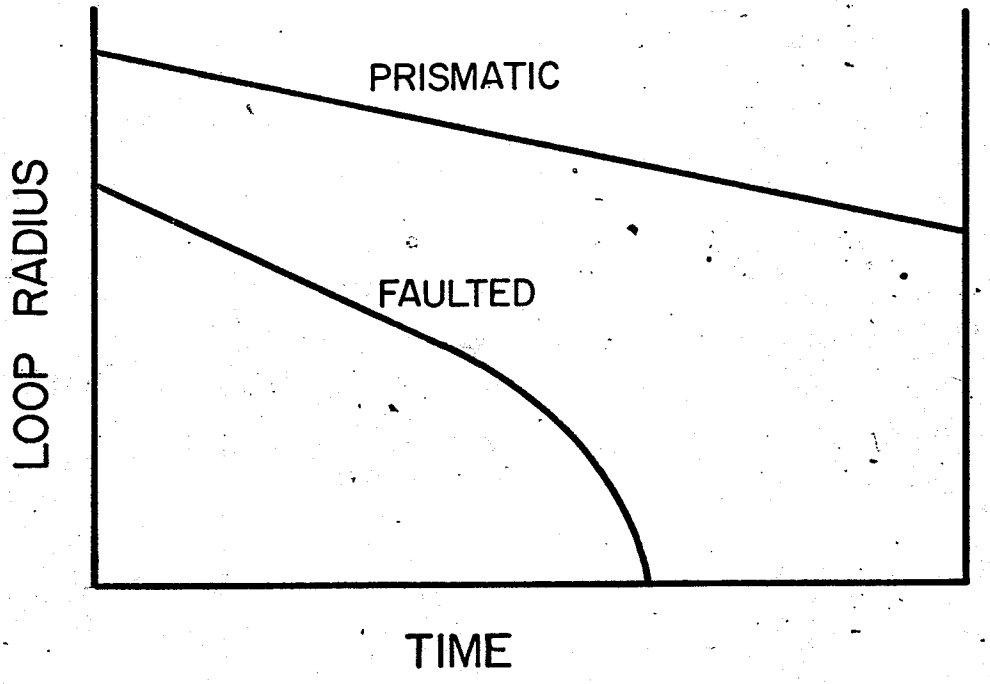

Fig.14a Schematic annealing curve for faulted and prismatic loops

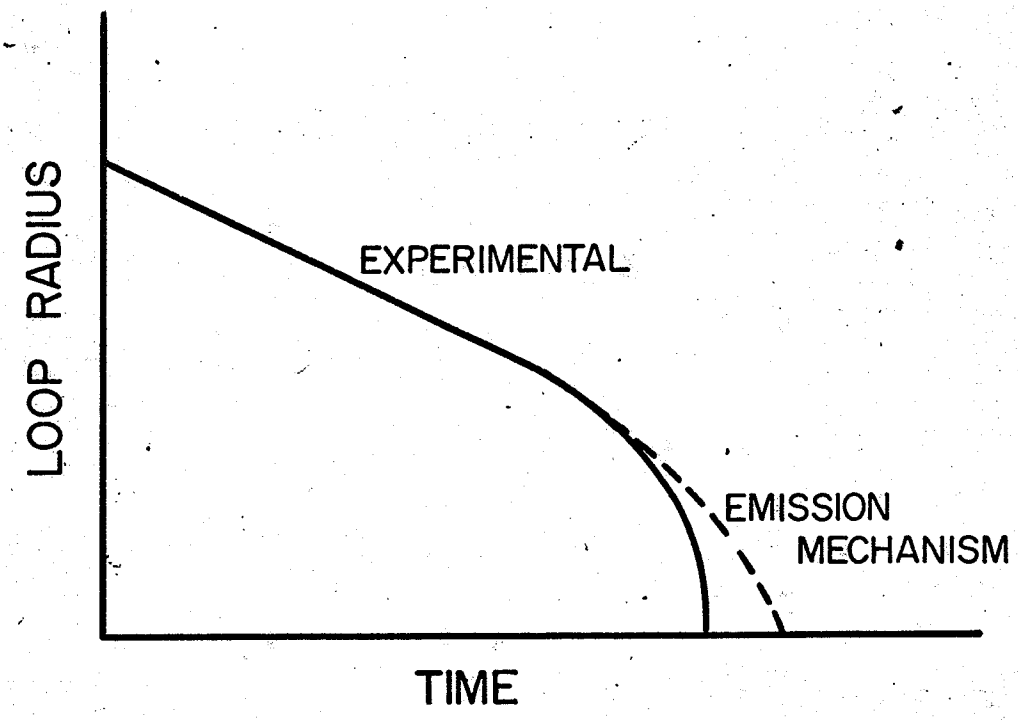

Fig. 14b Schematic annealing curve - experimental vs. theoretical

they found that the emission mechanism controlled annealing rate if $R/L < C_c$. The second case considered a small loop at the center of a sphere of radius L, with $L >> R$, i.e. spherical diffusion, and they found that emission mechanism governed if $C_c < 2$. For the first case, with loops of around 1000 Å in a typical foil of thickness about the same, R/L will probably be greater than the maximum value of $C_c = 1/2$, indicating diffusion control. However, the second case indicates emission control just as strongly and the authors concluded that this was the more likely case, i.e. a random distribution of small loops much smaller than the foil thickness.

Aside from the obvious criticism that loops of sizes roughly equal to the foil thickness have often been found, Seidman and Baluffi[161] questioned this model of the climb process, i.e. that $C_c = 1/2$ and that the emission rate per jog is sufficiently fast and correctly given by (3.12). They asserted that it is very difficult to specify the climb process at the dislocation core and avoided this assumption by using an "ideal source" dislocation loop in which the flux across a toroidal envelope around the loop is calculated. Their rather complex analysis led to an emission-controlled annealing rate roughly ten times greater than the diffusion-controlled rate, indicating the diffusion model as rate controlling.

Dobson et al[129] confirmed the diffusion control mechanism experimentally after coming to the conclusion that the two mechanisms have the same functional form of rate equation and differ only in the pre-exponential term (as mentioned earlier). This makes the difference between them too small to conclude anything on solely a theoretical basis.

They then examined three possibilities; a) emission control, b) diffusion control with R > t (foil half-thickness), and c) diffusion control with R < t. They calculated that the pre-exponential terms were 3D/b, D/b and 2D/b respectively ($D = \nu a^2 \exp(-U_d/kT)$). If, then, the diffusion mechanism was to be rate controlling, three experimental observations should result:

a) altered rates at different distances from the surface

b) the distance from internal sinks should also alter the rate

c) as the loop size decreases, the annealing rate increases, i.e. a switch from the cylindrical to the spherical case.

With regard to the first point, measurements on a number of large loops showed a variation in climb rate of roughly 10 per cent. The diffusion mechanism, being logarithmically dependent on depth in the foil, was found to allow a maximum variation of around 10 per cent for the depths measured, thus confirming the prediction. Regarding the loop to sink distance, it was observed that loops lying near dislocations annealed faster than those lying farther away, and that prismatic loops near faulted ones acted as sinks for the faster shrinking faulted loops, i.e. they annealed faster than those farther away from the prismatic loops. Finally, and most convincingly, a plot of loop radius vs. time showed a much more rapid decrease at small radii than predicted by the emission-controlled process. In other words, the complete annealing curve cannot be described by a single equation, as emission control predicts, i.e. the slope of (3.18) is not quite linear. The diffusion-controlled model, through its switch from cylindrical to spherical diffusion, does furnish this type of behaviour and is therefore likely to be the rate-controlling model.

Accepting this mechanism, a good experimental application of this method would be that of Hales et al[137] on Mg, in which the SFE was calculated from the growth of faulted loops. This growth, rather than shrinkage, is generally attributed[162,163] to oxidation of Mg atoms at the foil surface, resulting in a vacancy super-saturation by which the loops grow. The loops, in the form of stacking fault annuli as described in Sec. 3.2.1, climb as per Dobson et al[129] with

$$dR/dt = \frac{2\pi D}{B \ln(t/b)} \left(c_s/c_o - c_1/c_o\right) \quad \ldots\ldots\ldots\ldots\ldots \quad (3.21)$$

where c_s = vacancy concentration at the foil surface maintained by oxidation

c_1 = vacancy concentration in equilibrium with the loop = $c_o \exp \Delta F/kT$, where c_o is the equilibrium concentration of vacancies and

ΔF = the free energy change of the defect per vacancy emitted = $\pm\gamma B^2$ for the outer and inner loops respectively

Thus the two rates are:

$$dR/dt_{outer} = \frac{2\pi D}{B \ln t/b_1} \left(c_s/c_o - \exp \gamma B^2/kT\right) \quad \ldots\ldots\ldots \quad (3.22)$$

$$dR/dt_{inner} = \frac{2\pi D}{B \ln t/b_2} \left(c_s/c_o - \exp(-\gamma B^2/kT)\right) \quad \ldots\ldots\ldots \quad (3.23)$$

Now, for a high SFE, $\exp(-\gamma B^2/kT) \ll 1$, so that

$$dR/dt_{inner} = \frac{2\pi D}{B \ln t/b_2} \; c_s/c_o \quad \ldots\ldots\ldots\ldots\ldots\ldots \quad (3.24)$$

As evident, the inner loop grows at a faster rate than the outer one until they finally combine to form a prismatic loop, where it must be remembered

that two vacancies must be added to increase the loop area by B^2. Thus

$$dR/dt_{prismatic} = \frac{2\pi D}{2B \ln t/b_3} (c_s/c_o - (1 + \alpha b/R)) \quad . \quad . \quad . \quad . \quad . \quad . \quad . \quad (3.25)$$

Since these are large growing loops, $\alpha b/R \ll 1$ and can be neglected, thus

$$dR/dt_{prismatic} = \frac{\pi D}{B \ln t/b_3} (c_s/c_o - 1) \quad . \quad . \quad . \quad . \quad . \quad . \quad . \quad . \quad . \quad . \quad . \quad . \quad (3.26)$$

Comparing (3.24) and (3.26), the only unknowns are c_s/c_o and $\pi D/B$. Solving for these and substituting back into (3.22) gives a value for the SFE. Or, manipulation of (3.22), (3.24) and (3.26) yields[166]

$$\frac{dR/dt_{inner} - dR/dt_{outer}}{dR/dt_{inner} - 2dR/dt_{prismatic} \ln t/b_3/\ln t/b_1} = \exp\gamma B^2/kT. \quad . \quad . \quad . \quad (3.27)$$

If $\exp(-\gamma B^2/kT)$ is not neglected, it was recently found[166] that (+1) is added to the RHS of (3.27) and the SFE is decreased by about 20 per cent.

If the loops were shrinking rather than growing (i.e. no oxide film formed), an added advantage would be the absence of any doubts that the vacancy concentration gradient influences the growth rate more than the SFE, since $c_s/c_o = 1$ for shrinking loops. Also, the sign of $\pm\gamma B^2$ would be reversed so that the outer loop shrinks faster. There would be only two unknowns, $\pi D/b$ and γ, thus γ could be determined from (3.22) and (3.26) or (3.23) and (3.26), and the values should be identical.

From (3.27) above it is obvious that the critical factors are the annealing rate and temperature. Loop measurements are often difficult when they are asymmetrically shaped and even round loops often do not anneal in a continued circular fashion. In addition, the measuring error increases as the loop size decreases. Temperature accuracy in hot stage

microscopy has been estimated at ± 10°C at best[156,159,136] so that the normal procedure has been to immerse the specimen holder with thin foil in a carefully controlled bath, resulting in accuracies of ± 0.1[130] - 0.5°C[129]. Thus a typical error range is currently ± 20 per cent, which is not unreasonable. Again, results must be based on a reasonable number of measurements, as can be seen by the scatter in some of the studies[137]. From Table 8, compiling most of the work to date by this method, it is evident that the comparative technique leads to a much greater accuracy. The major assumption in this method is that the SFE, through F_c, does control, at least to a large degree, the shrinkage rate. Clarebrough et al[112] concluded that, for lower SFE metals such as Au and Cu, the jog nucleation and/or propagation rate could quite possibly exert more of a controlling influence due to the reduced magnitude of F_c, thus leading to erroneously low values. It would be interesting, though, to see how loop annealing values for these metals would compare to the established ones.

It might appear that an accurate value of the foil thickness would be required. However, using suitable values from Hales et al[137], a change in t of an order of magnitude (200 vs. 2000 Å) results in only a 15 per cent difference in SFE, thus an approximate value of t is all that is required. Of a more serious nature is B^2, the vacancy cross-sectional area, since it is directly related to the SFE. Some studies merely use the square of the interatomic distance[159], while others, apparently trying to account for the small lattice relaxation around a vacancy, reduce this by 10-15 per cent[136,139]. Some[129,164,137] make no mention at all of the value used. Thus the picture is rather vague

TABLE 8

SFE DETERMINATION - LOOP ANNEALING TECHNIQUE

MATERIAL (purity)	TECHNIQUE	SFE ($ergs/cm^2$)	REFERENCE
Al (99.97) (99.995)	emission-single measurements	int.=280±50 ext.=420	Edington and Smallman, 1965 (159)
Mg (99.95) Zn (99.9999)	emission-single measurements	280 ± 100 300 ± 150	Harris and Masters, 1966 (136)
Zn (99.999)	emission-single measurements emission-comparative diffusion-single measurements	290 220 230	Dobson and Smallman, 1966 (139)
Al (99.99)	diffusion-comparative	135 ± 20	Dobson et al, 1967 (129)
Al (99.99)	diffusion-comparative	ext.=1.3int.	Goodhew et al, 1967 (164)
Al-.65wt%Mg	diffusion-comparative	110 ± 20	Kritzinger et al, 1967 (165)
Mg (99.99) Zn	diffusion-comparative recalculation of data from (139)	125 ± 25 140	Hales et al, 1968 (137)
Al (99.999)	diffusion-comparative	110	Tartour and Washburn, 1968 (130)
Al-.65wt%Mg	diffusion-comparative, on same loop (double-faulted)	int.=110 ext.=157	Kritzinger et al, 1969 (60)
Mg	recalculation of data of (137)	102	Leighly, Jr., 1970 (166)
Cd (99.999)	diffusion-single measurements	205 ± 50	Westmacott, 1970 (167)

in applying an accurate correction factor, if any is needed at all, and none of the studies discuss the matter. However, the major advantages of the loop method are still: a) it is a direct method, b) it can be applied to high SFE metals, and c) it is applicable to solid solutions in which loops can be formed. The latter point is quite intriguing as the method could then be used in conjunction with the low SFE direct methods for a complete determination over the entire SFE range which can occur with alloying, in this way eliminating some of the rather inaccurate extrapolations of the past. Possibly the main drawback is the difficulty in creating the necessary loops. The experimental difficulties are controlled by such factors as quench rate, specimen purity, etc. and will be discussed shortly.

3.4 EXPERIMENTAL PROCEDURE

3.4.1 ZIRCONIUM

Reactor grade crystal bar Zr of roughly 99.9% purity (see Table 9) was obtained through the Whiteshell Nuclear Research Establishment at Pinawa, Manitoba. The Zr was reduced directly from 1/2 in. rod to sheets of 0.0075-0.015 cm. by cold rolling. Strips of 0.5-1.5 cm. by 6-10 cm. were cut out and cleaned ultrasonically in ethanol.

Initially the strips were annealed in sealed Vycor tubes at the quench temperature for 1-2 hr. before quenching. This was later changed to annealing under a dynamic vacuum of $\sim 1 \times 10^{-5}$ torr at temperatures of 830-845^{o}C for times of 1.5-40 hr. for degassing purposes. The surface layer of the foil was then removed by chemical polishing in a 45 nitric-45 lactic - 10 hydrofluoric acid solution.

TABLE 9

ANALYSIS OF CRYSTAL BAR ZIRCONIUM

ELEMENT	AMOUNT (ppm)	ATOM VOLUME ($Å^3$) (168)	MELTING PT. (^oC) (169)	SOLUBILITY @ 850^oC (at.%) (170)
Zr	-	23.3	1852	-
Al	25	16.6	660	8
B	0.2	7.7	2030	0
C	40	5.7	3727	2
Cd	0.3	21.6	320	16
Co	5	11.13	1495	0
Cr	10	12.0	1875	0
Cu	25	11.8	1083	0
Fe	105	11.8	1536	0
H	7	-	-	0
Hf	132	22.2	2222	100
Mg	10	23.2	650	small
Mn	10	12.2	1245	0
Mo	10	15.6	2610	0
N	36	-	-	22
Nb	100	18.0	2468	0
Ni	10	10.9	1453	0
O	130	-	-	29
Pb	5	30.3	327	0
Si	40	20.0	1410	0
Sn	10	27.65	232	5
Ta	200	18.0	2996	0
Ti	20	17.65	1660	100
U	0.5	20.8	1132	0
V	5	13.9	1900	small
W	25	15.85	3410	0
Zn	50	15.2	420	0
	988.5			

The encapsulation procedure for the furnace quenches was; evacuation to 1 x 10^{-5} torr, followed by several argon flushes (industrial grade), and finally sealing off the tube with varying amounts of argon (0-200 mm pressure). Additional precautions to reduce hydriding were taken; wrapping with Ta or Zr foil, inclusion of Zr shavings in a torch-heated portion of the tube outside the furnace, and/or double sealing.

Several furnace quenches were attempted from the BCC β region (from 1100-1250^{o}, as high as facilities permitted), and several from the HCP α region (from 840-858^{o}), into either 25^{o}C or iced water, some by breaking the tube and others by leaving it sealed. A few quenches into liquid N_2 were also attempted.

In an attempt to reduce hydriding and increase the quench rate, a switch was made to a bell jar attachment on a Balzar's Replicating Unit, where the foils were heated by electrical resistance under a dynamic vacuum (photos. 1 & 2). Temperature measurement was by means of Chromel-Alumel wires spot-welded on the foils and quenching was by admitting He gas (industrial grade) into the chamber through a specially-constructed feed-in and simultaneously cutting off the DC current. The He was first passed through a Cu coil in a Dewar flask to which liquid N_2 could be added. Thus a typical quench could consist of a 30 min. anneal at 700-800^{o}C and a quench from 830-850^{o} either into a static atmosphere of cooled He, a steady flow of either cooled or uncooled He or a "blast" of He (by increasing the pressure and opening the control valve as the current was shut off).

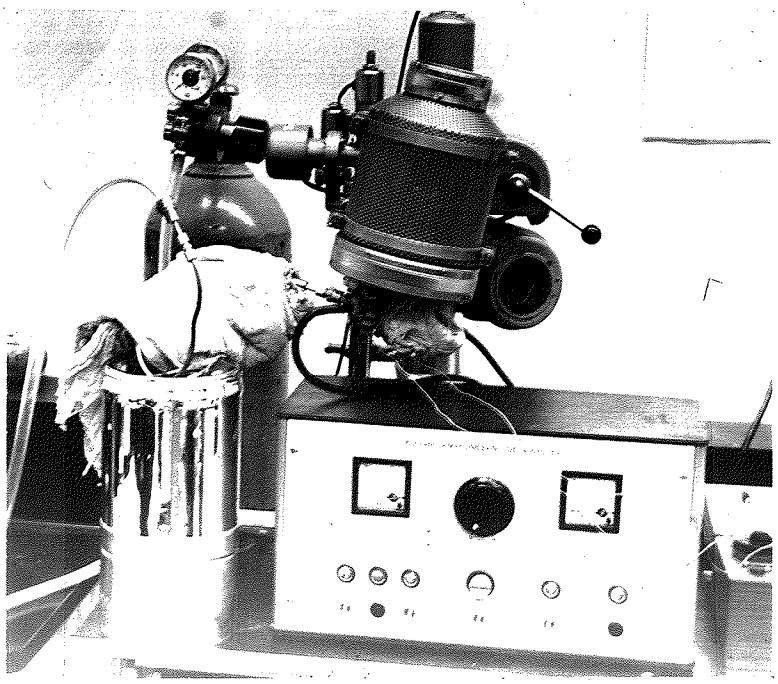

Photo.1 Apparatus for He quenching of Zr

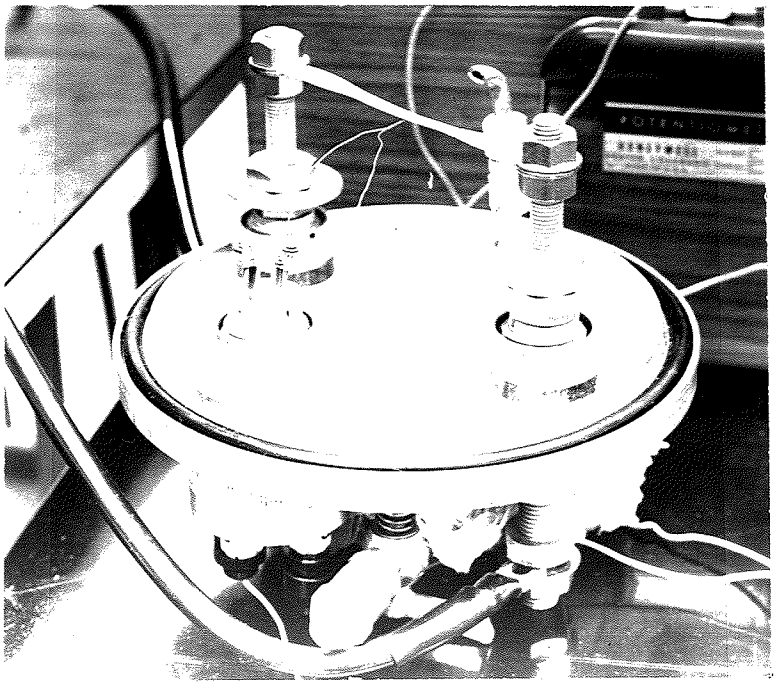

Photo.2 Close-up of Al foil ready for heating and quenching

An attempt was made to measure this quench rate by feeding the amplified thermocouple signal into a Tektronix Storage Oscilloscope. Several specimens were also prepared from rod that had been given 1-4 passes at 3/4-3 in./hr in an MRC Zone Refiner. A portion was sent to WNRE at Pinawa for partial impurity analysis.

Thin foils were prepared, after varying times of room temperature ageing, by the dual-jet electropolishing technique in a bath of 10 perchloric- 90 acetic at 10-15°C, a voltage of 18-20 v. and a jet flow setting of 3-4. The foils were immediately washed in acetic acid and then in ethanol (both cooled) and examined in a Phillip's EM-300 electron microscope. In addition to normal examinations several foils were heated in a special heating stage at temperatures of 110-250°C for times of a few minutes to an hour.

3.4.2 ALUMINUM

In order to check on the efficiency of the He quench, some foils of Al were similarly quenched, since many studies have produced quenched-in vacancy loops in this metal.

Al of 99.995 and 99.999% nominal purity obtained from the United Mineral and Chemical Corp. was used. The loop-producing abilities of the two grades were first checked by quenching specimens through techniques approximating those in previous studies. Specimens of 1 x 5 x 0.0075-0.015 cm were cut from cold-rolled 99.995 sheet, annealed 20-30 min. at 600°C in air and quenched by rapid extraction from the furnace into either room temperature water (once or five times) or room temperature oil. When very few loops were observed, this was switched to quenching from a vertical

furnace by cutting the wire holding the specimen, allowing the weighted foil to fall into the quench bath located directly below the mouth of the furnace. At the same time the specimen width was changed to 0.5 cm and the 99.999 material was used.

Longer strips, but with the same 0.5 x 5 cm gage length were quenched from close to 600^{o} in the Balzar's apparatus (in air) under a liquid N_2-cooled He blast once or five times. All ageing was at room temperature for at least 24 hours. Thin foils were prepared in a 20 perchloric- 80 ethanol bath at 5-15^{o}C, at a voltage of 19 v. and a jet flow of 3-4. Washing was in cooled ethanol. A few of these foils were also heated in the heating stage of the microscope.

3.5 OBSERVATIONS

From the outset, severe hydriding problems were experienced with the Zr specimens. Forming the vast majority of the second phase particles, the hydrides ranged from thin platelets usually present in the more rapidly quenched specimens (photo. 3), to the larger growths common to furnace-cooled specimens (photo. 4). These were definitely established as hydrides since they showed the same tetragonal lattice diffraction patterns found by Bailey[171]. It was discovered that reducing the final argon content in encapsulation to zero greatly reduced this problem. Wrapping with Ta or Zr foil and double sealing also helped but to a lesser extent. It was soon discovered that the dynamic vacuum annealing reduced hydriding substantially, although the degree of reduction did not increase appreciably with time, probably due to a limit imposed by the extent of the vacuum. Any slight oxide coating was easily removed by the chemical polishing.

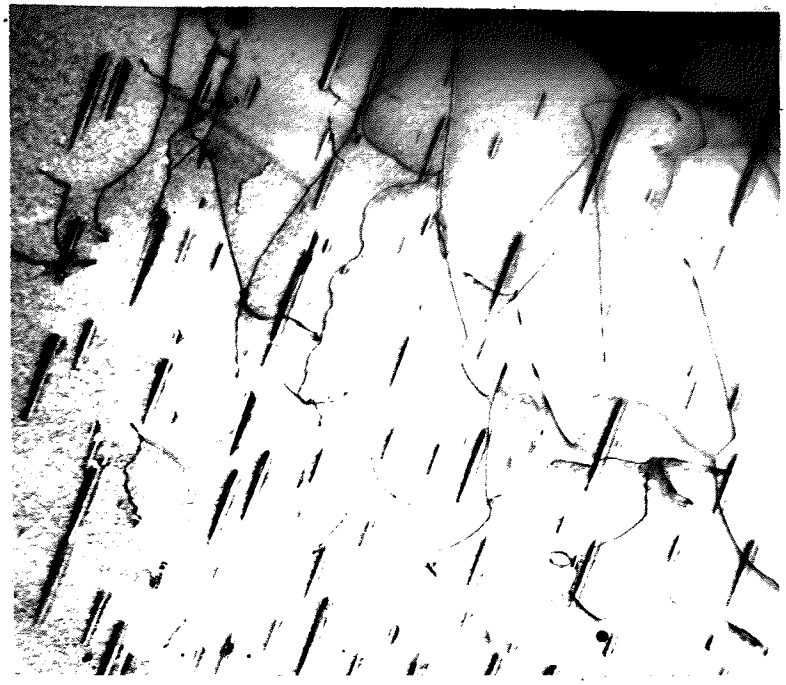

Photo.3 Typical hydride distribution in Zr quenched in sealed tube from 1250°C to 0°C water

X 40000

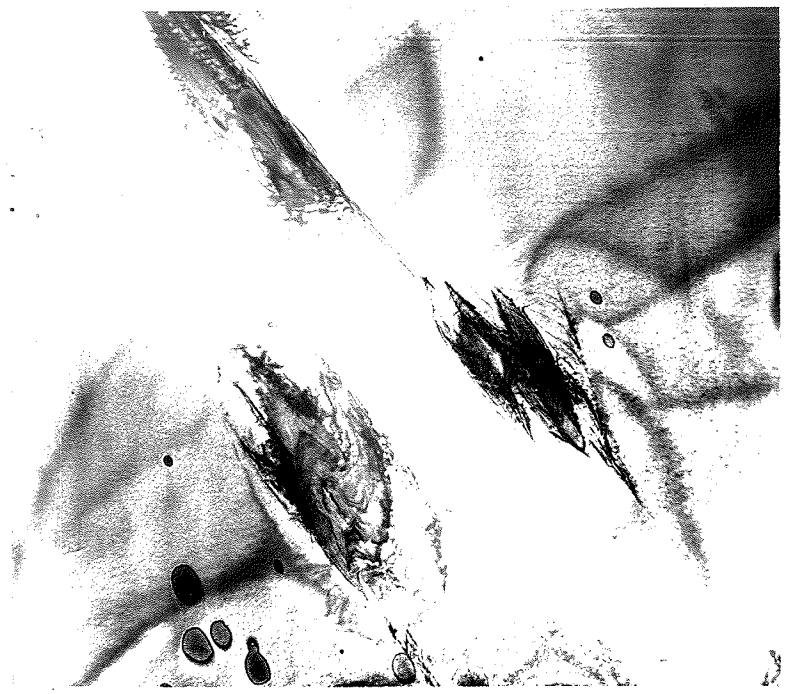

Photo.4 Large hydrides in Zr annealed 5 hr at 840°C and furnace cooled

X 28000

Virtually all of the quenches from the β temperature region showed a fairly high dislocation density, with many regular dislocation distributions (photo. 5) and networks (photo. 6). Even after the dynamic annealing, resulting in much shorter holding times at the quench temperature, some hydriding was still noticeable in all furnace quenches, with specimens that had been quenched by breaking the tube in water showing a very high hydride density. The quenches into liquid N_2 gave indications of being rather slow, as has been previously noticed[172].

The switch to the Balzar's apparatus led to new technical problems, most notably that of the thermocouple melting out or the strip melting through due to variations in foil cross-section. Even more damaging, the He used appeared to be sufficiently impure to drastically contaminate the specimen. A vacuum quenched specimen showed a very low impurity particle density whereas a He quench on the same strip resulted in a distribution as in photo. 7. Also, the attempt to measure the quench rate was unsuccessful as a "noise" signal from the unit itself completely masked the thermocouple signal and could not have been corrected without alteration of the equipment.

Most importantly, no loops were observed from any of the quenches, either after room temperature ageing or higher temperature ageing in the heating stage of the microscope. Small impurity clusters often gave loop-like contrast due to their strain fields, although dark field electron microscopy always revealed their true nature. This is demonstrated in photo. 8.

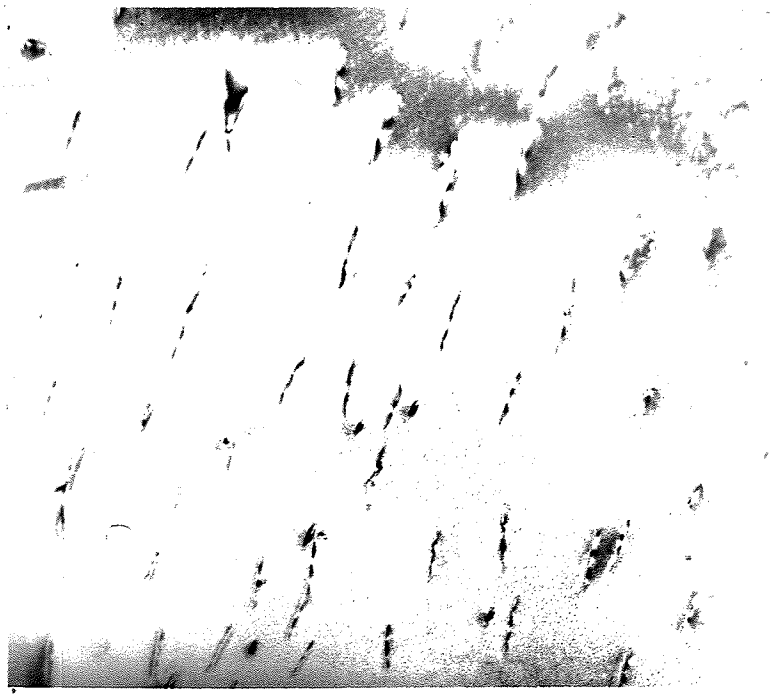

Photo.5 Uniform dislocation distribution in Zr
air quenched from 1020°C
X 40700

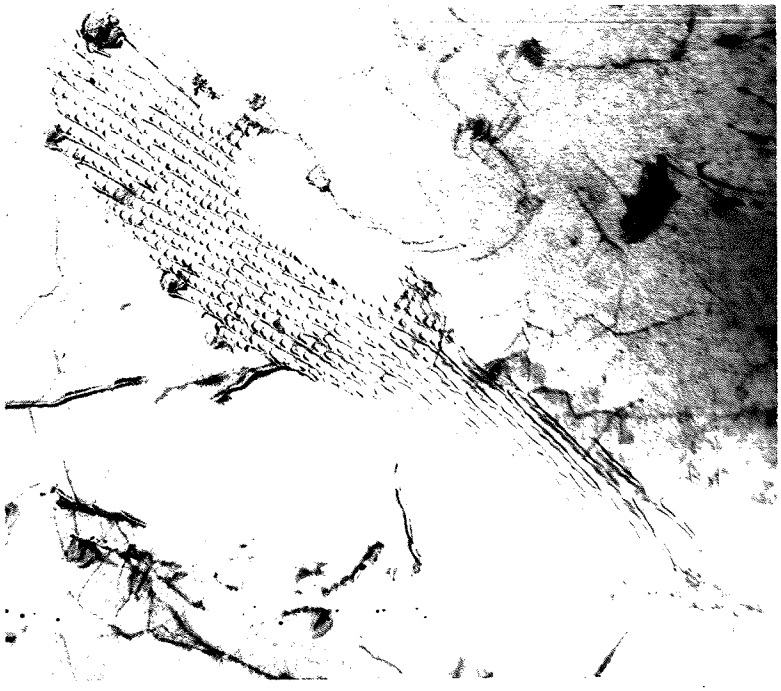

Photo.6 Dislocation network in Zr quenched in
sealed tube from 1250°C to 0°C water
X 49000

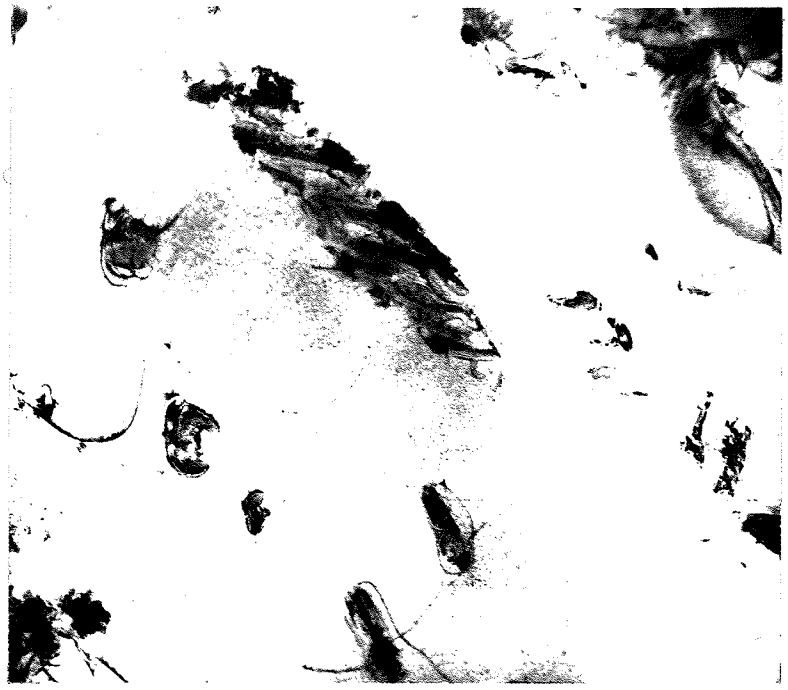

Photo.7 Large impurity clusters (probably hydrides)
in Zr quenched in He blast
X 33600

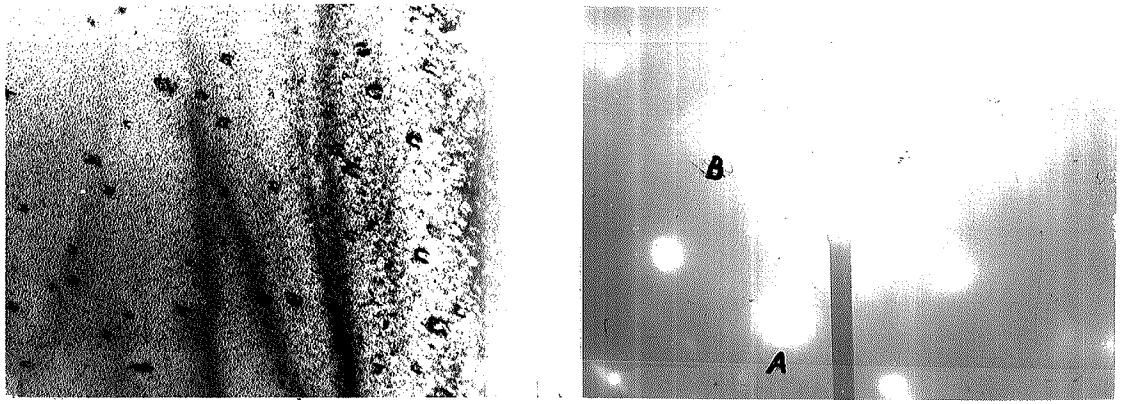

a) b)

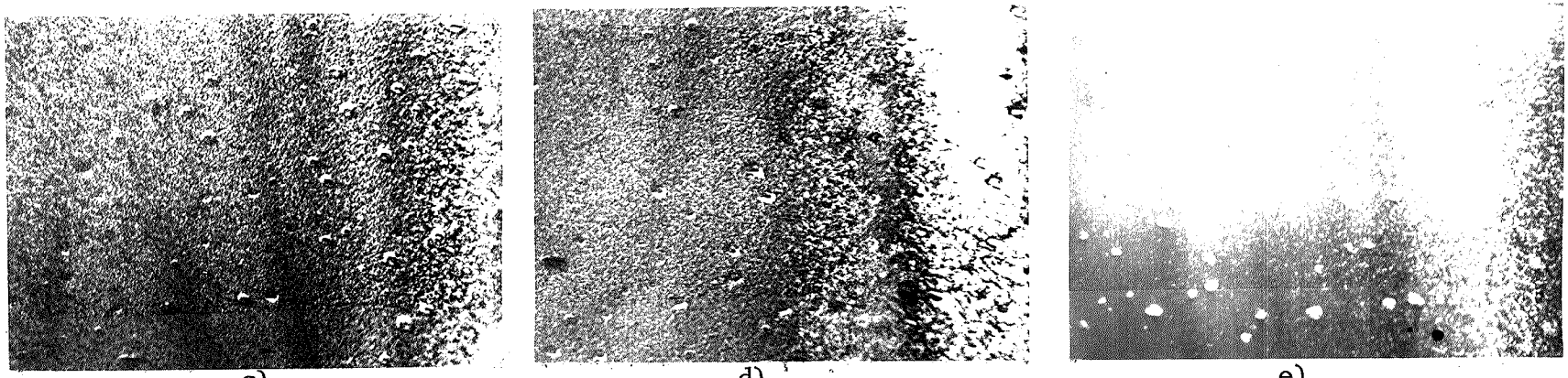

c) d) e)

Photo.8 Zr quenched from 856°C to liquid N_2 (in air)

a) bright field
b) selected area diffraction pattern
c) dark field from circled spot
d) dark field from spot A
e) dark field from spot B

X 41600

Due to the thinness and softness of the specimens, foil handling damage was very difficult to avoid and long straight dislocations in the thin areas (photo. 9) and dense tangles in the thicker areas (photo. 10) were often widespread. In addition to handling dislocations, the second phase particles often acted as dislocation sources due to their misfit strain with the lattice (photo. 11).

Some interesting defects which appeared to be stacking faults were observed in one specimen (photo. 12). Unfortunately, the foil was lost due to a mishap before they could be analyzed and they were not seen in any other specimen (although similar quenches were subsequently tried). Similar defects were seen in furnace-cooled foils, but these proved to be annealing twins from their symmetric bright field-dark field fringe contract[173] (photo. 13).

Finally, although the zone-refined specimens did appear to result in somewhat cleaner foils, the partial impurity analysis showed the refining effect to be minimal, with the 4 pass-3 in./hr sample showing slight Al and Fe decreases and no change in Ta, Nb and Hf impurity levels. The 4 pass-3/4 in./hr sample fated even worse, showing a tenfold O_2 increase and no change in Al, Fe, Nb and Hf.

The Al studies demonstrated how critical the quenching procedure, specimen size and purity can be. Pulling 99.995 specimens from the furnace into the quenchant resulted in no loop formation, probably due to the temperature decrease before contacting the quenchant (approximately 10% of T_q[172]). Even using the vertical furnace, the loop density was very low for 1 cm wide foils (although both faulted and perfect were present). Decreasing this to 0.5 cm increased the loop density

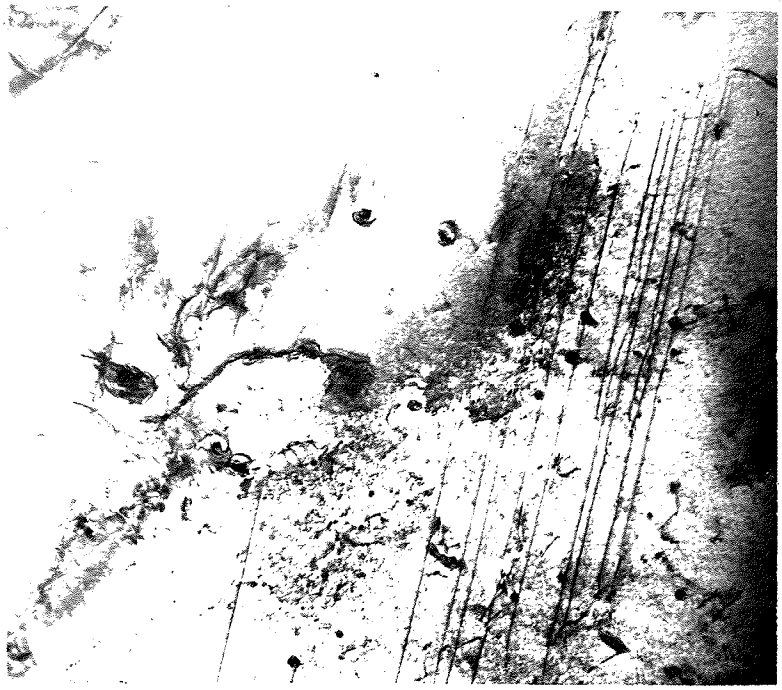

Photo.9 Probable foil handling dislocations in Zr common to thin areas of many foils

X 20000

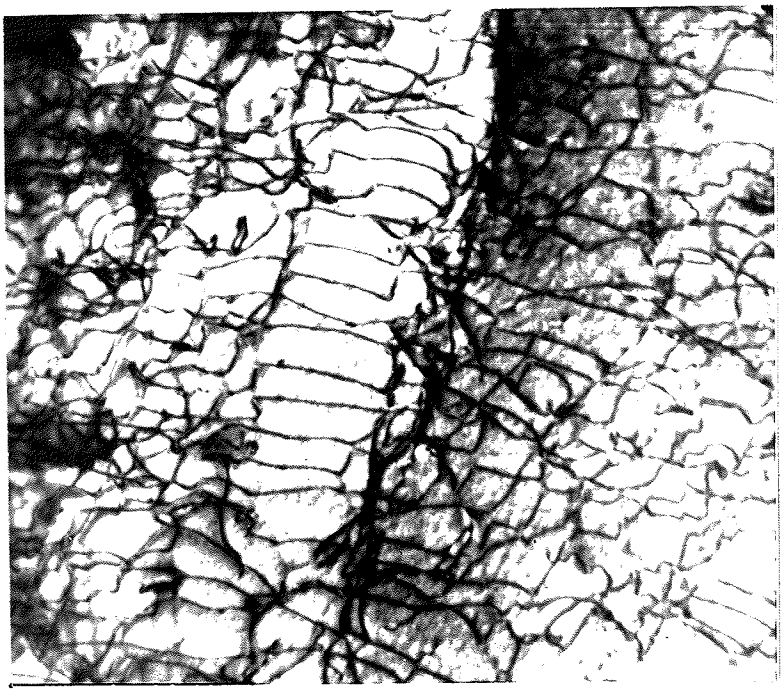

Photo.10 Dense dislocation tangles in Zr common to thicker areas of many foils

X 54000

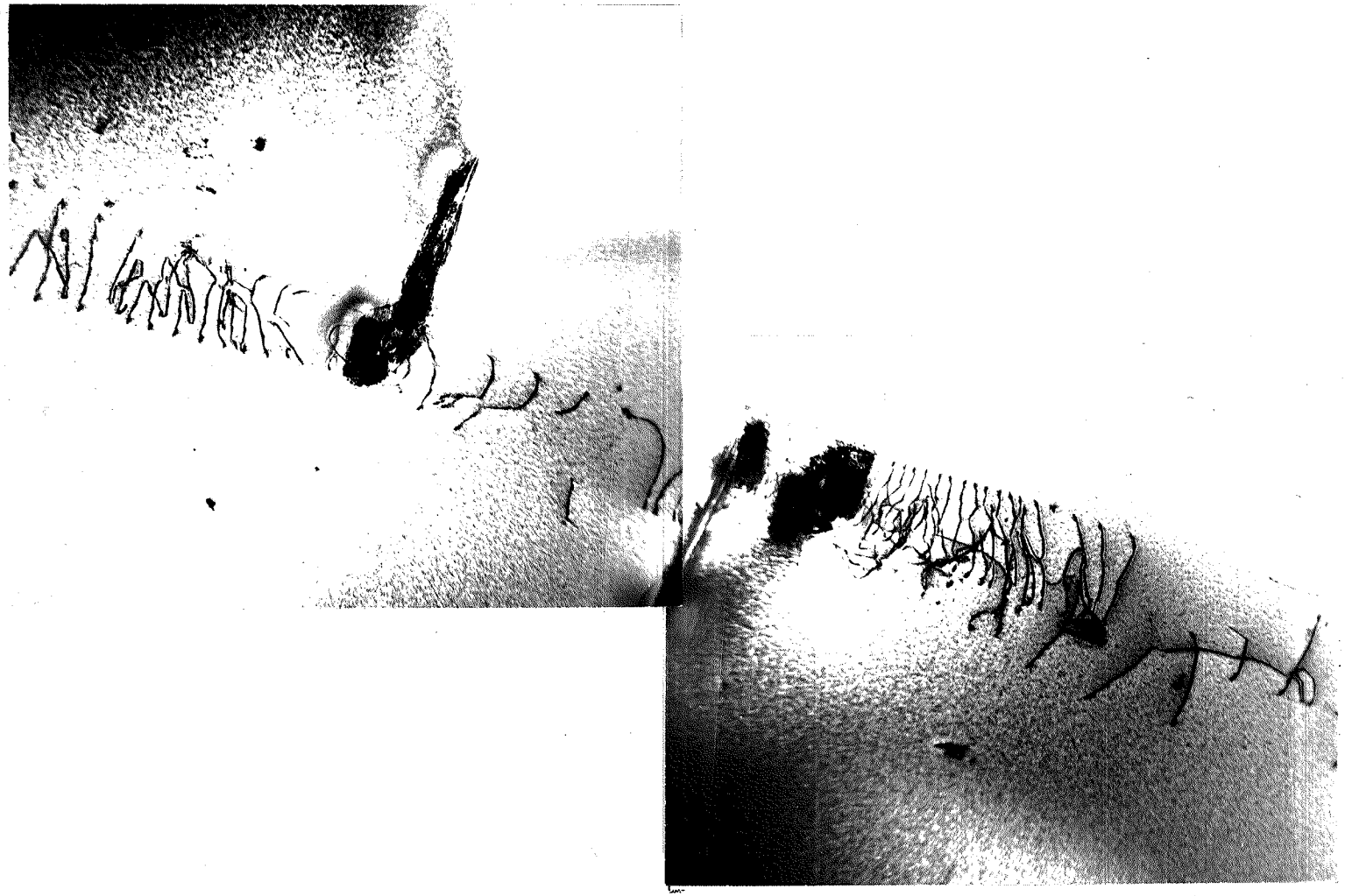

Photo.11 Particles as dislocation sources in Zr
furnace cooled from 840^{o}C
X 21000

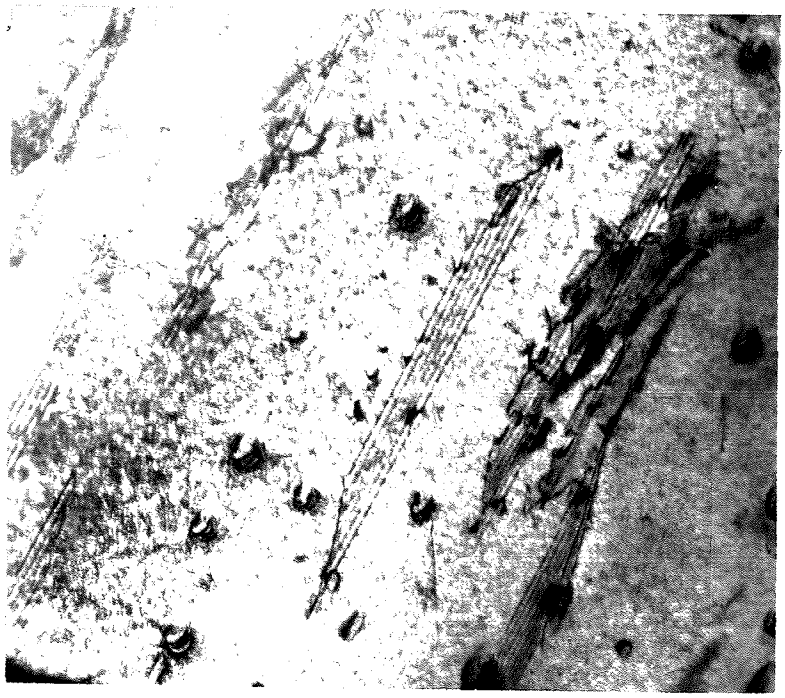

a)

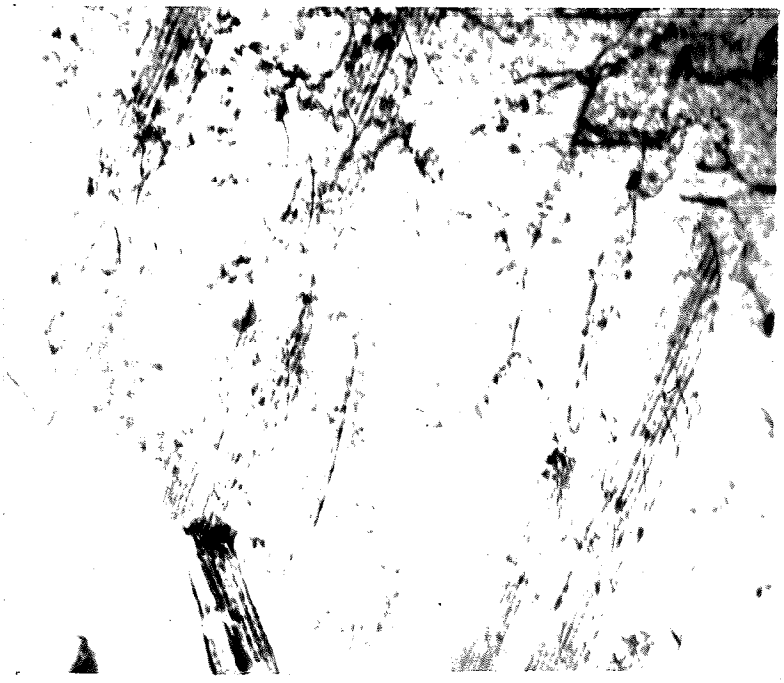

b)

Photo.12 Possible stacking faults in Zr quenched in sealed tube from 1250^{o}C to 0^{o}C water

X 49000

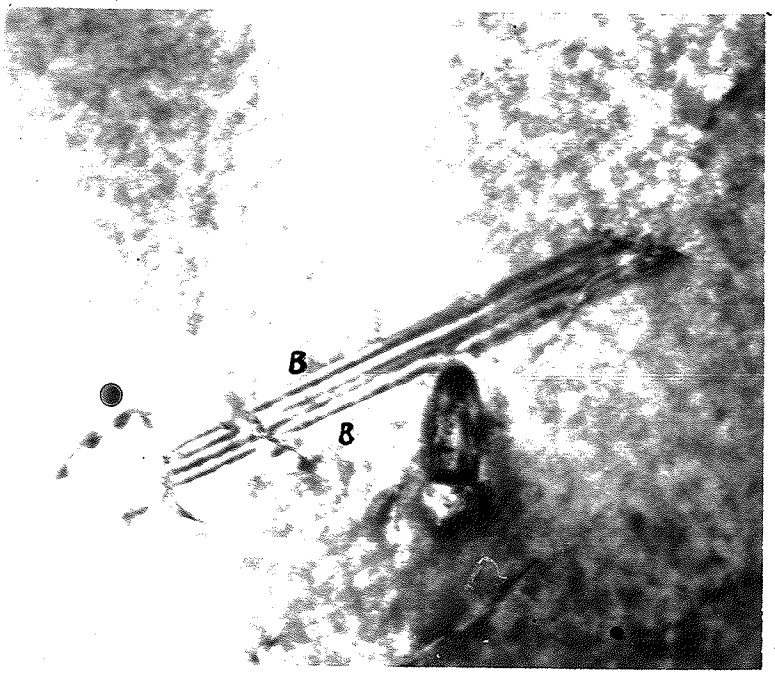

a)

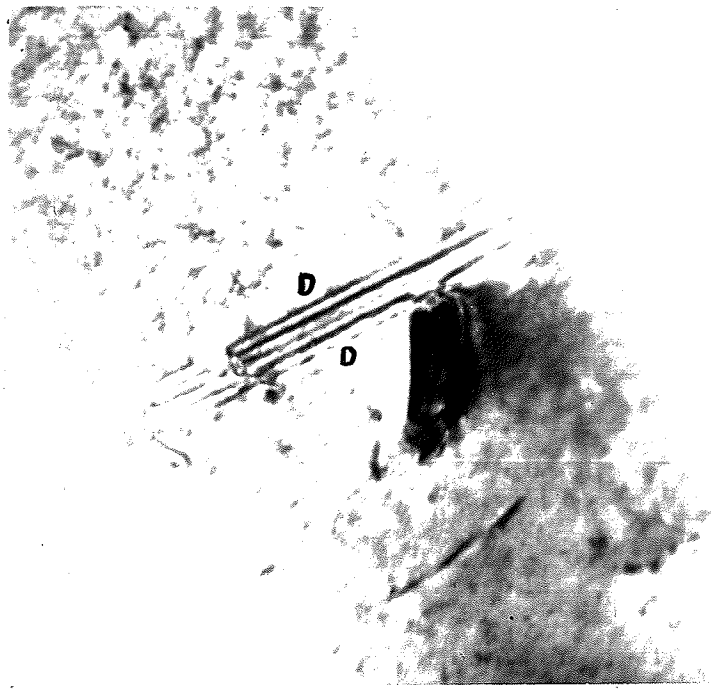

b)

Photo.13 Annealing twin in Zr annealed 5 hr at 840°C and furnace cooled a) bright field
b) dark field
X 76000

greatly, as did increasing the purity (compare photos. 14 and 15). The water quenches resulted in a high density of predominantly perfect loops, while the oil quenches resulted in a lower density of predominantly faulted loops.

The Balzar's quenches were even more difficult than the Zr ones with regard to the melt-through problem (especially in multiple quenches), since they were so near the melting point (0.9 mp). It was also noticed that the terminals holding the specimen often heated up somewhat, thus decreasing the quench efficiency. Typical results for a single He quench of 99.999 material are shown in photo. 16. Surprisingly, a multiple quench showed much poorer results, pointing to the difficulty of obtaining consistent reproducibility with this technique. It should be noted that, in all cases, the loop density varied greatly, from large areas with no loops at all to areas with densities as in photos. 14-16.

3.6 DISCUSSION

Providing that the Zr analysis is correct there are a number of possibilities to account for the hydriding experienced in this work:

a) impure argon or helium
b) diffusion into the tube while sealing off
c) backstreaming of cracked hydrocarbons from the diffusion pump
d) slow diffusion through the sealed tube in the furnace
e) poor vacuum levels
f) electropolishing or chemical polishing

a)

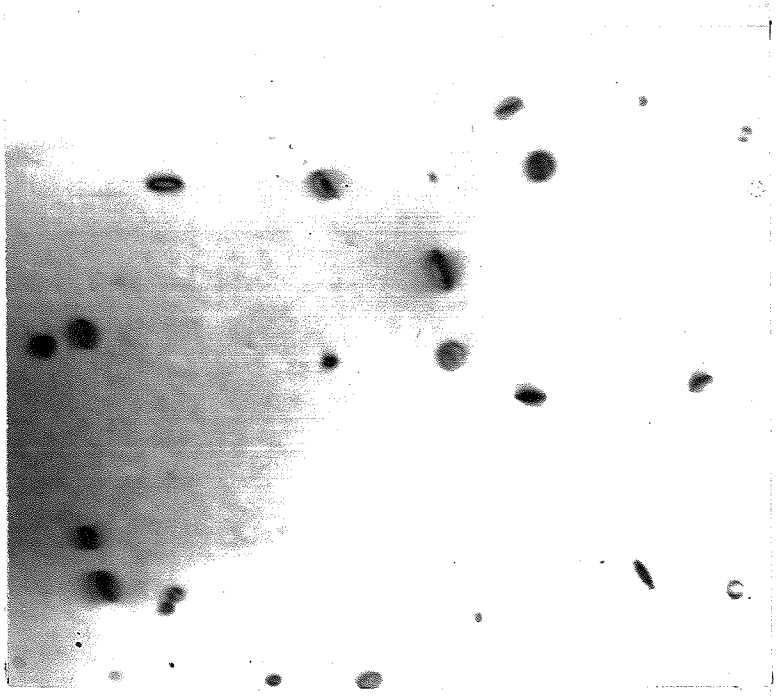

b)

Photo.14 Loop distribution in 99.995 Al quenched from $600^{o}C$ to $25^{o}C$ water a) once
b) five times
X 52500

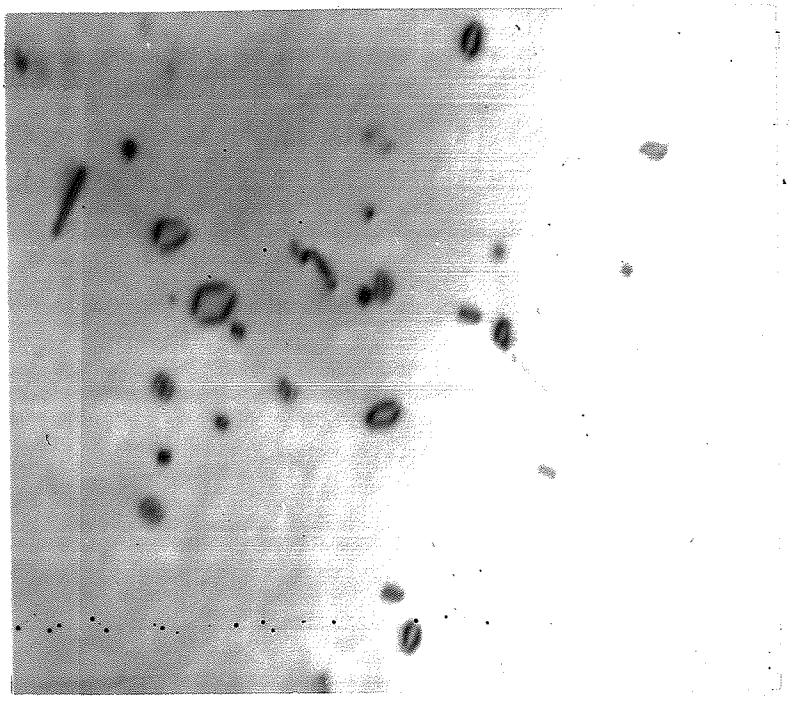

a)

b)

Photo.15 Loop distribution in 99.999 Al quenched from $600^{o}C$ to $25^{o}C$ water a) once
b) five times
X 52500

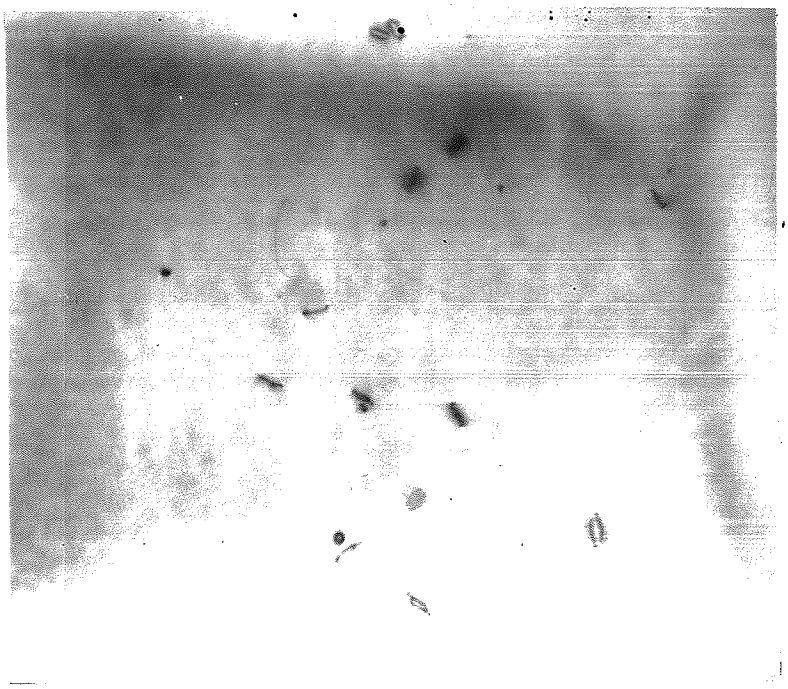

a)

b)

Photo.16 Loop distribution in 99.999 Al quenched once from approximately 600°C by pre-cooled He

X 52500

b), c) and d) are likely to be rather minor while polishing hydrides are generally small surface hydrides[171] that can be greatly reduced by careful polishing. Thus the main causes are likely a) and e). Both can be improved although e) can be severely limited by the capability and condition of the equipment. As noted earlier, a dynamic vacuum is much preferred to a static one and could greatly reduce gaseous impurities over a long anneal providing the degree of vacuum is very high, e.g. of the order of 10^{-7} - 10^{-8} torr for Zr[186,187]. Therefore, using Zr of low initial H_2 content, high vacuum dynamic annealing, a high purity gas quenchant and careful electropolishing, the hydriding should be severely curtailed.

As already stated, no quenched-in vacancy loops of any kind were observed in any of the Zr specimens. There are five major factors that influence the formation of these loops:

a) ageing procedure

b) specimen size

c) quench temperature (T_q)

d) quench rate

e) specimen purity

The ageing procedure used after quenching appears to be very important for determining the optimum loop size and distribution as seen in Table 10, which is a partial summary of many recent studies on quenched-in defects, or from the comprehensive analysis of Al ageing by Kiritani et al[188]. It would appear, though, that room temperature ageing for a period of a day or so should result in at least some loop formation. The

optimum conditions, i.e. those giving large, fairly isolated loops, can then be obtained by further ageing at higher temperatures or for longer times. It should be noted from Table 10 that the ageing temperature is higher for higher m.p. metals, although it could be argued that for metals with anomolously high diffusion coefficients, like Ti and Zr, it would not be as high as for, say, Au or Ni.

The specimen size should be as thin and narrow as possible since this makes the quench more uniform, reducing quenching strains. Both of these dimensions are, however, limited by technical difficulties such as the melt-through problem, deformation from the quenchant and/or electro-polishing procedures. A 'range of compromise' would appear to be roughly 0.0075 - .015 cm by 0.3 - 0.6 cm. In this regard it should be noted that the He-quenched Al foil (photo. 16) was slightly thicker (.0125 cm vs. .0106 cm) than the water-quenched foils (photos. 14 & 15).

From the earlier discussion in Sec. 3.2 it is obvious that T_q should be very close to the m.p. in order to start off with the maximum number of vacancies for loop formation. Thus, as seen in Table 10, T_q is usually around 0.9 m.p. As T_q nears the melting point the number of clusters nucleated increases, leading to a higher density of smaller loops. This is not, however, desireable for the loop annealing method, lowering T_q decreases the number of clusters, resulting in fewer loops, but of greater size, since there is still an appreciable vacancy 'reservoir' to draw upon. However, due to the exponential dependence of the vacancy concentration with temperature, this reduction in T_q cannot go on indefinitely since a point is soon reached where there are not enough single

TABLE 10

SUMMARY OF QUENCH-INDUCED DEFECTS

MATERIAL	t(cm)	QUENCH PROCEDURE (^{o}C)	AGEING	RESULTS(d is d_{avg} in Å)	REFERENCE
Al(99.999)	.005	620 (.94 mp) to -10 iced brine, in air	-----	only prismatic loops	(150)
Al(99.99)	.0075	600 (.91 mp) to iced brine	room temp.	only prismatic loops	(156)
Al(99.9999)& Al(99.995)	.0075	1) heating until contact with 25^{o} water 2) heating, then drop into 25^{o} water	-----		(155)
a) (99.9999)		from 650 by 1)		prismatic, d=325	
		from 600 by 1)		prismatic, d=400, 13% faulted, d=875	
		from 520 (.79 mp) by 1)		prismatic, d=275, 22% faulted, d=900	
		from 650 by 2)		prismatic, d=400, 50% faulted, d=1200	
		from 520 by 2)		prismatic, d=500, 65% faulted, d=1500	
b) (99.995)		from 650 by 1)		prismatic, d=250	
		from 520 by 1)		prismatic, d=500	
		from 650 by 2)		prismatic, d=400	
		from 520 by 2)		no loops	
		from 650 by 1) twice		prismatic, d=300, 2% faulted, d=750	
		from 650 by 2) twice		prismatic, d=400, 27% faulted, d=900	

* All Al quenches in air

TABLE 10 (continued)

MATERIAL	t(cm)	QUENCH PROCEDURE (^{o}C)	AGEING	RESULTS (d is d_{avg} in Å)	REFERENCE
Al(99.999)	----	640 (.97 mp) to 25^{o} water	-----	faulted, d=250	(174)
		520 to 25^{o} water		faulted, d=1000	
Al(99.995)& Al(99.97)	.0125		24 hr at 25^{o}		(159)
a) (99.995)		600 to room temp. oil		prismatic, d=2000, 88% faulted, d=3000	
		600 to room temp. water		prismatic, d=700, 5% faulted, d=700	
		600 to room temp. water 5 times		prismatic, d=600, 50% faulted, d=800	
b) (99.97)		650 to room temp. oil		prismatic, d=1000, 91% faulted, d=1000	
		600 to room temp. oil		prismatic, d=2000, 92% faulted, d=3000	
		600 to room temp. water		prismatic, d=700	
Al(99.99)	.01	600 to 50^{o} water or room temp. oil	1 hr at 50^{o}	faulted and prismatic	(129)
Al(99.999)	.02	610 (.925 mp) to 100^{o} water	-----	mostly faulted	(130)
Al & Al-In(at%)	.0125	600 to 45^{o} $CaCl_2$			(175)
a) Al-.006In			5 min at 20^{o}	very low density of prismatic	
			1 hr at 50^{o}	high density of small prismatic	
b) Al-.0375In			2 hr at 100^{o}	lower density of larger prismatic	
c) zone-refined (Z.R.) Al			1 hr at 50^{o}	medium density of large faulted	
Al-.65wt%Mg	.01	600 to silicone oil	room temp.	mostly faulted	(60)
Al-3wt%Mg	.0125	550 (.83 mp) to silicone oil	room temp.	mostly prismatic	(63)

TABLE 10 (continued)

MATERIAL	t(cm)	QUENCH PROCEDURE (^{o}C)	AGEING	RESULTS (d is d_{avg} in Å)	REFERENCE
Au(99.999)	.015	875 (.82 mp) to 25^{o} brine in air and deformed	-----	tetrahedra	(176)
Au(99.999)	.01	1000 (.94 mp) to ice water, in air	1-4 hr at 0-150^{o}	tetrahedra, largest at 100^{o}	(177)
Z.R. Au doped with Cd & Zn	.0037	980 (.925 mp) to -35^{o} bath, in air	-----	tetrahedra, l=400-1200	(178)
Au(99.9995)	-----	900 (.85 mp) to 25^{o} water	1 hr at 100^{o}	single, double tetrahedra and faulted loops, l=100-600	(179)
Au & Au-Pt(at%)	.005	940 (.89 mp) to -5^{o} $CaCl_2$			(180)
a) Au(99.999)			1 hr at 100^{o}	tetrahedra and high density small faulted loops .	
b) Au-1Pt			1 hr at 100^{o}	same as a)	
c) Au(99.999)			1 hr at 200^{o}	larger loops and tetrahedra	
d) Au-1Pt			1 hr at 200^{o}	slightly larger, prismatic also	
Mg(99.95)	.025	625 (.96 mp) to ice water, in argon	-----	mostly large faulted	(136)
Mg(99.9999) (99.9997) (99.95)	.0075		-----		(181)
a) (99.9999)		550, 500, 450 (.85, .77, .69 mp) to 20^{o} oil*		mostly perfect on prism planes with increasing size and decreasing density as T_q decreased	
b) (99.9997)		same as a)		mixture of perfect and basal faulted	
c) (99.97)		500 to 20^{o} oil		mostly large faulted	

* Measured as 21-24000 ^{o}/sec. A liquid N_2-cooled He blast (at 4 atmospheres) was 17-23000 ^{o}/sec.

TABLE 10 (continued)

MATERIAL	t(cm)	QUENCH PROCEDURE (^{o}C)	AGEING	RESULTS (d is d_{avg} in Å)	REFERENCE
Mg(99.99)	.02	620 to ice water, in argon	20 min at 100^{o}	mostly large faulted	(137)
Mg(99.99)	.01	630 to ice water	-----	mostly large faulted	(182)
Zn(99.999)		400 (.95 mp) to ice water	-----	mostly large faulted	
Zn(99.9999)	.0125	415 (.99 mp) to ice water	-----	mostly large faulted	(136)
Zn(99.999)	.0125	400 to iced brine	room temp.	mostly faulted	(139)
Ni(99.96 & Z.R.)	.0075	1400 (.96 mp) to 25^{o} oil, in 10^{-6} torr vacuum	1 hr at 350^{o}	tetrahedra, faulted and prismatic loops, in Z.R. only	(46)
Ni(Z.R.)	.0016	1200 (.83 mp) to liquid-N_2 cooled He	-----	low density of small faulted, increasing with increasing passes	(183)
Cu-Al(at%)	.0125		-----		(184)
a) Cu-9Al		(?) to 20^{o} oil, in CO		large faulted, d=5000	
b) Cu-15.6Al		(?) to 20^{o} oil, in argon		large faulted, d=5000	
Cu_3Au(99.98)	.005	900 (.94 mp) to 0^{o} silicone oil, in vacuum	1 hr at 100^{o}	prismatic, d=900, 65% faulted, d=700, tetrahedra, l=800	(185)
			1 hr at 150^{o}	prismatic, d=800, 65% faulted, d=700, tetrahedra, l=500	
			1 hr at 200^{o}	prismatic, d=500, 30% faulted, d=750, tetrahdera, l=800	
			1 hr at 300^{o}	prismatic, d=600, 50% faulted, d=700, tetrahedra, l=400	

vacancies present to interact and form clusters.

Another interesting point for FCC metals concerns the decrease in percentage of faulted loops as T_q is raised. This is generally considered[155] to be due to the Frank loops forming at temperatures sufficiently high to nucleate Shockley partials and convert them to prismatic loops. This would also account for the presence of perfect loops when the earlier-discussed energy considerations indicate that the great majority should be Frank loops. While the activation energy for Shockley nucleation is of the order of a few electron volts[155,189], it would appear that the high SFE metals, such as Al, are near enough to the upper limit for faulted loop stability so that the small amount of thermal energy available at these temperatures (a few tenths of an electron volt) is often sufficient to overcome the remaining portion of the nucleation barrier.

The effect of quench rate is very similar to that of T_q. Too slow a rate allows too many of the non-equilibrium vacancies to reach sinks, while too fast a rate cuts down the clustering time, leading to a high density of small loops. It is also possible that the higher quenching stresses from higher rates might be sufficient to cause the nucleation of Shockley partials, producing perfect loops.

The question of purity is important in that impurity atoms can lead to either vacancy-impurity complexes or second phase particles. The former may be mobile enough to allow the associated vacancies to reach sinks, or, if slower-moving, possibly result in cluster nucleation at temperatures high enough to permit Shockley nucleation. The latter, possible only if the impurity solid solubility is near zero, may generate

dislocations which can act as vacancy sinks, or act as sinks themselves to relieve the misfit strains often associated with precipitates. It should be mentioned here that it seems reasonable that any dislocations produced by precipitates, by quenching stresses or by phase transformations should act more as vacancy sinks than sources. That is, production of vacancies through tangling, cutting, jog formation, etc. of a sufficient quantity to affect the loop formation process, would not seem likely from these dislocations.

Further to the question of slow complexes, it could be argued that some amount are desireable for cluster formation, but too many complexes may result in severe depletion of the vacancy 'reservoir'. As mentioned in Sec. 3.2, the complex concentration depends on the relative sizes of solvent and solute. Thus, for relatively small matrix atoms, such as Al or Ni (see Table 9), high purities of the order of "5 or 6-9's" are needed while the requirements are not as stringent (around 4-9's) for larger matrix atoms, such as Mg. It is worthwhile to note that theoretically calculated homogeneous nucleation rates by Hirth and Davis[190] are much lower than actual rates, further lending credence to the likelihood of heterogeneous, i.e. impurity-induced nucleation.

In considering the above, one point that bears emphasis is the interchangeability of these parameters, e.g. re-examination of a 99.995 pure, 1 cm wide Al foil (water quenched 5 times), after a few weeks, showed a very reasonable mixed loop density close to that of photo. 14b or 15a. Since this mixed character is more desirable one might then take the 0.5 cm foils of these photos. (which are better for He quenching) and possibly achieve the same result by perhaps decreasing T_q, increasing the thickness slightly or reducing the quench rate through reduced pre-cooling or a lower

flow rate.

In applying the above criteria to Zr it would seem reasonable that specimen size and ageing procedure should present no special problems. As regards T_q, it may be intuitively argued that, as the solid state transformation is approached, more vacancies than normal are present due to the increasing instability of the HCP lattice. Thus T_q should be as close as possible to the transformation temperature of 862°C. In addition the quench rate should probably also be as high as possible since this approximation of the transformation to a melting point is most likely only a partial one at best. If this assumption is not valid, the possibility of loop formation in Zr would be very bleak because of the difficulties caused by quenching through the transformation, to say nothing of the technical problems arising from Zr's high melting point.

As is evident from Table 9, the impurity level in this Zr is indeed substantial, being approximately 1000 ppm. However, only 25 ppm of this total are larger than the Zr atom, and thus could form vacancy-impurity complexes. More seriously, roughly 600 ppm impurities could form precipitate particles because of their very limited solid solubility, arising mostly from the magnitude of their size difference with respect to the Zr atom, whether larger or smaller. It should be noted that hydrogen, easily picked up through contact with water vapor at high temperatures, is one of these impurities. It is to be further noted that roughly 200 ppm of the 625 ppm total, combining both the above factors, are impurities possessing melting points much less than Zr. These could perhaps be amendable to zone refining. Thus to obtain a satisfactory level of, say,

less than 100 ppm of undesirable impurities (those underlined in Table 9) would not seem as difficult a task as indicated by the total impurity level. Unfortunately, a closer analysis reveals that the majority of the undesirable impurities have rather high equilibrium distribution coefficients with Zr, which would necessitate a larger number of passes to significantly reduce their concentrations. At the same time, Zr's high affinity for gaseous elements would require very high vacuum levels for the refining. It is perhaps small wonder, then, that even the best purities obtained by the Materials Research Corporation[191] are only of the order of 99.96%.

Finally, it is possible that some difficulty could arise over the condensation mode of the vacancies in Zr. One study[192] has shown that neutron irradiation of Zr can result in interstitial perfect loops on prism planes (which have a slightly larger d spacing than basal planes in Zr), but, it could be argued that interstitials would condense on planes of largest d spacing, while vacancies, being strain relievers, should still condense on the closest-packed planes. If condensation was on the prism plane, it is difficult to visualize the exact mechanism or the final result, due to the fact that $\{10\bar{1}0\}$ planes can be considered as either flat low density planes having an ABCDA stacking sequence, or corrugated planes having a simple ABABA stacking[193].

It is apparent that several improvements could be made in the experimental technique used here. Besides those already mentioned (purity, vacuum level, etc.) it appears that the quench rate is on the low side. The method used resembles that of Lang and Canetoli[172], which they state as approximately equivalent to a liquid N_2 quench. However, as noted in Table 10, Levy et al[181] obtained a very high quench rate from gas quenching

by immersing the entire vacuum chamber in liquid He, which, unfortunately, would involve a complete restructuring of the apparatus. In addition it is probable that the uniformity of the quench could be increased by improved design, e.g. flared nozzles on both sides of the specimen, and a more uniform thickness from high quality rolls. An alternative to the latter might be a small furnace enclosed in the vacuum chamber.

Since none of these would help a great deal if the transformation cannot be approximated to a melting point to some degree, this approximation could be checked by a study of the quenched-in resistivity ($\Delta\rho$) near the transformation. If the assumption holds, an anomolous increase in ρ should occur at this point since an increase in vacancy concentration would result in a resistivity increase. However, it could be quite difficult to determine what portion of $\Delta\rho$ is ascribable to vacancies, since re-dissolution of impurities would also increase the resistivity. This is amply demonstrated by the study of Swanson et al[194] of quenched Zr wires, where, although they obtained $\Delta\rho$'s equivalent to point defect concentrations of roughly 10^{-4}, they could not definitely state what portion was due solely to vacancies.

If this assumption were invalid, there still remains the question of how best to measure the SFE of Zr. Ignoring the methods not applicable to HCP metals or those for which it is doubtful that an HCP theory could be derived, several alternative methods remain, but it is evident that their probabilities of being applicable are not very high. That is, the most accurate methods, the node, ribbon and fault-pair, require very low SFE's and it is doubtful that even maximum amounts of alloying can lower the SFE sufficiently for these methods to apply, since this requires a

substantial increase in e/a ratio. This is not likely because Zr may be, at best, only considered as di-valent[195] and, even then, higher valency solutes, such as Al or Sn possess small solid solubilities with Zr. This would appear to be experimentally confirmed, since for Ti-Al alloys[196,197] (Ti possessing a similar electronic structure), no extended defects (or even non-equilibrium faults) have been observed at Al contents up to 18 at%. The only other direct method, the grain boundary intersection method, depends entirely on the existence of equilibrium configurations.

It is doubtful that any alloying could lower the SFE sufficiently, for the X-ray method to be applicable (γ should be of the order of 10 ergs/cm^2 [198]). For the deformation methods the only proven possibility is the accurate determination of activation energy for prismatic slip in high purity single crystals and comparing this to equally accurate values for HCP metals of known SFE, such as Mg and Zn. The same format would apply to correlation of SFE with the Cottrell-Stokes ratio (if a correlation exists) or to the relative amounts of work softening.

The theoretical methods do not appear to be accurate enough at this time, except to be used as perhaps a rough check, cf. Ramaswami and Craig[83].

One final possibility, not previously discussed, would utilize the decrease of SFE with temperature. Although Gallagher[37] states that studies indicate little or no true temperature dependence of γ/G for a pure metal such as Ag, it could be reasoned that, since the SFE is lowered upon alloying by increasing the number of free electrons, i.e. expanding the Fermi surface, the same effect could occur by having the same number of free electrons increase in energy due to the temperature

rise. Unfortunately the work of Ericsson[199] on Co and Co alloys seems to indicate a very gradual decrease of SFE (in the order of 3 ergs/cm^2/100^{o}C) up to a few degrees from the phase change, followed by a precipitous drop and an equally steep rise to a similar value in the other phase, from which it gradually rises as the other phase stabilizes. This appears more reasonable than a linear decrease to zero at the transformation temperature, since this should evidence itself by wide splitting of dislocations in hot stage microscopy. No such evidence was obtained in specimens heated past the transformation, although severe oxidation after about 700^{o}C made any splitting thereafter very difficult to detect. Thus it might still be possible to heat the specimen to just past the transformation temperature and deform it as it is being quenched through the zero SFE point, resulting, hopefully, in fault formation and possibly even some good grain boundary intersections. Indeed, this may account for the supposed faults of photo. 12, since no similar defects were seen in any quenches from the α region.

3.7 CONCLUSIONS AND RECOMMENDATIONS

1) Many methods of determining the SFE of a metal exist, applicable over the whole range of possible values. It is especially important to remember though, that each method usually has several weak points or limiting conditions, thus a multi-method determination is emminently desirable, time and facilities permitting.
2) From previous work it appears that the SFE of Zr is high, probably in the range of 150-250 ergs/cm^2.

3) The present attempt to create faulted vacancy loops in Zr failed due to:

   a) low purity of the metal

   b) H_2 contamination from insufficient vacuum levels and quenchant impurities

   c) too low a quench rate

   d) an insufficient vacancy supersaturation due to the transformation not approximating to a melting point.

4) There still exist several possibilities of obtaining at least an estimate of Zr SFE (and, incidentally, for Ti as well). These would form the basis for any future work and are summarized as follows:

   a) another attempt at creating vacancy loops incorporating the previously-mentioned improvements only after a study of $\Delta\rho$ vs. T_q has shown some promise of an increase in vacancy concentration near the transformation temperature.

   b) accurate single crystal deformation studies to furnish a value of activation energy for prismatic slip, possibly in conjunction with X-ray studies of α vs'. alloying content. (It should be noted that work is currently in progress which may furnish the former for dilute Zr-Al alloys.)

   c) an electron microscope investigation of Al or Sn alloys of the highest solid solubility to determine if the SFE is lowered enough to obtain measureable equilibrium-extended defects.

   d) a study to determine if the Cottrell-Stokes law applies to Zr and, if it does, see if any correlation exists between it and other HCP C.-S. ratios. An investigation of work softening vs. SFE might also fit in here.

e) determine if it is possible, under certain conditions, to pull partials from grain boundaries and apply the critical tear stress idea of SFE determination.

f) deformation at or above the transformation temperature to see if any stacking fault-grain boundary intersections are formed. If extensive faulting proved possible, an optimum treatment of deformation and ageing for dilute alloys might result in strengthening through some form of precipitate association with the faults.

Of the above recommendations, only b) should definitely furnish some estimate of SFE, the others may or may not. If they did, a) would furnish the most accurate value. Finally, f) is the most intriguing possibility from a development standpoint.

4. ACKNOWLEDGEMENTS

I would like to express my gratitude to the National Research Council of Canada for their financial assistance, to Mr. J. Van Dorp and Dr. M. C. Chaturvedi for their aid with the electron microscope, and to Mr. S. N. Tiwari, who was responsible for the zone refining. Most of all I would like to thank my supervisor, Dr. K. Tangri, without whose teaching, comments and criticisms this study would not have been possible.

5. REFERENCES

1) Nabarro, F.R.N., Advances in Physics, 1, 355, 376 (1952)

2) Frank, F.C., Phil. Mag., 42, 809 (1951)

3) Frank, F.C., ibid., p. 1041

4) Frank, F.C. and Nicholas, J.F., Phil. Mag., 44, 1213 (1953)

5) Hirsch, P.B., Howie, A. and Whelan, M.J., Phil. Trans. Roy. Soc., 252A, 499 (1960)

6) Whelan, M.J. and Hirsch, P.B., Phil. Mag., 2, 1121, 1303 (1957)

7) Van Landuyt, J., Gevers, R. and Amelinckx, S., Phys. Stat. Sol., 9, 135 (1965)

8) Steeds, J.W., Phil. Mag., 17, 771, 785 (1967)

9) Shaw, A.M. and Brown, L.M., ibid., p. 797

10) Gevers, R., Art, A. and Amelinckx, S., Phys. Stat. Sol., 3, 1563 (1963)

11) Gevers, R., Art, A. and Amelinckx, S., Phys. Stat. Sol., ibid., p. 697

12) Seeger, A. and Shock, G., Report Bristol Conference on Defects in Crystalline Solids, p. 340 (1955)

13) Barnes, R.S., Acta Met., 2, 380 (1954)

14) Diehl, J., Mader, T. and Seeger, A., Z. Metallk., 46, 650 (1956)

15) Wyatt, O.H., Proc. Phys. Soc., 66, 459 (1953)

16) Mott, N.F., Symposium on Creep and Fracture, H.M.S.O., p. 21 (1956)

17) Hirsch, P.B. and Kelly, A., Phil. Mag., 11, 881 (1965)

18) Honeycombe, R.W., Warrington, D.H. and Van Aswegan, J.S., Phil. Mag., 9, 380 (1963)

19) Silcock, J.M. and Tunstall, W.J., Phil. Mag., 10, 361 (1964)

20) Hirsch, P.B., Phil. Mag., 7, 67 (1962)

21) Raty, R. and Miekk-Oja, H.M., Phil. Mag., 18, 1105 (1968)

22) Kotval, P.S., Trans. TMS-AIME, 242, 1651 (1968)

23) Chaturvedi, M.C., Honeycombe, R.W. and Warrington, D.H., J. Iron and Steel Inst., 206, 1236 (1968)

24) Nicholson, R.B. and Nutting, J., Acta Met., 9, 332 (1961)

25) Honeycombe, R.W., unpublished work

26) Venables, J.A., Phil. Mag., 7, 35 (1962)

27) Honeycombe, R.W., The Plastic Deformation of Metals, Arnold, p. 80 (1968)

28) Whelan, M.J., Proc. Roy. Soc., 249A, 114 (1959)

29) Brown, L.M., Phil. Mag., 10, 441 (1964)

30) Siems, R., Delavignette, P. and Amelinckx, S., Z. Physik, 165, 502 (1961)

31) Thornton, P.R., Mitchell, T.E. and Hirsch, P.B., Phil. Mag., 7, 1349 (1962)

32) Mader, S., Conference on Electron Microscopy and Strength of Crystals, Interscience, p. 183 (1963)

33) Gallagher, P.C.J., J. App. Phys., 37, 1710 (1966)

34) Brown, L.M. and Tholen, A.R., Disc. Far. Soc., 38, 35 (1964)

35) Siems, R., Disc. Far. Soc., 38, 42 (1964)

36) Christian, J.W. and Swann, P.R., Alloying Behavior and Effects in Concentrated Solid Solutions, Gordon and Breach, a) p. 195, b) p. 137, c) p. 216 (1965)

37) Gallagher, P.C.J., AIME Conference on the Measurement of Stacking Fault Energy, Pittsburgh (1969), publ. Met. Trans., 1, 2429 (1970)

38) Silcox, J. and Hirsch, P.B., Phil. Mag., 4, 72 (1959)

39) de Jong, M. and Koehler, J.S., Phys. Rev., 129, 49 (1963)

40) Kimura, H., Kuhlmann-Wilsdorf, D. and Maddin, R., App. Phys. Letters, 3, 4 (1963)

41) Hirsch, P.B., N.P.L. Conference on the Relation Between Strength and Structure in Metals and Alloys, 1, 440 (1963)

42) Loretto, M.H., Clarebrough, L.M. and Segall, R.L., Phil. Mag., 11, 459 (1965)

43) Vingsbo, O., Acta Met., 15, 615 (1967)

44) Czjzek, G., Seeger, A. and Mader, S., Phys. Stat. Sol., 2, 558 (1962)

45) Jossang, T. and Hirth, J.P., Phil. Mag., 13, 657 (1966)

46) Humble, P., Loretto, M.H. and Clarebrough, L.M., Phil. Mag., 14, 297 (1966)

47) Humble, P., Segall, R.L. and Head, Å.K., Phil. Mag., 14, 281 (1966)

48) Read, W.T., Dislocations in Crystals, McGraw-Hill, p. 131 (1953)

49) Amelinckx, S. and Delavignette, P., Electron Microscopy and Strength of Crystals, Interscience, p. 441 (1963)

50) Murr, L.E., Smith, P.J. and Gilmore, C.M., Phil. Mag., 17, 89 (1968)

51) Peterson, L.G. and Queeney, R.A., Trans. TMS-AIME, 245, 2098 (1969)

52) Ives, K.L. and Ruff, A.W., J. App. Phys., 37, 1831 (1966)

53) Lele, S., Trans. TMS-AIME, 239, 592 (1967)

54) Loretto, M.H., Phil. Mag., 10, 441 (1965)

55) Hirth, J.P. and Lothe, J., Theory of Dislocations, McGraw-Hill, a) p. 294, b) p. 764 (1967)

56) Gallagher, P.C.J., Phys. Stat. Sol., 16, 95 (1966)

57) Gallagher, P.C.J. and Washburn, J., Phil. Mag., 14, 971 (1966)

58) Murr, L.E., Thin Solid Films, 4, 389 (1969)

59) Gallagher, P.C.J., Trans. TMS-AIME, 242, 103 (1968)

60) Kritzinger, S., Smallman, R.E. and Dobson, P.S., Acta Met., 17, 49 (1969)

61) Steeds, J.W., Phil. Mag., 16, 771, 785 (1967)

62) Pande, C.S., Phys. Stat. Sol., 37, 151 (1970)

63) Edwards, O.S. and Lipson, H., Proc. Roy. Soc., 180A, 268 (1942)

64) Wilson, A.C.J., ibid., p. 277

65) Warren, B.E. and Warekois, E.P., J. App. Phys., 24, 951 (1953)

66) Paterson, M.S., J. App. Phys., 23, 805 (1952)

67) Vasamillet, L.F. and Massalski, T.B., J. App. Phys., 34, 3398 (1963)

68) Smallman, R.E. and Westmacott, K.H., Phil. Mag., 17, 669 (1957)

69) Gallagher, P.C.J. and Liu, Y.C., Acta Met., 17, 127 (1969)

70) Otte, H.M., J. App. Phys., 38, 217 (1967)

71) Ahlers, M., AIME Conference on the Measurement of Stacking Fault Energy, Pittsburgh (1969), publ. Met. Trans., 1, 2415 (1970)

72) Seeger, A., Handbuch der Physik VII, 2. Springer Verlag, Berlin (1958)

73) Seeger, A., Berner, R. and Wolf, H.Z., Z. Physik, 155, 247 (1959)

74) Seeger, A., Dislocations and Mechanical Properties of Crystals, Wiley, p. 259 (1957)

75) Wolf, H., Z. Naturf., 15a, 180 (1960)

76) Peissker, E., Acta Met., 13, 419 (1965)

77) Gallagher, P.C.J., J. App. Phys., 39, 160 (1968)

78) Kuhlmann-Wilsdorf, D., Work Hardening, Gordon and Breach, p. 97 (1968)

79) Bocek, M., Hotzch, G. and Simmon, B., Phys. Stat. Sol., 7, 833 (1964)

80) Bocek, M., Luckac, P., Smola, B. and Svaboda, M., Phys. Stat. Sol., 7, 173 (1964)

81) Luckac, P. and Svaboda, M., Phys. Stat. Sol., 8, 187 (1965)

82) Thornton, P.R. and Hirsch, P.B., Phil. Mag., 3, 738 (1958)

83) Ramaswami, B. and Craig, G.B., Trans. TMS-AIME, 239, 1226 (1967)

84) Cousland, S.M., Phys. Stat. Sol., 37, 159 (1970)

85) Tangri, K.K., private communication

86) Cottrell, A.H. and Stokes, R.J., Proc. Roy. Soc., 233A, 17 (1955)

87) Saarinen, A.V.A. and Miekk-Oja, H.M., Met. Sci. J., 1, 145 (1967)

88) Singh, R.N. and Tangri, K.K., Met. Trans., 1, 3151 (1970)

89) Dillamore, I.L., Smallman, R.E. and Roberts, W.T., Phil. Mag., 9, 517 (1964) and 12, 191 (1965)

90) Liu, Y.C. and Alers, G.A., Trans. TMS-AIME, 245, 1857 (1969)

91) Liu, Y.C., Trans. TMS-AIME, 230, 656 (1964)

92) Kamijo, T. and Sekine, K., Met. Trans., 1, 1287 (1970)

93) Fullman, R.J., J. App. Phys., 22, 448 (1951)

94) Inman, M.C. and Tipler, H.R., Met. Rev., 8, 105 (1963)

95) Greenough, A.P., App. Mater. Res., 6, 25 (1965)

96) Valenzuela, C.G., Trans. TMS-AIME, 233, 1911 (1965)

97) Fawley, R., Quader, M.A. and Dodd, R.A., Trans. TMS-AIME, 242, 771 (1968)

98) Saada, G., Theory of Crystal Defects, Academic Press, p. 210 (1966)

99) Jossang, T., private communication to Hirth and Lothe, ref.55, p. 295

100) Ducharme, A.R., Phys. Letters, 31A, 41 (1970)

101) Krasko, G.L., Telliyants, V.N., Pozvonkova, R.T. and Zazlavskii, Y.I., Sov. Phys.-Solid State, 9, 2414 (1968)

102) Tisone, T.C., Sundahl, R.C. and Chin, G.Y., Met. Trans., 1, 1561 (1970)

103) Davies, R.G. and Cahn, R.W., Acta Met., 10, 621 (1962)

104) Bolling, G.F., Massalski, T.B. and McHargue, C.J., Phil. Mag., 6, 491 (1961)

105) Vasamillet, L.F., J. App. Phys., 32, 778 (1961)

106) Beeston, B.E.P., Dillamore, I.L. and Smallman, R.E., Met. Sci. J., 2, 12 (1968)

107) Tisone, T.C., ASM Spring Meeting, Las Vegas (1970)

108) Loretto, M.H., Clarebrough, L.M. and Segall, R.L., Phil. Mag., 10, 731 (1964)

109) Gallagher, P.C.J., Ph. D. Thesis, Cambridge University, England (1964)

110) Wilkens, M., Rapp, M. and Differt, K., Z. Metallk., 10, 746 (1966)

111) Ruff, A.W. and Ives, L.K., Acta Met., 15, 189 (1967)

112) Clarebrough, L.M., Humble, P. and Loretto, M.H., Can. J. Phys., 45, 1135 (1967)

113) Berner, R., Z. Naturf., 15a, 689 (1960)

114) Buhler, S. and Lucke, K., Z. Metallk., 55, 722 (1964)

115) Ahlers, M., Z. Metallk., 56, 741 (1965)

116) Ahlers, M. and Haasen, P., Phys. Stat. Sol., 10, 485 (1965)

117) Seeger, A., Phil. Mag., 9, 887 (1964)

118) Haussermann, F. and Wilkens, M., Phys. Stat. Sol., 18, 607 (1966)

119) Hu, H., Cline, R.S. and Goodman, S.R., J. App. Phys., 32, 1399 (1961)

120) Suzuki, H. and Barrett, C.S., Acta Met., 6, 156 (1958)

121) Haasen, P. and King, A., Z. Metallk., 51, 722 (1960)

122) Peissker, E., Acta Met., 13, 419 (1965)

123) Fisher, J.C. and Dunn, C.G., Imperfections in Nearly Perfect Crystals, Wiley, p. 317 (1952)

124) Seeger, A. and Schock, G., Acta Met., 1, 519 (1953)

125) Inman, M.C. and Khan, A.R., Phil. Mag., 6, 937 (1961)

126) Nordstrom, T.V. and Barrett, C.R., Acta Met., 17, 139 (1969)

127) Blewitt, T.H., Coltmann, R.R. and Redman, J.K., J. App. Phys., 28, 651 (1957)

128) Kannan, V.C. and Thomas, G., J. App. Phys., 37, 2363 (1966)

129) Dobson, P.S., Goodhew, P.J. and Smallman, R.E., Phil. Mag., 16, 9 (1967)

130) Tartour, J.-P. and Washburn, J., Phil. Mag., 18, 1257 (1968)

131) Haasen, P., Phil. Mag., 3, 384 (1958)

132) Saulnier, A., private communication to Friedel, J., Electron Microscopy and Strength of Crystals, Interscience, p. 605 (1963)

133) Seeger, A., Defects in Crystalline Solids, London: Phys. Soc., p. 328 (1955)

134) Price, P.B., Electron Microscopy and Strength of Crystals, Interscience, p. 41 (1963)

135) Seeger, A., Electron Microscopy and Strength of Crystals, Interscience, p. 680 (1963)

136) Harris, J.E. and Masters, B.C., Proc. Roy. Soc., 292A, 240 (1966)

137) Hales, R., Smallman, R.E. and Dobson, P.S., Proc. Roy. Soc., 307A, 71 (1968)

138) Spreadborough, J., Phil. Mag., 3, 1167 (1958)

139) Dobson, P.S. and Smallman, R.E., Proc. Roy. Soc., 293A, 423 (1966)

140) Roy, R.B., Aktiebolaget Atomenergi, AE-130 (1963)

141) Chou, T.Y., Acta Met., 10, 739 (1962)

142) Lele, S. and Anantharaman, T.R., Phil. Mag., 15, 1035 (1967)

143) Mogard, J.H. and Averbach, B.L., Acta Met., 6, 552 (1958)

144) Krishnan, R., Z. Metallk., 58, 811 (1967)

145) Damask, A.C. and Dienes, G.J., Point Defects in Metals, Gordon and Breach, p. 31 (1963)

146) Koehler, J.S., Seitz, F. and Bauerle, J.E., Phys. Rev., 107, 1499 (1957)

147) Panseri, C. and Federighi, T., Phil. Mag., 3, 1223 (1958)

148) Eikum, A. and Thomas, G., J. Phys. Soc. Jap., 18, Supp. III, 7 (1963)

149) Devoit, B., Octer, H. and Scherrer, S., Int. Conf. on Vacancies and Interstitials in Metals, Julich, Germany (1968)

150) Kuhlmann-Wilsdorf, D. and Wilsdorf, H.G.F., J. App. Phys., 31, 516 (1960)

151) Dohkner, R., Sov. Phys.-Solid State, 11, 916 (1969)

152) Berghezan, A., Fourdeux, A. and Amelinckx, S., Acta Met., 9, 464 (1961)

153) Cottrell, A.H., Dislocations and Plastic Flow in Crystals, Oxford University Press (1953)

154) Smallman, R.E., Westmacott, K.H. and Coiley, J.H., J. Inst. Met., 88, 127 (1959)

155) Cotterill, R.M.J. and Segall, R.L., Phil. Mag., 8, 1105 (1963)

156) Silcox, J. and Whelan, M.J., Phil. Mag., 5, 1 (1960)

157) Freidel, J., Les Dislocations, Paris, Gauthier-Villars, p. 72 (1956)

158) Frank, F.C., Plastic Deformation of Crystalline Solids, Office of Naval Research, p. 89 (1958)

159) Edington, J.W. and Smallman, R.E., Phil. Mag., 11, 1109 (1965)

160) Saada, G., Phil. Mag., 13, 1307 (1966)

161) Seidman, D.N. and Baluffi, R.W., Phil. Mag., 13, 649 (1966)

162) Hales, R., Smallman, R.E. and Dobson, P.S., Met. Sci. J., 2, 224 (1968)

163) Spalding, D.R., Edington, J.W. and Villagrana, R.E., Phil. Mag., 20, 1203 (1969)

164) Goodhew, P.J., Dobson; P.S. and Smallman, R.E., Met. Sci. J., 1 198 (1967)

165) Kritzinger, S., Smallman, R.E. and Dobson, P.S., Phil. Mag., 16, 217 (1967)

166) Leighly, Jr., H.P., Phil. Mag., 22, 209 (1970)

167) Westmacott, K.H., Int. Met. Soc., Proceedings, p. 353 (1969)

168) Barrett, C.S. and Massalski, T.B., Structure of Metals, McGraw-Hill, p. 626 (1966)

169) ASM Metals Handbook, vol. 1, p. 46 (1961)

170) Hansen, M., Constitution of Binary Alloys, McGraw-Hill (1958)

171) Bailey, J.E., Acta Met., 11, 267 (1963)

172) Lang, E. and Canetoli, S., Euratom EUR4283e (1969)

173) van Landuyt, J., Gevers, R. and Amelinckx, S., Phys. Stat. Sol., 9, 135 (1965)

174) Studel, J.L. and Washburn, J., Phil. Mag., 9, 491 (1964)

175) Duckworth, F.C., Ramachandran, T.R. and Burke, J., Int. Conf. on Vacancies and Interstitials in Metals, Julich, Germany (1968)

176) Seidman, D.N. and Baluffi, R.W., Phil. Mag., 10, 1067 (1964)

177) Yokota, M.J. and Washburn, J., Phil. Mag., 16, 461 (1967)

178) Quader, M.A. and Dodd, R.A., Phil. Mag., 17, 575 (1968)

179) Eades, J.A. and Rojo, J.M., Phil. Mag., 18, 1093 (1968)

180) Camanzi,A., Mancini, N.A., Rimini, E. and Schianchi, G., Int. Conf. on Vacancies and Interstitials in Metals, Julich, Germany (1968)

181) Levy, V., Hillairet, J. and Schumacher, D., ibid.

182) Hales, R., Dobson, P.S. and Smallman, R.E., Met. Sci. J., 2, 224 (1968)

183) Scherrer, S., Lozes, G. and Devoit, B., Int. Conf. on Vacancies and Interstitials in Metals, Julich, Germany (1968)

184) Clarebrough, L.M. and Morton, A.J., ibid.

185) Camanzi, A. and Schianchi, G., Phil. Mag., 16, 1207 (1967)

186) Wilson, J.C. and Picklesimer, M.L., Electron and Ion Beam Science and Technology, Wiley, p. 502 (1965)

187) Rapperport, E.J., Acta Met., 7, 254 (1959)

188) Kiritani, M., Nishikawa, T. and Yoshida, S., J. Phys. Soc. Jap., 27, 67 (1969)

189) Saada, G.V., Int. Conf. on Crystal Lattice Defects, J. Phys. Soc. Jap., 18, Supp. III, p. 41 (1963)

190) Hirth, J.P. and Davis, T.L., J. App. Phys., 37, 2112 (1966) and 38, 2390 (1967)

191) Materials Research Corporation, New York, private communication

192) Gulden, T.D. and Bernstein, I.M., Phil. Mag., 14, 1087 (1966)

193) Regnier, P. and Dupouy, J.M., Phys. Stat. Sol., 39, 79 (1970)

194) Swanson, M.L., Piercey, G.R., Kidson, G.V. and Quennville, A.F., J. Nuc. Mater., 34, 340 (1970)

195) Douglass, D.L., Atomic Energy Review, 1, 141 (1963)

196) Williams, J.C. and Blackburn, M.J., Boeing Scientific Research Laboratories Document D1-82-0928, Sept. (1969)

197) Lutjering, G. and Weissmann,S., Acta Met., 18, 785 (1970)

198) Salonen, L.O., Kajamaa, J.P. and Saarinen, A.V., Z. Metallk., 60, 802 (1970)

199) Ericsson, T., Acta Met., 14, 853 (1966)